VARNA SCIENTIFIC AND TECHNICAL UNIONS

TECHNICAL UNIVERSITY - VARNA

# SEVENTEENTH INTERNATIONAL CONFERENCE ON MARINE SCIENCES AND TECHNOLOGIES


## The Conference is Dedicated to the 50th Anniversary of the Establishment of the Shipbuilding Faculty at the Technical University of Varna

# PROCEEDINGS

ISSN 1314 - 0957

October 18th, 2024

Varna, Bulgaria

# SEVENTEENTH INTERNATIONAL CONFERENCE ON MARINE SCIENCES AND TECHNOLOGIES

## The Conference is Dedicated to the 50th Anniversary of the Establishment of the Shipbuilding Faculty at the Technical University of Varna


# PROCEEDINGS

## ISSN 1314 - 0957

**October 18th, 2024**
**Varna, Bulgaria**

**VARNA SCIENTIFIC AND TECHNICAL UNIONS**

**BULGARIA**
**9000 VARNA**
**25, "TSAR SIMEON I" Str.**

**Phone: +35952 630 532**
**E-mail: nts@nts.varna.net**
**URL: nts.varna-bg.org**
**DOI: https://doi.org/10.7546/IO.BAS.2024.10**

# ISSN 1314 - 0957

**Organized by:**

**VARNA SCIENTIFIC AND TECHNICAL UNIONS**

**AND**

**TECHNICAL UNIVERSITY - VARNA**

**With the Cooperation of:**

**BULGARIAN NATIONAL ASSOCIATION OF SHIPBUILDING AND SHIPREPAIR (BULNAS)**

**"N. VAPTSAROV" NAVAL ACADEMY - VARNA**

**BULGARIAN ACADEMY OF SCIENCES (BAS):**

**INSTITUTE OF OCEANOLOGY - VARNA**

**BULGARIAN SHIP HYDRODYNAMICS CENTRE**

* * *

## Main Topics of the Conference:

**(1) Oceanology**

**(2) Shipbuilding and Ship Repair**

**(3) Decarbonization in Shipping**

**(4) Ship Hydrodynamics**

**(5) Maritime Transportation and Port Operations**

## INTERNATIONAL ADVISORY COMMITTEE

**Ionel CHIRICA,**
Dunarea de Jos University of Galati, ROMANIA

**Leonard DOMNISORU,**
Dunarea de Jos University of Galati, ROMANIA

**Yordan GARBATOV,**
University of Lisbon, PORTUGAL

**Mathias PASCHEN,**
Universität Rostock, DEUTSCHLAND

**Pentscho PENTSCHEW,**
Universität Rostock, DEUTSCHLAND

**Carlos Guedes SOARES,**
University of Lisbon, PORTUGAL

**Volodymyr ZAYTSEV,**
Admiral Makarov National University of Shipbuilding, Ukraine

## EXECUTIVE COMMITTEE

### Chairman:
**Stefan VACHKOV,**
Chairman of the Varna Scientific and Technical Unions

### Co-Chairmen:
**Atanas PALAZOV,**
Head of Institute of Oceanology - Varna

**Rumen KISHEV,**
Bulgarian Ship Hydrodynamics Centre

**Petar GEORGIEV,**
Technical University - Varna

**Scientific Secretary:**
**Stefan KYULEVCHELIEV,**
Bulgarian Ship Hydrodynamics Centre

### Organization Secretary:
**Nedelcho VICHEV,**
Varna Scientific and Technical Unions

## Members:

**Dragomir PLAMENOV,**
Rector of Technical University - Varna

**Boyan MEDNIKAROV,**
“N. Vaptsarov” Naval Academy - Varna

**Svetlin STOYANOV,**
Chairman of the Bulgarian National Association of Shipbuilding and Shiprepair (BULNAS)

**Ivan IVANOV,**
Technical University - Varna

**Dimitar TODOROV,**
ODESSOS Ship repair Yard, J. S. Co - Varna, Executive Director

**Kiril PALAVEEV,**
ULA Ltd. - Varna, Manager

**Elena VELIKOVA,**
Bulgarian National Association of Shipbuilding and Ship repair (BULNAS),
Executive Secretary

# C O N T E N T S

## (1) Oceanology:



## (2) Shipbuilding and Ship Repair:



## (3) Decarbonization in Shipping:

## (4) Ship Hydrodynamics:



## (5) Maritime Transportation and Port Operations:


# OCEANOLOGY

# EVOLUTION OF THE BULGARIAN NATIONAL OPERATIONAL MARINE OBSERVING SYSTEM

**Atanas PALAZOV*, Veselka MARINOVA*, Violeta SLABAKOVA*, Asen STEFANOV*,Olexandr UMANOV***

**Abstract**: *The Bulgarian National Operational Marine Observing System (NOMOS) is a system of systems introduced on 2012 and designed to allow the real-time assessment of weather and marine conditions in the coastal, shelf and open sea areas of the western part of Black Sea. The main goal of NOMOS is to support sustainable development of the Bulgarian Black Sea coast and EEZ, and the main task is to provide operational information for the needs of: national security, civil protection, Search and Rescue, government and local authorities, port authorities, shipping, marine industry, fishery and aquaculture, tourist industry, environmental protection, coast protection, oil spills combat and other interested. In 2018 NOMOS become a module of MASRI - Infrastructure for Sustainable Development of Marine Research and Participation in The European Infrastructure Euro-Argo - a project of the National roadmap for scientific Infrastructure (2020 - 2027) of Republic of Bulgaria. As a result of this and operational experience, the system has evolved both in terms of scope and measured parameters. The evolution of NOMOS is aimed at technical improvement and increasing its efficiency. The NOMOS real time data is one of the most important sources of multi-parameter operational information in the Black Sea which serves for monitoring, verification and improvement of model results and forecasts as well as for collecting long time series of data needed for climatic research, marine physics, chemistry and biology. Free real time data access and developed user-friendly WEB and WAP interfaces made the system useful not only for science, marine industry and governmental agencies but also for general public, especially for fishermen, yachtsmen and windsurfers.*

**Keywords**: *Black Sea; observing systems; operational oceanography; oceanographic data management.*

## INTRODUCTION

Development of modern oceanography has begun with the establishment on July 1, 1973 of the Institute of Oceanology to the Bulgarian Academy of Sciences (IO-BAS). First complex International coastal experiments “Kamtchia” were performed 1977-1981 at the coastal research base (RB) “Shkorpilovtci” [1]. First computer controlled automated coastal measurements with capability to provide operational information is putted into practice at the RB “Shkorpilovtci” during 1983-1988 [2]. On year 2001 the BlackSeaGOOS MoU was signet and first GOOS activities in the Black Sea were ARENA EC FP5 project 2003-2006 [3] and ASCABOS EC FP6 project 2006-2009 [4]. Last twenty years significant efforts were applied towards building the Bulgarian National Operational Marine Observing System (NOMOS) [5]. NOMOS was established on the basis of several independently built subsystems: POMOS, Galata, Shkorpilovtci, BulSeaL and BulARGO. POMOS was an observing system located in the ports (14 measuring sites, 45 instruments, 14 weather and seastate parameters), designed to provide weather and sea state operational information for the areas of major Bulgarian ports (Varna, Burgas and Balchik), intended to secure safety shipping in ports, canals and bays [6]. Galata is a gas extraction platform and the instruments installed on it provided open sea Real-time meteorological and oceanographic information from 24 sensors, measuring 31 major oceanographic and meteorological parameters [7,8]. Shkorpilovtci is a coastal oceanographic station compiling: weather station, sea level gauge, UV radiation sensor and Recording Doppler Current Profiler with wave sensor. BulSeaL is a network of sea

*** Institute of Oceanology, Bulgarian Academy of Sciences, Varna, Bulgaria**

level stations including four historical sites, measuring sea level from more than 90 years. BulARGO [9] was a set of Argo floats deployed in the frame if the project supported by Bulgarian National Science Fund, Ministry of education, youth and science. The purpose of the BulARGO project was to develop a new national marine research infrastructure for in situ observation in Black Sea based on autonomous profiling floats as a Bulgarian component of the Euro Argo network.

These subsystems are collected real-time data using various sensors and instruments deployed at different strategic locations. All instruments are connected to communication system via Internet which provides direct access to the sensors or data collected. The measured data are transmitted to the central collecting system, where the information is processed and stored in the database. Access to database is through internet with the help of web browsers. Actual data is controlled by Data Management System and can be displayed on the computer screens using report server supporting thereby needs of different group of users. Since 2018 NOMOS has become a module of MASRI - Infrastructure for Sustainable Development of Marine Research and Participation in The European Infrastructure Euro-Argo - a project of the National roadmap for scientific Infrastructure (2020 -2027) of Republic of Bulgaria.

**NOMOS ARCHITECTURE**

In the frame of MASRI, NOMOS has been redesigned with the focus on the coastal and shelf areas. The BulArgo only remains as a basin scale system. Thus, NOMOS has become a system of systems designed mainly to provide real-time assessment of weather and marine conditions in the coastal and shelf areas of the western part at Black Sea for wide user community. Nowadays NOMOS consists of five independent marine observing systems, four of them are coastal and one open sea which cover different regions and are targeted to serve different users. The system includes the next subsystems:

- BulArgo
- WAVES - waves and currents monitoring system
- BulSeaL - Sea Level Monitoring System
- MOORINGS - Moorings network
- Coastal stations

Integration of the systems is on data and dissemination level. NOMOS architecture is shown on Figure1.

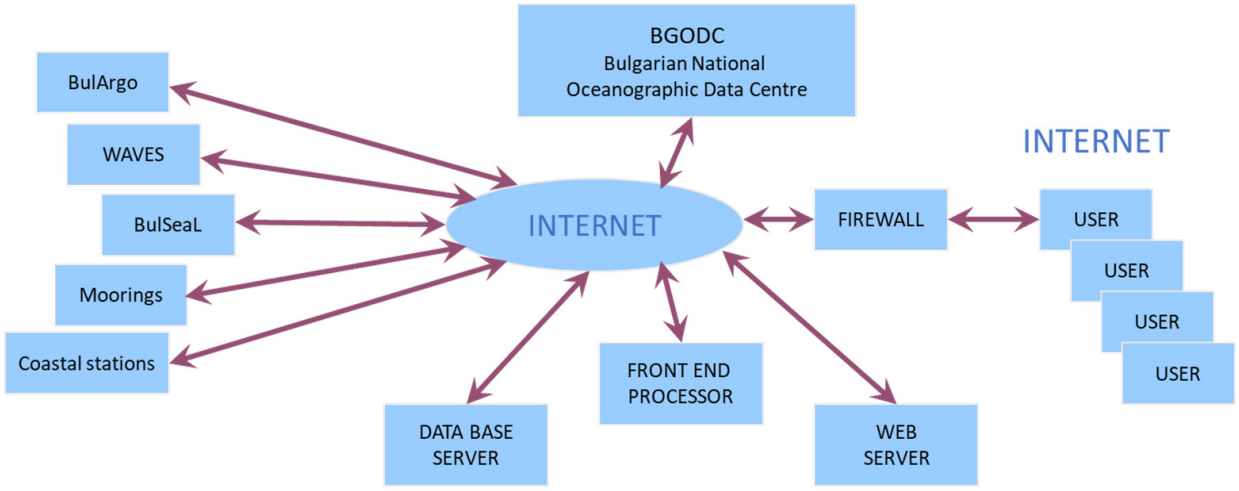


**Figure 1.**
**NOMOS architecture**

All data collected by NOMOS instruments are stored in the National Oceanographic Data Centre (BGODC) and are freely and openly available in real time through the BGODC website.

## DESCRIPTION OF NOMOS COMPONENTS

NOMOS consists of five components:

### *A. BulARGO*

In 2018 Bulgaria become a member of Euro-Argo ERIC and since then BulArgo received permanent funding from MASRI. The main objective of BulArgo is to develop and sustain the Black Sea Ocean observing system that monitors essential physical and ecosystem variables. Its targets are: to continue and extend the already established Argo infrastructure in the Black Sea with improved coverage and extension into shallow water areas such as the north west part of the Black Sea; to include floats with biogeochemical (BGC) - sensors and to contribute to the Euro-Argo ERIC Roadmap and the international Argo programs.

Till nowadays 51 Argo floats have been deployed in the Black Sea, provided mainly by MASRI and partly by EuroArgo and MedArgo programmes and some national and EU projects such as DOORS, PERSEUS, DEKOSIM, EIMS and EA-RISE . Currently there are 11 BulArgo floats active in the Black Sea out of 13 in total - Figure 2. Since establishment of the BulArgo programe, more than 2700 CTD and 1660 Disslved Oxygen profiles have been collected collected by Bulgarian Argo floats. The data are freely and openly available through the BulArgo and other Argo data websites (http://bulargo.io-bas.bg; https://fleetmonitoring.euro-argo.eu/dashboard; https://www.nodc.noaa.gov/; http://www.coriolis.eu.org/Observing-the-Ocean/ARGO; https://www.ocean-ops.org/board).

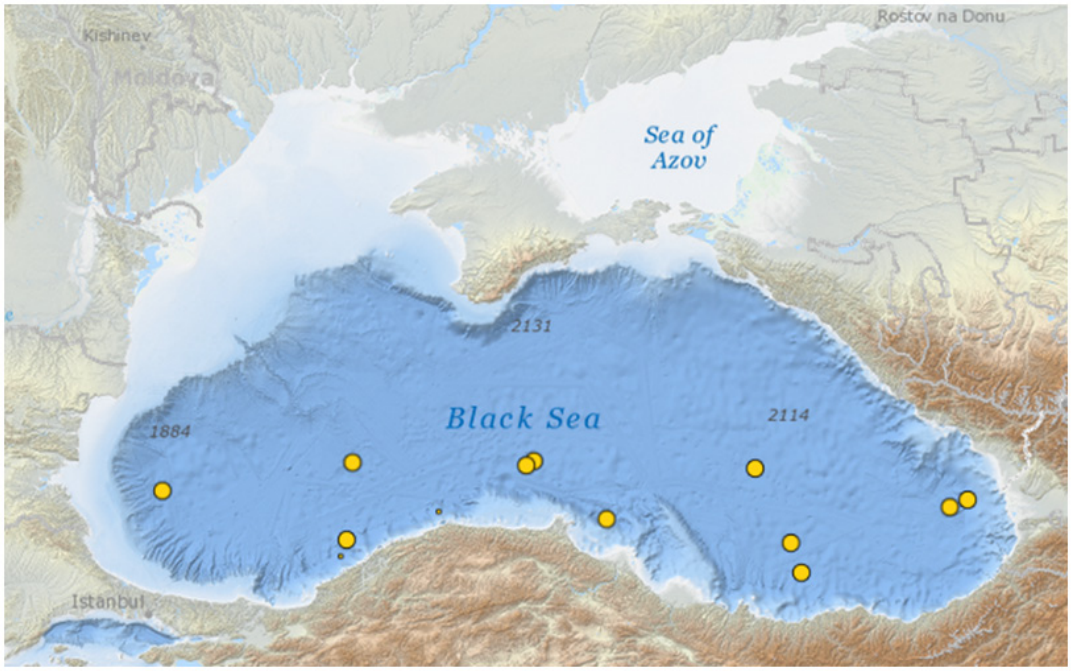


**Figure 2.**
**BulArgo floats in the Black Sea - 2024**

### *B. WAVES*

The development of the Sea wave observing system started in 2020 with the deployment of six moored wave buoys, three by IO-BAS and three by National Institute of Meteorology and Hydrology (NIMH) [10]. Next year another three wave buoys were deployed by NIMH. The buoys ware two types: six Spotter and three Anteia. The deployment positions were chosen to provide optimal coverage of the Bulgarian Black Sea coast. Figure 3 shows the wave data published on the BGODC and NIMH websites.

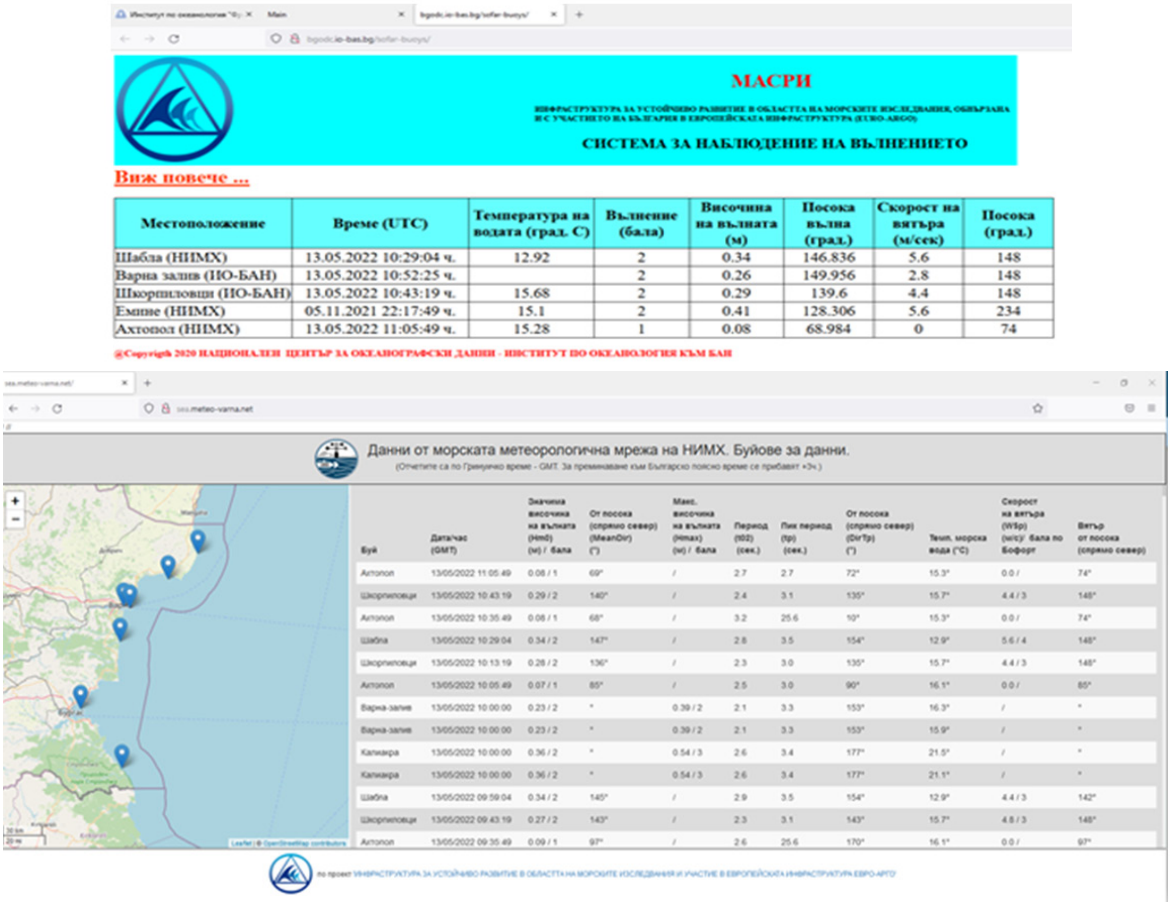


| Местоположение | Време (UTC) | Температура на водата (град. С) | Вълнение (бала) | Височина на вълната (м) | Посока вълна (град.) | Скорост на вятъра (м/сек) | Посока (град.) |
|---|---|---|---|---|---|---|---|
| Шабла (НИМХ) | 13.05.2022 10:29:04 ч. | 12.92 | 2 | 0.34 | 146.836 | 5.6 | 148 |
| Варна залив (ИО-БАН) | 13.05.2022 10:52:25 ч. | | 2 | 0.26 | 149.956 | 2.8 | 148 |
| Шкорпиловци (ИО-БАН) | 13.05.2022 10:43:19 ч. | 15.68 | 2 | 0.29 | 139.6 | 4.4 | 148 |
| Емине (НИМХ) | 05.11.2021 22:17:49 ч. | 15.1 | 2 | 0.41 | 128.306 | 5.6 | 234 |
| Ахтопол (НИМХ) | 13.05.2022 11:05:49 ч. | 15.28 | 1 | 0.08 | 68.984 | 0 | 74 |

**Figure 3.**
**Wave data websites**

In 2023 under the DOORS project and in 2024 under MASRI, three SPOTTER type buoys were delivered for expansion and maintenance of the system.

***C. BulSeaL***

BulSeaL is the Bulgarian sea level service. Systematic sea level measurements started in Bulgaria in the beginning of 20th century. In 2012 the processes of modernization of the coastal sea level stations (SLCS) started and consist of using of radar sea level sensors and communication equipment which allowed providing real-time sea level data every 2 minutes [11, 12]. Nowadays Bulgarian sea level service is provided in cooperation between Geodesy, Cartography and Cadastre Agency, Ministry of Regional Development and Public Works together with National Institute of Geophysics, Geodesy and Geography, Bulgarian Academy of Sciences and Institute of Oceanology, Bulgarian Academy of Sciences. The number, location and observational period of the Bulgarian sea level stations are shown in Table 1.

Sea level data are freely and openly available in real time through the website of the BGODC (http://bgodc.io-bas.bg/sea-level/).

**Table 1. Number and location of the Bulgarian sea level coastal station**

| No | SLCS | Latitude N | Longitude E | Established | Years in operation |
|---|---|---|---|---|---|
| 1 | Balchik | 43° 24′ | 28° 10′ | 2009 | 15 |
| 2 | Varna | 43° 12′ | 27° 57′ | 1928 | 96 |
| 3 | Shkorpilovtci | 42° 57′ | 27° 54′ | 2010 | 14 |
| 4 | Pomorie | 42° 33′ | 27° 38′ | 2009 | 15 |
| 5 | Burgas | 42° 29′ | 27° 29′ | 1928 | 96 |

Dedicated websites were developed for the needs of local authorities and general public. Figure 4 shows the location of the Sea level coastal stations (left) and Pomorie sea level station data (right). Future plans are to reopen two old stations: Irakli and Ahtopol.

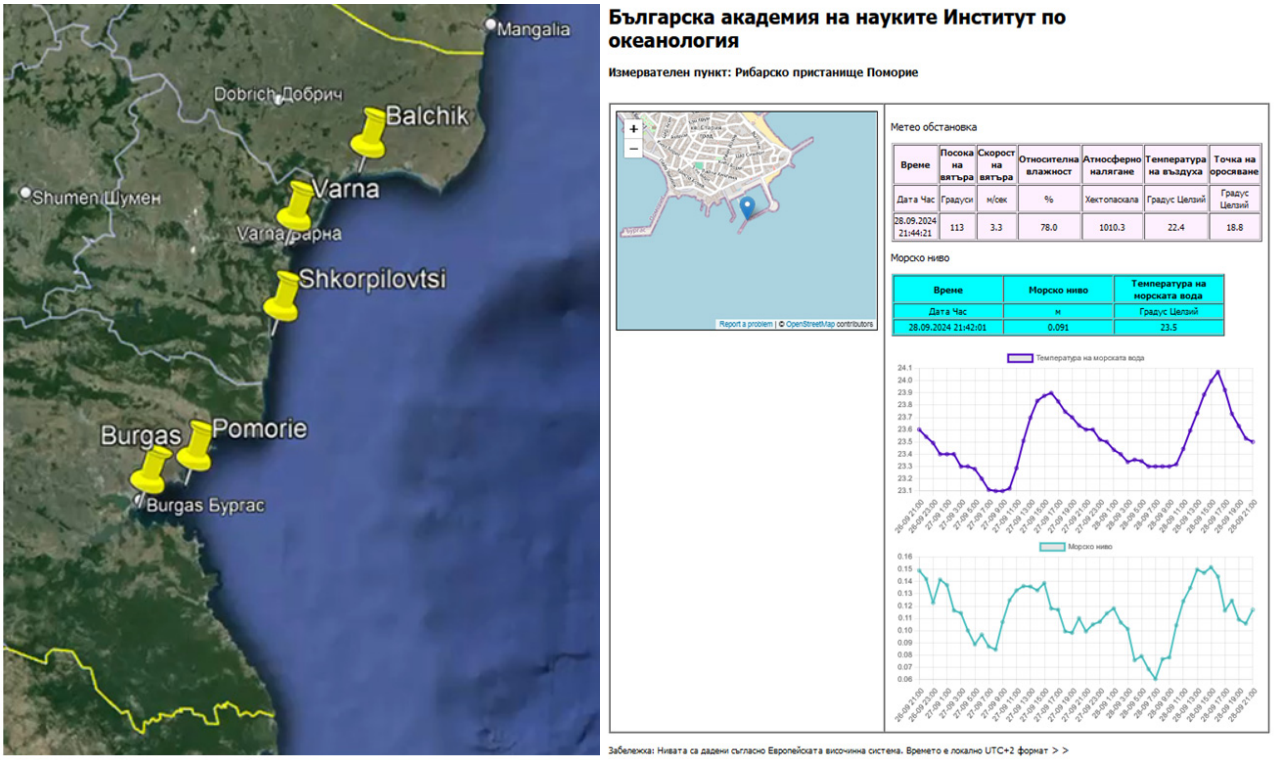


**Figure 4.**
**Location of the Sea level stations (left) and Pomorie sea level station data (right)**

***D. Moorings***

In the frame of IMAMO - Improved Marine Waters Monitoring project a system for real time monitoring was developed consists of two moorings [13, 14]. Surface buoys and bottom stations were deployed in Burgas and Varna bays in 2016 (Figure 5). Several marine variables had been provided by the two moorings in real time: Wind speed and direction, Air Temperature, Atmospheric pressure, Relative humidity, Turbidity, Conductivity, Dissolved oxygen, Chlorophyll, Dissolved organic matter (CDOM), Sea water temperature, Currents speed and direction, Significant wave height and Wave period.


**Figure 5.**
**Deployment of moored buoy and bottom station in Varna bay**

One of the main challenges faced by these in situ marine systems is the maintenance required to ensure their proper functioning. The Black Sea is known for its intense biofouling, especially during the spring and summer seasons. This phenomenon often renders optical sensors unusable after just a few months of operation (Figure

6). To maintain the systems' functionality, regular cleaning was necessary, which had to be performed every one to three months, depending on seasonal conditions. Optical sensors are particularly sensitive components, and their windows can easily become obstructed or damaged by biofouling if not cleaned regularly.

**Figure 6.**
**Bio-fouling of in situ sensors after three months**

Due to these maintenance issues, we decided to temporarily stop the operation of these systems. We plan to bring them back into service at a later date, after upgrading their components to improve their durability and functionality.

***E. Coastal stations***

Collection of long data series of biogeochemical characteristics of seawater is an important task to provide information for assessing the state of the marine environment. Long-term ecosystem research is an essential component of efforts to better understand ecosystems and the mechanisms by which they provide ecosystem services to humans. One of the main practical tasks before the LTER-BG project is the creation of a suitable research infrastructure that will allow the upgrading of these results to the creation of applied scientific products for specific groups of interested parties, including representatives of central and municipal administrations, businesses and the general public [15]. The mission of the project is to provide relevant scientific information for understanding and predicting ecosystem processes for the needs of society through long-term ecosystem research on the territory and water basins of the country.

To achieve the goals of this project, the Institute of Oceanology at the Bulgarian Academy of Sciences (IO-BAS) has established two coastal stations equipped with state-of-the-art water quality multiparameter instruments. These stations are strategically located in the Varna and Cape Kaliakra regions and continuously measure several key parameters, including seawater temperature, conductivity (salinity), turbidity, dissolved oxygen levels, chlorophyll A fluorescence, and acidity (Figure 7). The data collected from these stations is recorded every 15 minutes and is made available in both tabular and graphical formats on dedicated websites, ensuring accessibility to a wide audience (Figure7).

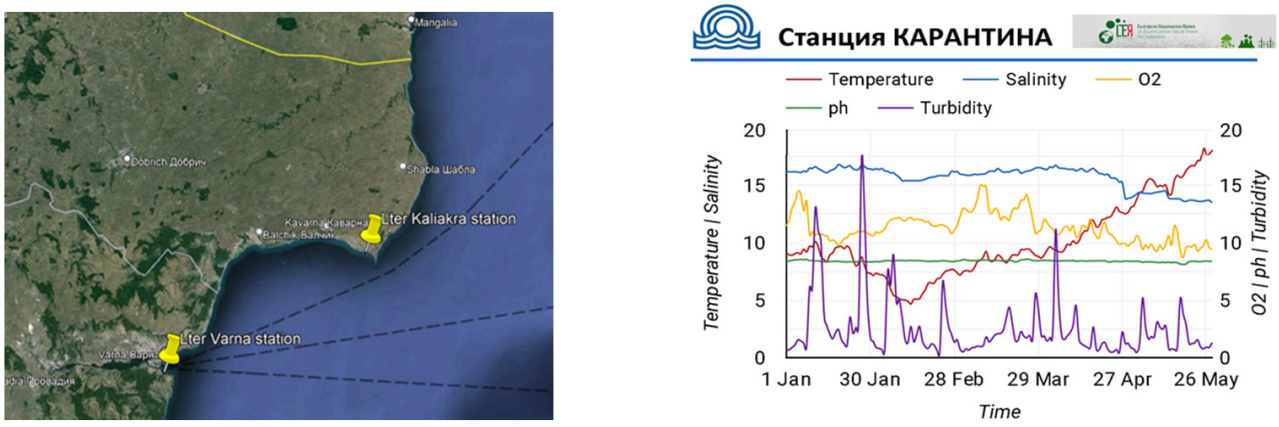


**Figure 7.**
**LTER-BG coastal stations along the Bulgarian Black Sea coast**

A similar coastal station was established in 2022 on the pier of the Shkorpilovtsi research base operated by IO-BAS. This station is equipped with a FerryBox system, developed as part of a collaborative project between IO-BAS and HEREON in Germany (Figure 8). The FerryBox system is designed to continuously collect data on various marine parameters while sailing, providing valuable information on marine conditions and contributing to the overall understanding of the Black Sea ecosystem.

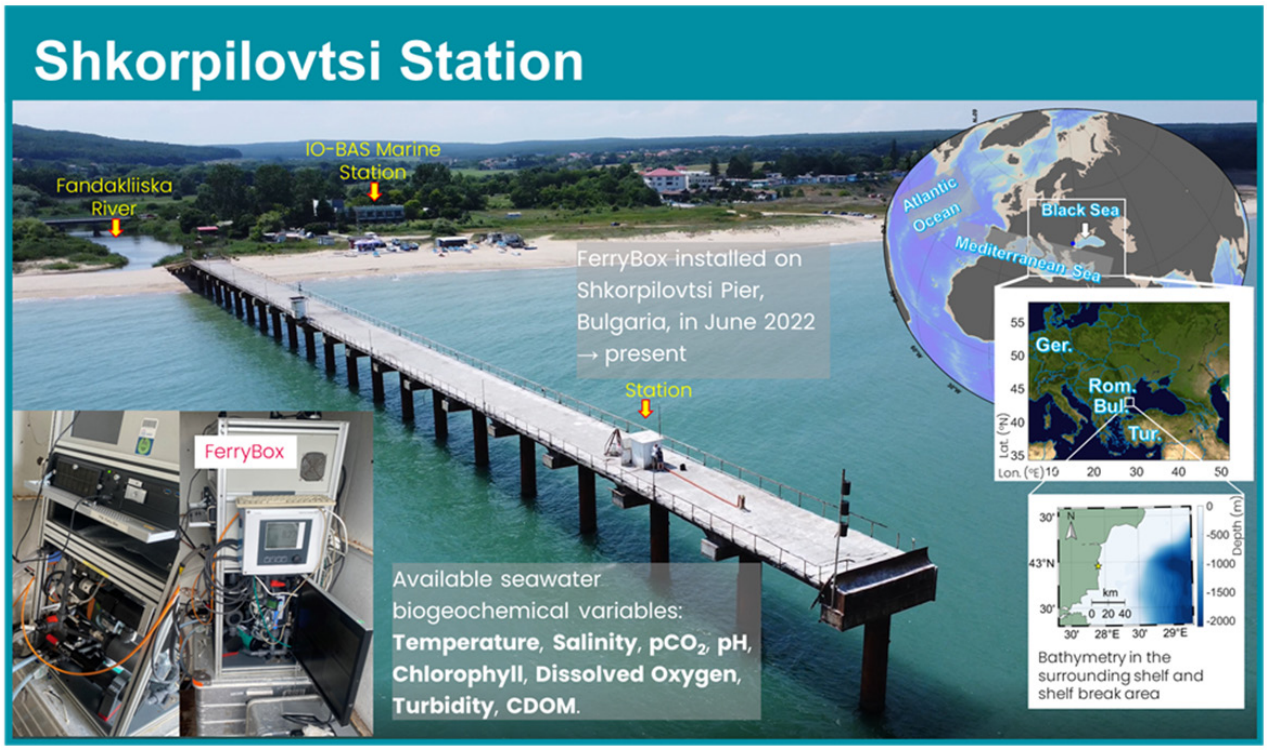


**Figure 8.**
**Shkorpilovtsi coastal station**

## FUTURE DEVELOPMENT

The plans for future developments include:

- New systems, sensors and sites: NOMOS will be continuously developed by including new observing systems, new technologies, modern sensors and extending number of sites;
- Integration - System of Systems: All system will be integrated in common portal;
- Data management and dissemination: New computer technologies for the data management system will be used to serve the integrated systems. New dissemination tool will be developed;
- Products and forecasts: Collected data will be used to generate new products to benefit Blue economy and for forecasts verification.
- European scale integration: Integration of NOMOS in the European Ocean Observing Systems will benefit science and industry and will generate added value.

## CONCLUSIONS

The NOMOS system is a unique source of in-situ data in the Black Sea that provides real time data for science, government and Blue economy. The system is in a continuous process of technological and scope development in an effort to meet the needs of its users from science to government bodies, maritime industry and society.

NOMOS data are freely and openly available in real time through Internet. They are also distributed by Copernicus Marine Environment Monitoring Service (CMEMS) and used for the assimilation in models and quality assessment of forecasts and reanalyzes.

NOMOS will be Bulgarian contribution to European Ocean Observing System (EOOS). BulArgo as a part of NOMOS made Bulgaria among the 34 countries contributing to the world's program Argo.

**ACKNOWLEDGMENTS**

The systems presented in this paper were realized with the support of Bulgarian Academy of Sciences, Infrastructure for Sustainable Development of Marine Research and Participation in the European Infrastructure Euro-Argo - MASRI and LTER-Bulgaria The Bulgarian National Network for Long-Term Ecosystem Research - a projects of the National roadmap for scientific Infrastructure (2020–2027) of Republic of Bulgaria and many EU projects as:, Euro Argo ERIC, H2020 DOORS and BRIDGE, t SEA-ReCap project - Helmholtz Association Program for Advanced Challenges and European Partnership, etc. The authors thank to MASRI project for the support to prepare and present this paper.

**REFERENCES**

[1] D y n a m i c a l processes in coastal regions, Popov. V., Antsyferov, S.M., Belberov, Z.K., Massel, S. (Eds.), Results of the Kamchia International Project, Publ. H. Bul. Acad. Sc., Sofia, 1990, p. 190

[2] Д а н д о л о в, И. В., Димитров, Х. А., Палазов, А. В., Топалов, П. Р. - Автоматизированная информационная система “Камчия”, Автометрия, 1, 1989, с. 114-117.

[3] S l a b a k o v, H., A. Palazov, S. Besiktepe, G. Korotaev, S. Nikolaev, K. Bilashvili, A. Kubryakov, V. Dorofeev, A. Postnov, T. Oguz, G. Kordzakhia, V. Malciu, H. Dahlin, N. Valchev - Recent Advance in the Black Sea Operational Oceanography within the Arena Project, Proceedings of the First Biannual Scientific Conference “Black Sea Ecosystem 2005 and Beyond”, Istanbul, 8-10 May 2006 , pp. 1229-1244.

[4] P a l a z o v, A., N. Valchev - Advance in the Black Sea regional efforts to build and sustain the operational status of oceanographic services, Proceedings of EuroGOOS Conference 2008, Coastal to Global Operational Oceanography: Achievements and Challenges, 20-22 May 2008 Exeter, 2010, pp. 380-387.

[5] P a l a z o v, A., A. Stefanov, V. Marinova, V. Slabakova, Bulgarian National Operational Marine Observing System, OCEANS, 2012 - Yeosu , vol., no., pp.1-9, 21-24 May 2012, doi: 10.1109/OCEANS-Yeosu.2012.6263526.

[6] P a l a z o v, A., A. Stefanov, V. Marinova, V. Slabakova, Operational Marine Observing System to Support Safety Port Navigation, Proceedings of the Tenth International Conference on Marine Sciences and Technologies “Black Sea 2010”, Varna, Bulgaria, 7-9 October, 2010, pp. 308-312.

[7] P a l a z o v, A., H. Slabakov, A. Stefanov , Galata platform weather and seastate observing system, Marine Industry, Ocean Engineering and Coastal Resources - Guedes Soares & Kolev (eds), Taylor & Francis Group, London, 2007, vol. 2, pp 755-760.

[8] S t e f a n o v, A., A. Palazov, H. Slabakov - Data management in offshore real-time monitoring, Marine Industry, Ocean Engineering and Coastal Resources - Guedes Soares & Kolev (eds), Taylor & Francis Group, London, 2007, vol. 2, pp 827-831.

[9] P e n e v a, E., E.Stanev, A. Palazov, G. Korchev, V. Slabakova, M. Milanova, A. Gencheva, BULARGO national research infrastructure: the present state and perspectives for the Argo data in the black sea, Proceedings of the Tenth International Conference on Marine Sciences and Technologies “Black Sea 2010”, Varna, Bulgaria, 7-9 October, 2010, pp. 318-323.

[10] P a l a z o v, A., Ivanov, I., Marinova, V., and Ivanova, V.: Sea wave observing system - initial results, EGU General Assembly 2022, Vienna, Austria, 23–27 May 2022, EGU22-3123, https://doi.org/10.5194/egusphere-egu22-3123, 2022.

[11] P a l a z o v, A., Development of the Bulgarian Sea Level Service, Geophysical Research Abstracts Vol. 15, EGU2013-2377, 2013.

[12] P é r e z G ó m e z, B., Vilibić, I., Šepić, J., Međugorac, I., Ličer, M., Testut, L., Fraboul, C., Marcos, M., Abdellaoui, H., Álvarez Fanjul, E., Barbalić, D., Casas, B., Castaño-Tierno, A., Čupić, S., Drago, A., Fraile, M. A., Galliano, D. A., Gauci, A., Gloginja, B., Martín Guijarro, V., Jeromel, M., Larrad Revuelto, M., Lazar, A., Keskin, I. H., Medvedev, I., Menassri, A., Meslem, M. A., Mihanović, H., Morucci, S., Niculescu, D., Quijano de Benito, J. M., Pascual, J., Palazov, A., Picone, M., Raicich, F., Said, M., Salat, J., Sezen, E., Simav, M., Sylaios, G., Tel, E., Tintoré, J., Zaimi, K., and Zodiatis, G.: Coastal sea level monitoring in the Mediterranean and Black seas, Ocean Sci., 18, 997-1053, https://doi.org/10.5194/os-18-997-2022, 2022.

[13] A t a n a s Palazov, Evgeniy Yakushev, Tanya Milkova, Violeta Slabakova, and Ognyana Hristova, Improved MarineWaters Monitoring, Geophysical Research Abstracts, Vol. 19, EGU2017-10579, 2017, EGU General Assembly 2017

[14] A t a n a s Palazov, Violeta Slabakova and Veselka Marinova. New sources of in-situ marine data to support EC Marine Strategy Framework Directive Implementation in the Black Sea, in Operational Oceanography serving Sustainable Marine Development. Proceedings of the Eight EuroGOOS International Conference. 3-5 October 2017, Bergen, Norway. E. Buch, V. Fernández, D. Eparkhina, P. Gorringe and G. Nolan (Eds.), EuroGOOS. Brussels, Belgium. 2018. D / 2018 / 14.040 / 1, ISBN 978-2-9601883-3-2. 516 pp. 89-96.

[15] http://project.lter-bulgaria.net/.

[16] Petersen, W.: FerryBox systems: State-of-the-art in Europe and future development, Journal of Marine Systems, 140, Part A, 4-12, 2014.

# BUILDING A FREE BEACH THROUGH WAVE MANAGEMENT IN THE COASTAL AREA OF THE SOUTHERN BAY IN FRONT OF THE CITY OF NESSEBAR

**Lyubomir DIMITROV*, Gencho GEORGIEV***

**Abstract.** *The disadvantage of the free beach is the lack of methodology for sufficiently accurate assessment of the consumption of sediments from the coastal zone. However, the factors influencing these processes and their main dependencies are already known, which in a relatively short period of time cause major changes in the outline of the coastline and the relief of the seabed. Based on this, the main essence of the proposed method is to solve the opposite problem: artificial creation of conditions for dynamic resilience through intervention formation of the main factors influencing the equilibrium profile of the underwater coastal slope and sediment balance management in the desired direction. The report examines a specific section of our Black Sea coast. An example is given for construction of a free beach by means of disturbance management in the coastal zone of the Southern Bay in front of the city of Nessebar.*
**Keywords:** *free beach; artificial beach; sea beach.*

Mastering the energy of the sea and being able to manage it in the direction we want is the unfulfilled dream of all oceanologists. We will present a step towards solving this task in this report.

The task is simplified by finding a specific site with suitable exposure, bathymetry and coastal zone geology. This site is the South Bay in Nessebar (Figure 1).


**Figure 1.**
**South bay of Nessebar**

The surface geology at the bottom of the site is characterized by sands of varying grain size.

This allows the deepening of the bottom in front of the object to reduce the coefficient of transformation of the excitation in front of the object of the study. The grain size composition of the sand where the bottom will be deepened in front of the site is analogous to the composition of the beach on the southern bay of the town of Nessebar.

*** Institute of Ocanology - Bulgarian Academy of Sciences, Bulgaria**
**E-mail: geos@io-bas.bg; g.georgiev@io-bas.bg**

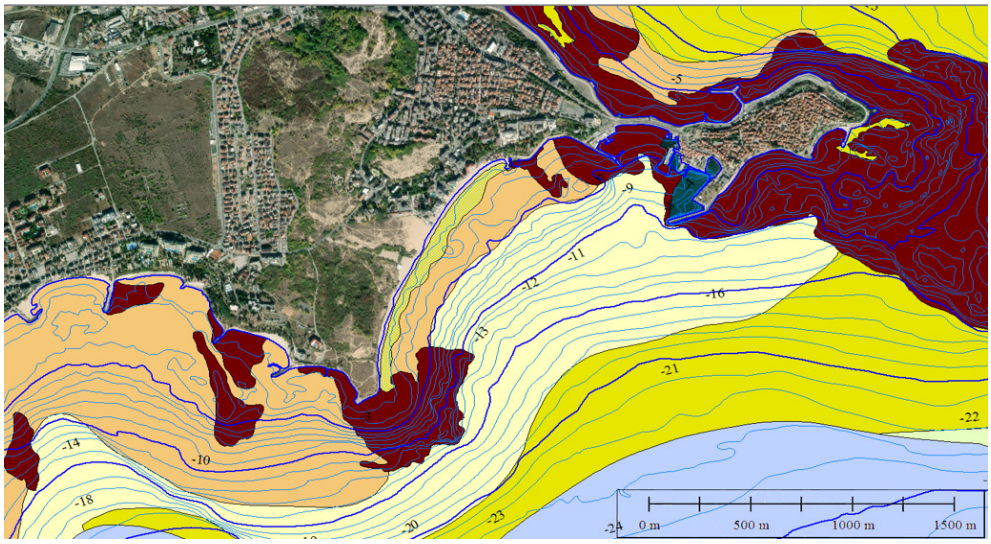


**Figure 2.**
**Bathymetry and Surface Geology**

**We can have a significant effect on the mastery of wave energy and its purposeful use by building in front of the engineering facilities or the coast of artificial bottom sand relief forms and facilities that manage the transformation of the wave and the movement of sediments in the coastal zone.**

With the construction of sand relief forms and facilities on the seabed, successive zones of divergence and convergence of wave propagation will be created, which will lead to the quenching of wave energy and its targeted use for the growth and multi-year maintenance of existing or created with suitable grain size composition , roughness and slope free beaches [1].

The simplest solution to the posed question is the increase of the depth along the bottom of the section to $H_2$ ($H_2 > H_1$) in the limits of a rhombus with side length a and vertices located at both ends of the section along the wave propagation. In Figure 3 the bottom deepening area is shaded. The length of the rhombus in the direction of wave propagation is equal to L = 2.a.sinα (where α is the angle between the limit of depth variation and the perpendicular to the axis of the rhombus, and the total area of the deepening of the bottom is:

(1) $$S= \mathbf{a}.(2.\cos \boldsymbol{\alpha} \,.\, \sin \boldsymbol{\alpha})$$

where a is the length of the side of the rhombus.

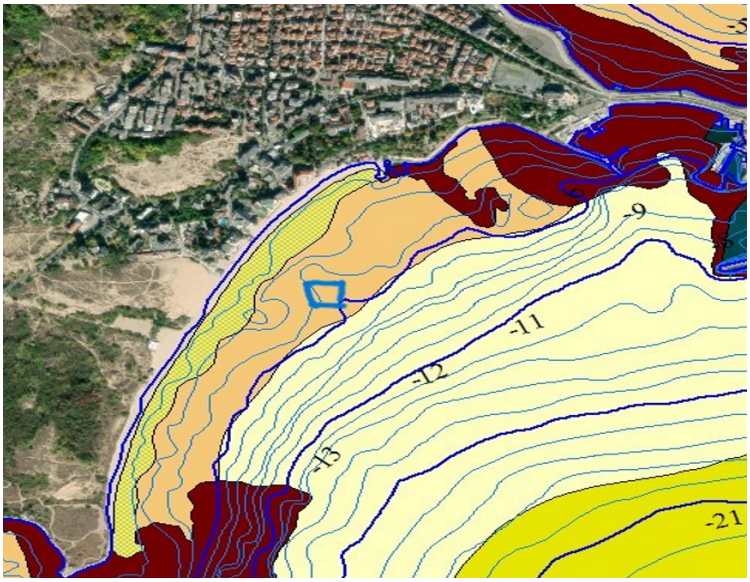


**Figure 3.**
**Figural deepening of the bottom**

With such deepening of the bottom, wave rays initially parallel to the axis of the rhombus will deviate from this direction twice, and in different directions. This will happen once when crossing the boundary from depth $H_0$ to $H_2$ and a second time when crossing the boundary from $H_2$ to $H_0$. Ultimately, the output distance between the wave rays lo in the region of the second refraction of the wave rays will acquire a value $l_1 > lo$ , and at a distance R from the top of the rhombus the distance between the refracted wave rays will be $l_2 > l_1$. Using the law of conservation of the flow of wave energy between wave beams, it will be obtained that the coefficient of reduction of the wave height $Kr_2$ at a distance R from the beginning of the bottom deepening region (R = 250 m) will be:

**(2)**
$$\mathbf{Kr_2} = \sqrt{\frac{lo}{l2}}$$

where according to [1] when solving a simple trigonometric problem we get:

**(3)**
$$l_2 = 2.(2a - l_0.\ tg\propto - \frac{2a.ctg\alpha - lo}{tg\Delta 1\alpha + ctg\alpha}).\frac{[\sqrt{a^2.(1-sin\propto}) - lo/2]}{\sqrt{\left(a - \frac{lo}{2cos\propto}\right)^2 - [\sqrt{a^2.(1-sin\propto}) - lo/2]^2}} + 2.\{R - \sqrt{a^2 + sin\alpha} - \sqrt{\left(a - \frac{lo}{2cos\propto}\right)^2 - [\sqrt{a^2.(1-sin\propto}) - lo/2]^2} + (2a - l_0.\ tg\propto - \frac{2a.ctg\alpha - lo}{tg\Delta 1\alpha + ctg\alpha})\}.tg(\Delta\alpha_1 + \Delta\alpha_2)$$

We enter the following parameter values from the equation, where λ is the wavelength and $\Delta_{1\alpha}$ and $\Delta_{2\alpha}$ are the refraction angles at the first and second deviation of the wave rays, respectively, which we determine graphically using the nomogram for building the refraction plan and determining the angles of wave beam deflection (according to G. G. Kuzminskoi). [3]

For the construction of the wave beams, it is convenient to use the formula [2]:

**(4)**
$$\Delta_{i+1}\alpha = \arcsin\{[\ (1+ 0{,}032\ \lambda_0\ /d_{i+1})\ /\ (1+ 0{,}032\ \lambda_0\ /d_i)].\ sin\Delta_i\alpha\}$$

where

$\Delta_{i+1\alpha}$ - refraction angle; $\Delta_{i\alpha}$ - angle of incidence; $d_{i,\ i+1}$ - water depth.

We substitute in equation 3 all the parameters with the set and determined values (Figure 4.) and get the result $l_2$ = 53.08 m. It follows from this that for the coefficient of reduction of the wave height at a distance R = 250 m from the beginning of the deepening to the depth of the first collapse of the wave in a calm sea, we will get the following value:

**(5)**
$$\mathbf{Kr_2} = \sqrt{\frac{lo}{l2}} = \sqrt{\frac{40}{53{,}08}} = \mathbf{0{,}868}$$

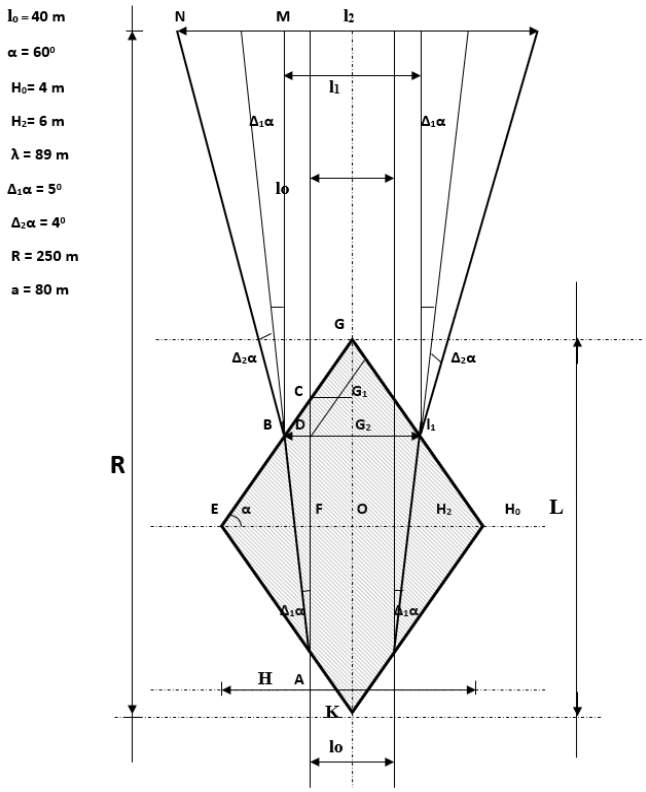


**Figure 4.**

**A very important condition in solving the problem is the washing of the excavated sand masses directly on the shore in front of the section and obtaining a ready-made free beach with a grain-metric composition similar to the underwater coastal slope of the section.**

In the considered case, the volume of washed sand masses will be about 5,000 $m^3$.

Sizing the effect of wave energy attenuation will be complicated when the natural depth is not constant but varies within the development section. Within a first approximation, we can safely assume that the results of the proposed sizing will be significant in this case as well, when the depths of the excavated bottom of the section follow the natural slope of the bottom.

## CONCLUSION

What has been stated so far determines the need to deepen the knowledge of the regional hydrological and lithological processes along the shores of the Black Sea. The scientific research included in the project is oriented towards issues of international importance and for this reason is characterized by high international visibility.

These studies have their place insofar as they pursue important societal challenges such as the growth of the country's territory and the provision of extensive beaches for the development of tourism, which will increase the significance of the achieved scientific results.

The implementation of the proposed project will create specific mechanisms for the rapid commissioning and conduct of scientific research in response to urgent specific needs and problems of national or regional importance.

## REFERENCES

[1] G e o r g i e w, G., Natural Method For Management Of Wave Transformation And Construction Of Free Beaches; Sixteenth International Conference on Marine Sciences and Technologies, Oktober 2022.

[2] С м и р н о в а, Т. Г., Правдивец, Ю. П., Смирнов, Г. Н. Берегозащитные сооружения. Издательство Ассоциации строительных вузов. Москва 2002.

[3] СНиП 2.06.04-82 Нагрузки и воздействия на гидротехнические сооружения (волновие, ледовие и от судов) Гостстрой - М; Стройиздат, 1983.

# OXIDATIVE STRESS ECOLOGY OF THE PACIFIC OYSTER (*Crassostrea gigas* Thunberg, 1793) INVASION IN THE BULGARIAN BLACK SEA

**Georgi PETROV*, Albena ALEXANDROVA*, Nesho CHIPEV*, Plamen MITOV**, Lyubomir KENDEROV**, Elina TSVETANOVA*, Almira GEORGIEVA*, Madlena ANDREEVA* and Georgi PRAMATAROV***

**Abstract.** *Recently, Pacific oysters (Magallana gigas Thunberg, 1793) were found to invade the natural habitats of the Bulgarian Black Sea coast. The present study aims to evaluate the oxidative stress ecology of the Pacific oyster invasion. Oxidative stress (OS) in organisms is a general reaction towards the environmental multi-stressor effect and results from the imbalance of pro-oxidative and antioxidative processes. Oysters were gathered from four sites (Kavarna, Varna Lake, Burgas, Sozopol Bay) manually by SCUBA diving and from farm owners. A set of OS indicators were measured spectrophotometrically, using commercially available kits. The obtained results indicated that oysters from the more polluted localities had higher OS that however was effectively compensated by their antioxidant system. This strongly indicates that the Pacific oysters are already acclimated to the special conditions of the Black Sea and their continued distribution could be expected. Further studies and monitoring of the spread of Pacific oysters along the Bulgarian Black Sea coast are urgently needed together with possible prevention actions.*

**Keywords:** *adaptability, Bulgarian Black Sea, oxidative stress, Pacific oyster.*

## INTRODUCTION

The Pacific oyster (*Magallana gigas* Thunberg, 1793), is native to the coastlines of the Sea of Japan [1]. This oyster species has been widely introduced elsewhere for aquaculture purposes. Oysters are highly nutritious shellfish that offer a wide array of health benefits. They are a valuable source of high-quality protein, omega-2 fatty acids, vitamins, minerals, and antioxidants and at the same time they are naturally low in carbohydrates, total and saturated fat [2]. The European Union classifies the Pacific oyster as a useful resource for the aquaculture industry (Council Regulation (EC) No 708/2007, 2022). Apart from its high rate of exploitation and production in aquaculture in many countries, it has been widely spread also unintentionally via ships. At present M. gigas is further expanding its distribution in European coastal waters across the former ranges of native oyster taxa, whose habitats have suffered extermination for various reasons [3], leading to its near-global distribution [4]. The Pacific oyster is considered an invasive species and this sets the question if it is harmful to the local biodiversity and ecosystems and to what extent.

Between 1980 and 1991, *M. gigas* was also extensively introduced to the Black Sea from its native range, with active acclimatization efforts continuing from 1989 to 2016, primarily to assess its potential for mariculture. These efforts took place along various coastal areas, including Romania (near Constanta) and the Ukrainian, Crimean, and Caucasian coastlines [5,6]. Skifian Oyster, the first modern oyster farm along the Black Sea coast appeared in 2014 in Ukraine. The first and only Bulgarian producer of oysters (Kranea oysters est. 2017) is a farm situated 23 km north of the city of Varna, supposed to be located in an ideal biotope for growing the Pacific oyster.

Since 1989 individual feral specimens of the Pacific oyster have been also found in natural Black Sea habitats, outside of farms and areas where they were initially introduced [5-11]. In the past decade, reports of not just isolated feral individuals but also wild micropopulations of *M. gigas* in the Black Sea have increased. Such wild populations have been observed along the Ukrainian coast [11], the Romanian coast [12], the Crimean coast (2015), and the Caucasian coast (2018) [6]. The species has also become increasingly common along the

*** Institute of Neurobiology - Bulgarian Academy of Sciences**

**** Faculty of Biology at Sofia University "St. Kliment Ohridski"**

Bulgarian Black Sea coast, with the first observations recorded in 2010 at Sts. Constantine and Helena Resort, followed by additional observations in 2015 near Burgas [9]. The successful acclimatization of the Pacific oyster in the Black Sea has led some researchers, such as Mitov [9], to consider *M. gigas* as a permanent allochthonous species in the Black Sea fauna.

Oxidative stress (OS) has been recognized as a valuable tool for the assessment of the effect of environmental stressogenicity and adaptation of organisms [13-15]. A common effect of environmental stressors on marine organisms is the induced OS, which corresponds to an imbalance between pro-oxidative processes and antioxidant defense mechanisms in the cells, with levels depending also on organisms' sensitivity (i.e. sensitive, tolerant, or resistant organisms) which is at the basis of stress ecology [16]. This imbalance can lead to cellular and tissue damage. In the marine environment many stressors, such as pollutants (incl. heavy metals, polycyclic aromatic hydrocarbon, microplastics, etc.), temperature changes, UV radiation, etc., can induce OS in organisms [17]. Oxidative stress biomarkers (such as lipid peroxidation, protein oxidation, and antioxidant enzyme activity) are commonly measured to evaluate the biological impacts of environmental pollutants and stressors. These biomarkers serve as indicators of the organism's stress response and its potential to experience cellular damage, making OS a reliable tool for environmental monitoring and ecotoxicology studies.

Given the above, the present study aimed to evaluate the oxidative stress ecology and adaptability of the Pacific oyster invasion of the Bulgarian Black Sea coast through the oxidative stress response.

## MATERIALS AND METHODS

### Sampling

Specimens of *M. gigas* were collected from four locations along the Bulgarian Black Sea coast (Figure 1). Oysters from Burgas (Foros Bay, Port of Burgas Shipyard, Ship-Repair Factory) and Sozopol Bay (Chernomorez coast) were manually gathered by SCUBA diving from their natural attachment sites. Specimens from the oyster farm in the aquatory of Kranevo and experimentally laid down from Varna Lake were obtained from farm owners. All specimens were transported on dry ice to the laboratory, where they were stored at -80°C until biochemical analyses were conducted.

### Oxidative stress analyses

After thawing, each oyster's length, width, and thickness were measured. The soft tissues were then separated from the shells and homogenized using a Potter Elvehjem homogenizer with a Teflon pestle (Thomas Scientific, USA). The resulting homogenate was centrifuged at 3,000 rpm for 10 minutes to obtain the post-nuclear fraction, in which lipid peroxidation, protein oxidation, and glutathione levels were measured. This fraction was subsequently centrifuged at 20,000 rpm for 20 minutes to isolate the post-mitochondrial fraction, where antioxidant enzyme activities were assessed. All procedures were carried out at 4°C. All tested OS biomarkers were measured spectrophotometrically using commercially available kits: Lipid Peroxidation (MDA) Assay Kit MAK085, Protein Carbonyl Content Assay Kit MAK094, Glutathione Assay Kit CS0260, Catalase Assay Kit CAT100, Glutathione Reductase Assay Kit GRSA, Glutathione Peroxidase Cellular Activity Assay CGP1, Glutathione-S-Transferase Assay Kit, CS0410, purchased from Sigma-Aldrich Co. LLC, USA. The protein concentrations were measured according to the method of Lowry et al. [18] using bovine serum albumin to generate the standard curve.

### Statistical analyses

All measurements were performed in triplicate and their average was taken as the response variable. The calculations and statistical analyses of data were carried out using the STATISTICA 10 package (Stat Soft Inc., USA). Differences were considered significant at $p < 0.05$ in the statistical tests.

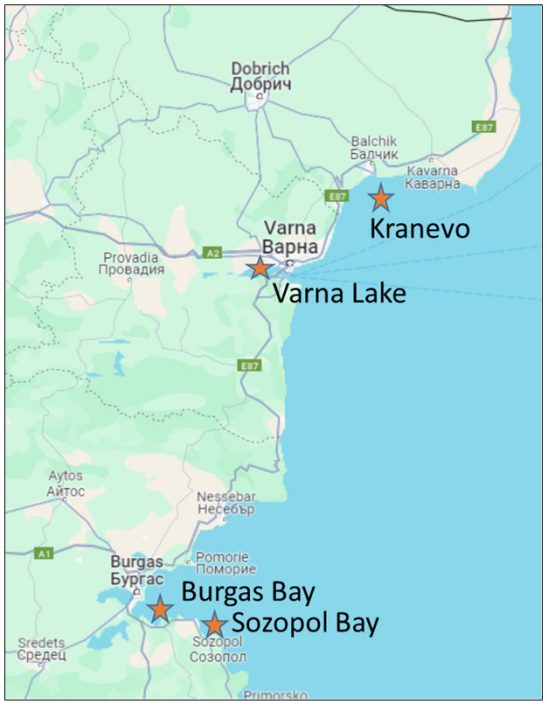


Locality № 1. **Kranevo**, 10 specimens (L: 3.60-6.82 cm, H: 3.31-6.74 cm, W: 1.93-3.26 cm).

Locality № 2. **Varna Lake** (Tortuga marina), 10 specimens (L: 6.26-9.06 cm, H: 7.05-7.27 cm, W: 2.93-3.18 cm); hard bottom: shell sand with fine mud and stones; 1.8 m depth.

Locality № 3. **Burgas** (Foros Bay, Port of Burgas Shipyard, Ship-Repair Factory), 9 specimens (L: 3.86-5.6 cm, H: 2.42-5.65 cm, W: 1.27-2.37 cm); attached to wave-dissipating tetrapods, above and at the water level.

Locality № 4. **Sozopol Bay** (sites at Chernomorez coast), 14 specimens (L: 6.96-10.04 cm, H: 5.68-8.30 cm, W: 1.77-4.08 cm); attached to the rocks.

**Figure 1.**
**Sites of collected *M. gigas* specimens with biometrical characteristics, and substrate type**

**RESULTS**

The measured OS biomarkers (Mean±SD) in *M. gigas* specimens from the studied sites are presented in Figure 2.

The *M. gigas* individuals from Kranevo and those from the Sozopol Bay, showed average values of the measured OS indicators. This suggested low OS levels, i.e. good adaptability of these oysters to the local environment, which is a prerequisite for their good development and survival.

The oysters from Lake Varna showed higher values of lipid peroxidation (LPO), protein oxidation (PO), glutathione concentration (GSH), and glutathione-S-transferase (GST) activities compared to the individuals from the other investigated locations. The measured higher values of LPO and PO here indicated increased OS levels. Possibly as a protective response, the oysters reacted with increased levels of the non-enzymatic antioxidant GSH. The high activity of GST suggested activation of the xenobiotic neutralization system, associated with the known serious pollution of Lake Varna.

Among studied oysters, the specimens from Burgas exhibited the highest activities of superoxide dismutase (SOD), catalase (CAT), glutathione peroxidase (GPx), and glutathione reductase (GR) along with low levels of LPO, PO and GSH concentration. These results suggested higher environment stressogenicity, which activated the enzymatic antioxidant system and thus led to OS suppression.

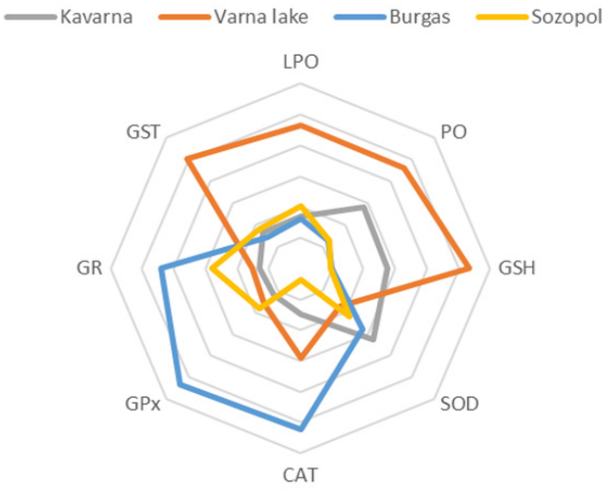


| Locality | LPO | PO | GSH | SOD | CAT | GPx | GR | GST |
|---|---|---|---|---|---|---|---|---|
| | nM MDA/ mg protein | nM PC/ mg protein | ng/mg protein | U/mg protein | U/mg protein | U/mg protein | U/mg protein | U/mg protein |
| Kranevo | 3.28 | 11.59 | 329.64 | 7.77 | 3.74 | 8.78 | 10.93 | 15.71 |
| | ±0.57 | ±1.91 | ±10.72 | ±2.60 | ±2.91 | ±3.24 | ±1.79 | ±2.57 |
| Varna Lake | 9.05* | 18.83* | 641.16* | 4.20 | 7.42 | 12.06 | 12.84 | 47.74* |
| | ±0.76 | ±4.66 | ±140.7 | ±1.55 | ±4.38 | ±2.67 | ±5.05 | ±3.98 |
| Burgas | 3.11 | 5.17 | 117.60 | 13.34* | 13.34* | 39.72* | 37.11* | 13.47 |
| | ±0.28 | ±1.14 | ±46.91 | ±3.61 | ±0.39 | ±3.98 | ±8.21 | ±1.13 |
| Sozopol Bay | 3.97 | 5.25 | 117.12 | 5.30 | 1.95 | 13.74 | 23.41 | 17.37 |
| | ±2.08 | ±1.66 | ±29.61 | ±2.23 | ±0.17 | ±5.58 | ±6.41 | ±5.75 |

**Figure 2.**
**Oxidative stress biomarkers (Mean±SD) in *M. gigas* specimens from the studied sites (* - statistical significance p<0.05)**

## DISCUSSION

For the first time in this study, the adaptability of the Pacific oysters from different localities of the Bulgarian Black Sea coast was assessed. Particularly, the stress ecology of *M. gigas* from four habitats was characterized and their adaptability was assessed by the induced OS in cells, which indicates to what extent the organisms are sensitive, tolerant, or resistant to stress [16]. Different levels of OS stress were present in *M. gigas* individuals from the studied sites with different local environmental conditions. Specifically, the marine environment of Kranevo and Sozopol Bay seemed to induce little OS in the *M. gigas* individuals. On the other hand, the Pacific oysters from Burgas and especially from Varna Lake (which are known as more polluted regions) showed the presence of much higher OS which however seemed to be effectively compensated by the antioxidant cell system of the oysters. Recent measurements showed that the surface sediments of Varna Lake, which are a source of nutrients, are contaminated with heavy metals (Hg, As, Fe, Cu, Pb) and petroleum products [19]. Oysters are susceptible to both waterborne and sediment-bound contaminants due to their filter-feeding and sessile nature [20]. Environmental pollution, particularly from heavy metals, organic contaminants, and microplastics, can significantly increase OS levels in oysters. Similar to our results, oyster species exposed to a contaminated environment with metals, polycyclic aromatic hydrocarbons (PAHs), and pesticides showed elevated LPO levels and increased antioxidant enzyme activities [21-23]. These findings strongly suggested the high adaptability of *M. gigas* to the different local ecological conditions of the Bulgarian Black Sea habitats. Hence, the acclimatization of the Pacific oyster in the Bulgarian Black Sea seems to be at an advanced stage which is in agreement with other

views [9,11,24] defining *M. gigas* as a permanent allochthonous species for the Black Sea fauna. However, the question arises to what extent is the invasion of *M. gigas* potentially harmful to the Bulgarian Black Sea's local biodiversity and ecosystems. In fact, the negative effects of *M. gigas* invasions is a controversial subject and it is under debate both among scientific experts and also in the mainstream popular press [25-28]. Practically, in Bulgaria there are so far no such studies.

## CONCLUSIONS

The present research was the first to analyze the adaptability of *M. gigas* to the specific environmental conditions of the Bulgarian Black Sea littoral. The results obtained confirmed that *M. gigas* displayed a high adaptive capacity and can effectively compensate the OS caused by multiple stressors of the marine environment. In conclusion, the acclimatization of the Pacific oyster in the Bulgarian Black Sea seems to be at an advanced stage. In Bulgaria, detailed research on the dispersal and adaptation of *M. gigas* to the ecological conditions of the Black Sea coast is still lacking, and specific monitoring is not carried out either. This set limits to the evaluation of the long-term effects of this alien species on the local biodiversity and ecosystem of the Bulgarian Black Sea, and especially the need for control measures. Further detailed research on the possible effects of the spread of *M. gigas* along the Black Sea coast of Bulgarian is urgently needed.

## ACKNOWLEDGMENTS

This study was supported by Grant КП-06-Н61/11 of the Bulgarian National Science Fund.

## REFERENCES

[1] L a u g e n, A., Hollander, J., Obst, M., Strand, Å. The Pacific Oyster (*Crassostrea gigas*) invasion in Scandinavian coastal waters in a changing climate: impact on local ecosystem services. In: Clode JC (ed), *Biological Invasions in Changing Ecosystems - Vectors, Ecological Impacts, Management and Predictions*. De Gruyter Open, 2015, 230-252.

[2] W r i g h t, A. C., Fan, Y., Baker, G. L. Nutritional value and food safety of bivalve molluscan shellfish. Journal of Shellfish Research, 37(4), 2018, 695-708.

[3] M c A f e e, D., Connell, S. D. The global fall and rise of oyster reefs. Front Ecol Environ., 19(2) 2021, 118-125.

[4] M o r t e n s e n, S., Bodvin, T., Strand, Å., Holm, M. W., Dolmer, P. Effects of a bio-invasion of the Pacific oyster, *Crassostrea gigas* (Thunberg, 1793) in five shallow water habitats in Scandinavia. Management of Biological Invasions, 8(4), 2018, 543-552. https://doi.org/10.3391/mbi.2017.8.4.09.

[5] P o p o v, M. A., Schurov, S. V. Findings of spat of bivalve mollusc *Crassostrea gigas* (Thunberg, 1793) in Donuzlav Lake and Artillery Bay (Crimea, the Black Sea). Marine Biological Journal, 4(4), 2019, 97- 99. doi: 10.21072/mbj.2019.04.4.10

[6] P e r e l a d o v, M. V. Pacific oyster (Crassostrea gigas) in the Black Sea. Modern natural settlements and prospects for further expansion. VIII International Conference «Marine Research and Education» Moscow, 28-31 October 2019, Conference Proceedings, Volume II (III), 2020, 343-347. Tver: OOO «PoliPRESS», 2020, 518.

[7] M i c u, D. Annotated checklist of the marine Mollusca from the Romanian Black Sea. International Workshop on the Black Sea Benthos. 18-23 April 2004. Istanbul. Turkey. 2004, 89-152.

[8] S k o l k a, M., Gomoiu, M. T. Specii invazive în Marea Neagră. Impactul ecologic al pătrunderii de noi specii în ecosistemele acvatice. Ovidius University Press Constanț. 2004, 180.

[9] M i t o v, P., Uzunova, S., Kenderov, L., Dimov, S., Yanachkov, P. Pacific oyster invasion along Bulgarian black sea coast. Kliment's Days 2020, Faculty of Biology, file:///C:/Users/Admin/Downloads/%D0%95&SD-15%20(3).pdf.

[10] P e r e l a d o v, M. V. The current state of the population of the Black Sea oyster. Trudy VNIRO, 144. Coastal hydrobiological research, 2005, 254-274.

[11] K o v t u n, O. A., Zolotarev, V. N. The first find of the oyster Crassostrea gigas (Bivalvia, Ostreidae) in Odessa Bay (the Black Sea). Vestnik Zoologii 42, 2008, 262.

[12] K r a p a l, A-M., Ioniţă, M., Caplan, M., Buhaciuc-Ioniţă, E. Wild Pacific oyster Magallana gigas (Thunberg, 1793) populations in Romanian Black Sea waters - friend or foe? Travaux du Muséum National d'Histoire Naturelle "Grigore Antipa" 62(2), 2019, 175-183. https://doi.org/10.3897/travaux.62.e49074.
[13] L i v i n g s t o n e, D. R. Contaminant-induced oxidative stress in marine organisms. Marine Pollution Bulletin, 42(8), 2001, 656-666.
[14] L u s h c h a k, V. I. Environmentally induced oxidative stress in aquatic animals. Aquatic Toxicology, 101 (1), 2011, 13-30.
[15] R i b e i r o, R., Silva, A. Oxidative stress as an indicator of environmental stress in marine organisms. Ecotoxicology, 24, 2015, 919-933.
[16] S t e i n b e r g, C. E. W. Stress Ecology: Environmental Stress as Ecological Driving Force and Key Player in Evolution; Springer: London, UK; 2012, ISBN 978-94-007-2071-8.
[17] G a u t h i e r, J. M., Moffatt, P. The role of oxidative stress in the toxicity of environmental pollutants. Toxicology Reports, 8, 2021, 482-490.
[18] L o w r y, O. H., Rosebrough, N. J., Farr, A. L., Randall, R. J. Protein measurement with the Folin phenol reagent. Journal of Biology and Chemistry, 193(1), 1951, 265-275.
[19] G a n c h e v, T., Markova, V., Valcheva-Georgieva, I., Dobrev, I. Pollution of Varna Lake and possibilities of using the pollutants as resources. E3S Web Conf. Volume 404, 2023, International Conference on Electronics, Engineering Physics and Earth Science (EEPES 2023), 03002
[20] G a n, N., Martin, L., Xu, W. Impact of Polycyclic Aromatic Hydrocarbon Accumulation on Oyster Health. Frontiers in physiology, 12, 2021, 734463.
[21] F e r r e i r a, C. P., Lima, D., Paiva, R., Vilke, J. M., Mattos, J. J., Almeida, E. A., Grott, S. C., Alves, T. C., Corrêa, J. N., Jorge, M. B., Uczay, M., Vogel, C. I. G., Gomes, C. H. A. M., Bainy, A. C. D., Lüchmann, K. H. Metal bioaccumulation, oxidative stress and antioxidant responses in oysters *Crassostrea gasar* transplanted to an estuary in southern Brazil. Science of the Total Environment, 685, 2019, 332-344.
[22] S a r k a r, A., Bhagat, J., Sarker, M. S., Gaitonde, D. C. S., Sarker, S. Evaluation of the impact of bioaccumulation of PAH from the marine environment on DNA integrity and oxidative stress in marine rock oyster (*Saccostrea cucullata*) along the Arabian sea coast. Ecotoxicology 26, 2017, 1105-1116.
[23] C a p p a r e l l i, M. V., Ponce-Vélez, G., Dzul-Caamal, R., Rodriguez-Cab, E. M., Cabrera, M., Lucas-Solis, O., Moulatlet, G. M. Multi-level responses of oysters *Crassostrea virginica* for assessing organochlorine pesticides in a Ramsar coastal lagoon in southern Mexico, Chemosphere, 320, 2023,138064.
[24] H a n s e n, B. W., Dolmer, P., Vismann, B. Too late for regulatory management on Pacific oysters in European coastal waters? Journal of Sea Research, 191, 2023, 102331.
[25] H o l l a n d e r, J., Blomfeldt, J., Carlsson, P., Strand, Å. Effects of the alien Pacific oyster (*Crassostrea gigas*) on subtidal macrozoobenthos communities. Mar Biol., 162, 2015, 547-555.
[26] H o l m, M. W., Davids, J. K., Dolmer, P., Holmes, E., Nielsen, T. T., Vismann, B., Hansen, B. W. Coexistence of Pacific oyster Crassostrea gigas (Thunberg, 1793) and blue mussels Mytilus edulis Linnaeus, 1758 on a sheltered intertidal bivalve bed? Aquatic Invasions, 11(2), 2016, 155-165.
[27] B o n g a r t s L e b b e, T., Rey-Valette, H., Chaumillon, É., Camus, G., Almar, R., Cazenave, A., Claudet, J., Rocle, N., Meur-Férec, C., Viard, F., Mercier, D., Dupuy, C., Ménard, F., Rossel, B. A., Mullineaux, L., Sicre, M-A., Zivian, A., Gaill, F., Euzen, A. Designing coastal adaptation strategies to tackle sea level rise. Front. Mar. Sci. 8, 2021, 740602.
[28] Z w e r s c h k e, N., Eagling, L., Roberts, D., O'Connor, N. Can an invasive species compensate for the loss of a declining native species? Functional similarity of native and introduced oysters, Marine Environmental Research, 153, 2020, 104793.

# WAVE MONITORING ALONG THE BULGARIAN BLACK SEA COAST

**Veselka MARINOVA*, Violeta SLABAKOVA*, Atanas PALAZOV***

**Abstract.** T*he Bulgarian Coastal Wave System (WAVE), established in 2020 as part of the National Operational Marine Observing System (NOMOS), monitors wave conditions along the Bulgarian Black Sea coast. The system developed in collaboration between the Institute of Oceanology at the Bulgarian Academy of Sciences (IO-BAS) and the National Institute of Meteorology and Hydrology (NIMH) uses GPS buoys to collect real-time data on wave height, period, and direction. This information supports maritime safety, coastal management, and scientific research, including climate change analysis. By providing timely wave data, the WAVE enhances decision-making across sectors like fisheries, shipping, ports operations and tourism.*
**Keywords:** *data buoys, coastal management, directional wave measurement, physical oceanography, Black Sea.*

## INTRODUCTION

Wave monitoring along the Bulgarian Black Sea coast began in 2020 with the establishment of a national buoy system, marking a significant advancement in marine observation. This system, part of the Bulgarian National Operational Marine Observing System (NOMOS) [5-7], was developed through a collaboration between the Institute of Oceanology at the Bulgarian Academy of Sciences (IO-BAS) and the National Institute of Meteorology and Hydrology (NIMH). Its primary aim is to provide real-time data on wave conditions, which are essential for maritime safety, coastal management, and long-term climate analysis.

The system uses advanced GPS buoys to collect critical wave parameters, including wave height, period, and direction. These measurements are crucial for forecasting and managing extreme weather events, as well as for supporting various sectors such as fisheries, shipping, and tourism. In addition, the data collected by the buoys contribute to the study of coastal dynamics and the effects of climate change on the Black Sea environment.

By providing timely and accurate information, the buoy system plays a vital role in improving decision-making processes for both scientific research and practical applications, enhancing the resilience of coastal communities, and promoting sustainable management of marine resources.

## WAVE BUOY INSTRUMENTS

Two types of directional GPS wave buoys have been used in the system: Sofar Ocean Spotter and Zunibal Antea (Tables 1). Both instruments are small-format buoys that measure the wave field by recording their horizontal and vertical movement using a satellite positioning receiver, rather than by measuring buoy motion and orientation physically using onboard mechanical instruments, such as accelerometers, gyros and compass. One of the most beneficial advantage, is that the GPS do not need any kind of calibration, due to its work with and absolute reference frame obtained by the satellites. The data obtained from the systems related to all wave parameters (i. e., wave heave, period and direction), both statistical and spectral data, every 30 minutes and include the possibility of having wave-by-wave information in real time. Key differences between the Spotter and Antea buoys include the shape, fabrication materials and weight of their hulls, power systems, data storage and transmission, satellite positioning systems, and the frequency at which they record their displacement.

The Spotter buoy has a pentagonal upper/spherical lower plastic hull of 0.42 m diameter and weighs 7.6 kg as deployed with ballast chain (Figure 1 a). Operating on a solar-battery power system with five 2W solar panels the Spotter buoy can be deployed indefinitely, although biofouling limits deployment duration in practice. The satellite receiver measures displacement using the Doppler shift and position data and records its displacement at 2.5 Hz, resulting in 4500 records per half-hour sampling period. The data are stored on an SD data card. Spotter

*** Institute of Oceanology, Bulgarian Academy of Sciences (IO-BAS)**

buoy Versions 1 and 2 are featured with Iridium satellite telemetry of half-hourly onboard-computed wave spectra (coefficients) or a limited set of bulk waves parameters (describing wave height, period and direction), wind speed (inferred from measured wave spectra) and buoy position. A water surface temperature sensor has been added in version 2 and a cellular system data telemetry option in Version 3.

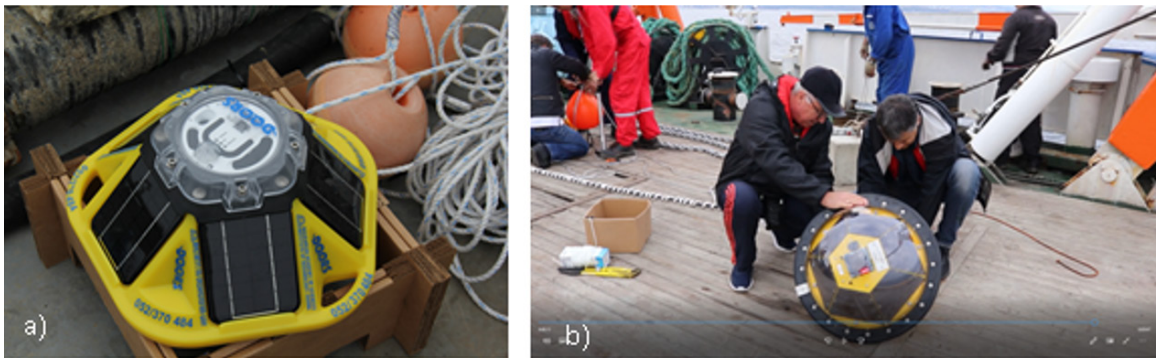


**Figure 1.**
**Wave buoy instruments:**
**a) Sofar Spotter wave buoy and b) Zunibal Antea wave buoy**

The Antea buoy (Figure 1b) is characterized by being small (26Kg - Ø 0.6m), requiring anchoring and staying close to the coast, and continuously provide data of interest related to wave conditions (height, direction and wave period). Anteia wave buoy has a GPS as its main sensor, for the buoy movement's estimation. Anteia GPS sensor, bases its measurement's, by obtaining a 3D absolute reference speed (North, East and Down), and with this speed, an integration is done, and a 3D displacement is obtained. This buoy has a bespoke mooring system, allowing free movement for optimum wave parameters detection. This mooring is specially designed for the buoy and can be fitted to different depths and current conditions.

## DEPLOYMENT LOCATIONS

Between 2020 and 2023, IO-BAS and NIMH deployed nine moored buoys along the Bulgarian Black Sea coast, with the main goal to improves the coastal wave monitoring and data collection. The selection of deployment locations was strategically chosen in nearshore areas with water depths of less than 25 meters, targeting the regions that fall under the specific coastal hazards (Figure 2, Table 1).

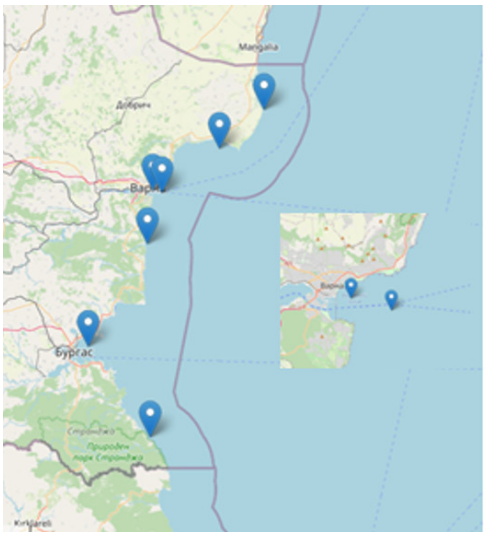

**Figure 2.**
**Location of wave buoys**

| Station | Longitude (degrees) | Latitude (degrees) | Depth (m) | Instruments |
|---|---|---|---|---|
| Shabla | 43.5392 | 28.6116 | 17 | Antea |
| Kaliakra | 43.3717 | 28.3438 | 17 | Antea |
| Varna | 43.182 | 27.9947 | 22 | Spotter |
| Varna bay | 43.1942 | 27.9415 | 17 | Spotter |
| Shkorpilovtci | 42.9577 | 27.9081 | 22 | Spotter |
| Emine | 42.6964 | 27.9067 | 17 | Antea |
| Burgas | 42.9577 | 27.9081 | 22 | Spotter |
| Burgas bay | 42.5117 | 27.5562 | 17 | Spotter |
| Ahtopol | 42.1144 | 27.9277 | 17 | Spotter |

**Table 1.**
**Buoy deployment positions and depth**

The selection of deployment sites was driven by two main factors. First, the need to sample a wide variety of coastal environments, each characterized by unique bathymetric and geomorphological features, in order to obtain a representative dataset on wave conditions. Second, the sites were chosen for their vulnerability to coastal hazards such as erosion, flooding, and storm surge, or because they were active research areas for studying coastal processes.

This site selection ensures that the wave buoy system provides not only broad scientific insights but also practical information for local coastal management initiatives. By collecting data in high-risk zones, the system helps to inform disaster risk management and coastal protection efforts, supporting the development of more resilient coastal communities.

## MOORING DESIGNS AND MANAGEMENTS

The buoys were deployed in accordance with the practical guidelines provided by Sofar Ocean (Sofar Mooring Guideline) and Zunibal Antea for moored applications. The mooring system consists of various buoys and mooring lines anchored to the sea floor. To secure the Spotter buoys, a double catenary mooring system was established, comprising two buoys and tether lines connected to an anchor on the seabed (Figure 3, left).

However, the moorings and buoys are vulnerable to fouling by marine organisms prevalent in the shallow coastal waters where these deployments are situated. The biofouling can significantly increase the weight of the mooring system, potentially compromising its stability. Additionally, it can reduce the effectiveness of the surface floats, which play a crucial role in minimizing the mooring's influence on the buoy's data collection capabilities.

To mitigate these challenges, regular maintenance and cleaning are essential to ensure the optimal performance of the monitoring system. Service visits have been conducted approximately every 3-4 months, during which the buoys and mooring system are inspected, and any biofouling is physically removed (Figure 3, right). While heavy fouling has been observed during these visits, such instances usually occur when the service schedule is delayed due to operational constraints. By adhering to a proactive maintenance regimen, the reliability and accuracy of the data collected by the buoys can be preserved, enhancing the overall effectiveness of the wave monitoring system.

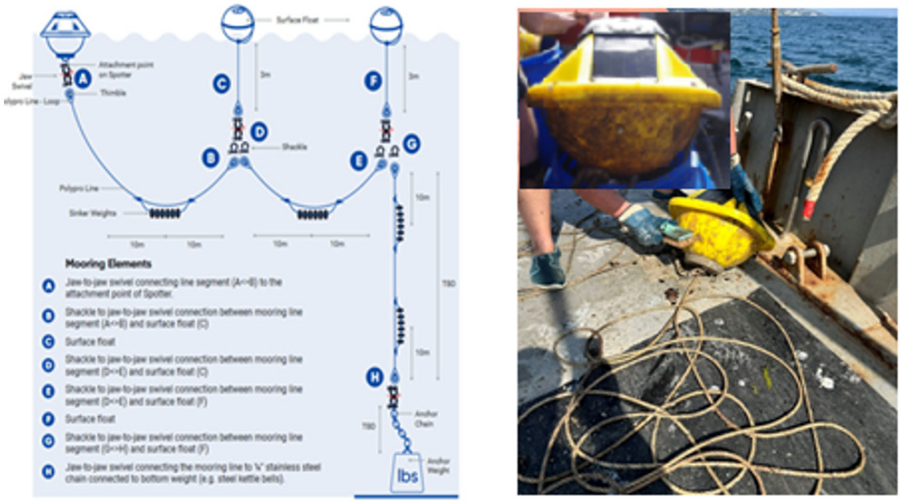


**Figure 3.**
**The Sofar Spotter buoy mooring general design (left, source Spotter Mooring Guidelines v1.2) and maintenance and cleaning of Spotter buoy (SPOT-30889C) deployed in Burgas Bay (right)**

## WAVE OBSERVATION DATA OUTPUT

The buoys are equipped to measure a variety of observational data, providing a comprehensive description of wind waves, including parameters such as height, period, and direction. Additionally, they monitor sea surface temperature (SST) and atmospheric (barometric) pressure, with the capability to integrate other sensors for more extensive data collection.

The data are transferred in near-real-time (every hour) via cellular or satellite connections. This information

is subsequently stored in databases at the Bulgarian National Oceanographic Data Center (BGODC) and the National Institute of Meteorology and Hydrology (NIMH) through API integration, ensuring efficient access and management.

The quality control (QC) of wave data is crucial for ensuring the accuracy, reliability, and usability of information collected by wave buoys. The main objective is to preserve the maximum amount of data while identifying any compromised or less reliable data, allowing end users to interpret such data with caution. QC processes follow established standards for wave data quality control and flagging, ensuring consistent and dependable results [1-4].

The near-real-time data are made publicly available through websites hosted by IO-BAS and NIMH, enabling users to monitor current wave conditions directly (Figure 4). These platforms significantly enhance situational awareness, facilitating the ongoing monitoring of the coastal and marine environment, which is essential for various stakeholders including researchers, policymakers, and the maritime industry.

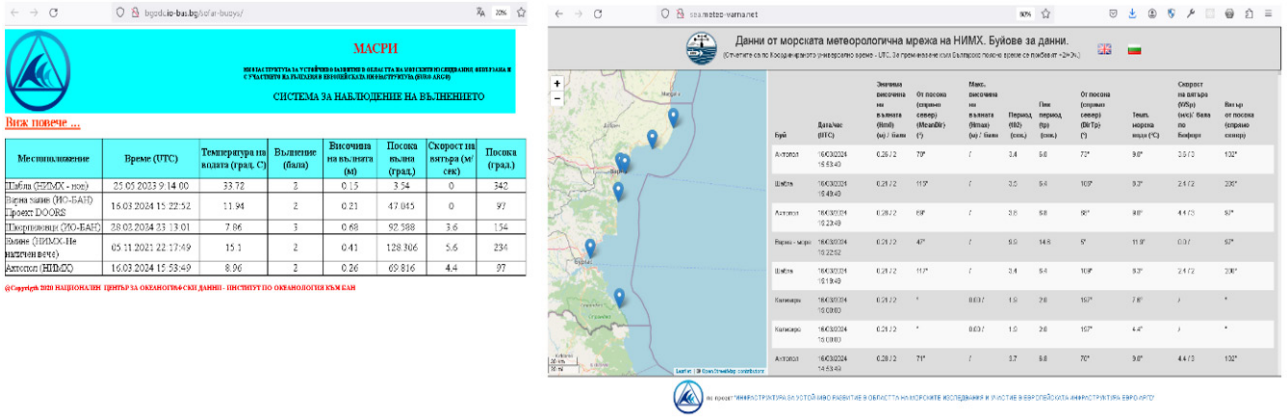


**Figure 4.**
**IO-BAS and NIMH websites**

A recent example of wave height and wind speed data relating to tropical cyclone (TC) Federico, which struck the Bulgarian Black Sea waters on 19 November 2023, was recorded by the buoys deployed along the northern coast. With wind speed approaching hurricane strength, the storm generated significant sea waves, with heights exceeding 4.5 meters, as registered by the wave buoy deployed off Shabla (Figure 5a).

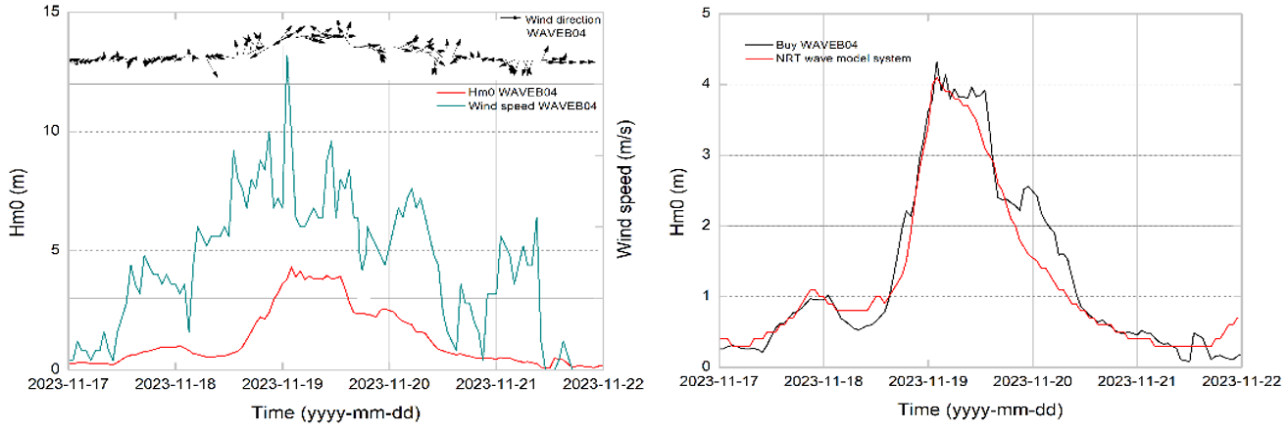


**Figure 5.**
**a) Progression of spectral significant wave height (Hm0), wind speed at 10 m above the sea surface and direction during storm Frederico measured by the buoy off Shabla (WAVEB04);**
**b) CMEMS Black Sea wave model results validated by Shabla buoy data**

## COMPARING MONITORING BUOY DATA WITH MODEL DATA

In situ observations from monitoring buoys provide high-resolution climate data, enabling comparisons with other observational sources, such as global and regional gridded model- and satellite-derived data. Numerous weather and climate models run by scientific institutions worldwide generate forecasts and future climate projections across different timescales, but these models require validation through observational data. For instance, Figure 5b demonstrates the validation of the CMEMS Black Sea wave model output with in situ buoy observations during the storm period. In the case of significant wave height, the model performs well over the whole time period.

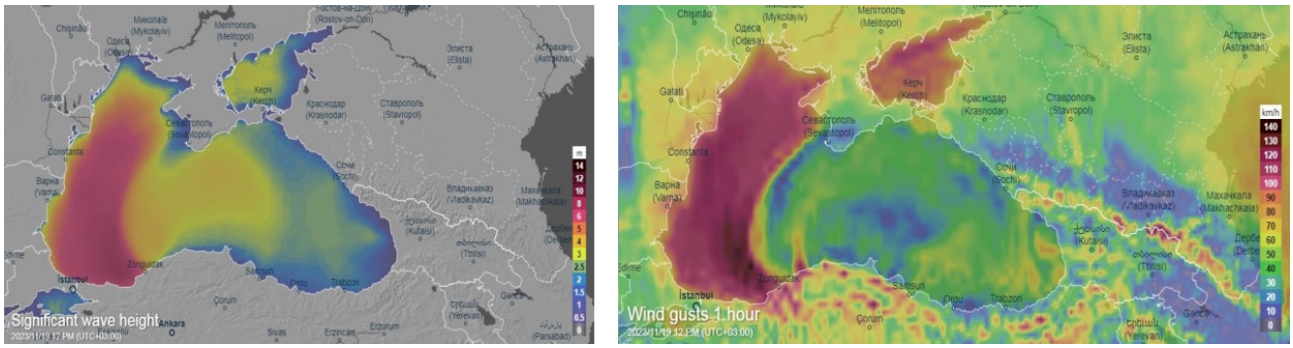


**Figure 6.**
**Storm significant wave heights (left) and wind gust (right) which occurred during the TC Frederico over Black Sea (19 November, 2023), as simulated by the ICON model (source https://www.ventusky.com)**

Figure 6 illustrates the simulation of TC Frederico across the Black Sea using the ICON weather and climate model, showing the distribution of maximum wave heights and wind gusts during the storm period. In the storm center the wave heights exceeded 7 m, while those near Shabla, Kaliakra, and Varna reached between 3 and 5 meters. Without reliable, high-resolution ocean observations for validation, it is challenging to assess whether the models are functioning correctly and to determine the confidence level in future climate projections and their associated impacts.

## CONCLUSIONS

The deployment of a wave buoy system along the Bulgarian Black Sea coast has significantly enhanced the capacity for real-time wave monitoring and climate data collection. The recent impacts of tropical storm illustrate the critical role that in situ observations play in understanding extreme weather events and validating climate models. With recorded wave heights exceeding 4.5 meters and wind speeds nearing hurricane levels, the data gathered from buoys deployed off Shabla, Kaliakra, and Varna coats provide invaluable information on the dynamics of marine conditions during such events.

Additionally, the integration of buoy data with advanced modeling systems, such as the CMEMS Black Sea Wave model, underscores the importance of continuous monitoring for improving predictive accuracy and informing decision-making processes in various sectors, including maritime safety and coastal management. As climate change continues to pose challenges to coastal communities, the ongoing development and maintenance of the wave monitoring system is essential for enhancing resilience and promoting sustainable management of marine resources in the Black Sea region.

## ACKNOWLEDGEMENTS

Sea wave observing system is developed and maintained with the support of MASRI - Infrastructure for Sustainable Development of Marine Research and Participation in the European Infrastructure Euro-Argo, a project of the National roadmap for scientific Infrastructure (2020 - 2027) of Republic of Bulgaria. The upgrade of the system was partly supported by European project DOORS - Developing Optimal and Open Research Support for the Black Sea.

**REFERENCES**

[1] C o p e r n c u s Marine in Situ Team (2020). Copernicus In Situ TAC, Real Time Quality Control for WAVES. Ref. CMEMS-INS-WAVES-RTQC. Copernicus in situ TAC. https://doi.org/10.13155/46607.

[2] C o p e r n i c u s Marine in Situ tac Data Management Team (2023). Copernicus Marine In Situ TAC NetCDF format manual. Copernicus Marine in situ TAC. https://doi.org/10.13155/59938.

[3] d e A l f o n s o alonso-muñoyerro Marta, Manzano Muñoz Fernando (2018). Copernicus Marine In Situ TAC quality information document for REProcessed waves (QUID REP WAVES). Copernicus Marine In Situ TAC.

[4] O c e a n Data Standards - Volume 3: Recommendation for a Quality Flag Scheme for the Exchange of Oceanographic and Marine Meteorological Data. Report IOC/2013/MG/54-3 (Intergovernmental Oceanographic Commission, 2013).

[5] P a l a z o v, A., A. Stefanov, V. Marinova, V. Slabakova, Operational Marine Observing System to Support Safety Port Navigation, Proceedings of the Tenth International Conference on Marine Sciences and Technologies “Black Sea 2010”, Varna, Bulgaria, 7-9 October, 2010, pp. 308-312.

[6] P a l a z o v, A., A. Stefanov, V. Marinova, V. Slabakova, Bulgarian National Operational Marine Observing System, OCEANS, 2012 - Yeosu , vol., no., pp.1-9, 21-24 May 2012, doi: 10.1109/OCEANS-Yeosu.2012.6263526.

[7] P a l a z o v, A., Ciliberti S., Peneva E., Gregoire M., Staneva J., Lemieux-Dudon B., Masina S., Pinardi N., Van denbulcke L., Behrens A., Lima L., Copinni G., Marinova V., Slabakova V., Lecci R., Creti S., Palermo F., Stefanizzi L., Valcheva N., Agostini P. 2019. Black Sea Observing System. Frontiers in Marine Science June 2019, Volume 6, Article 315.


# SHIPBUILDING AND SHIP REPAIR

# FEATURES OF STRENGTH CALCULATIONS DURING SALVAGE OPERATION OF A WRECKED BUNKER TANKER

**Alexander EGOROV *, Alexander NILVA **,**
**Nataliia BUTENKO ***, Vladimir NILVA******

**Abstract.** *The article describes the features of strength calculations when lifting and towing a wrecked bunker tanker, and presents a calculation justification for the chosen scenario of the ship-lifting operation, which was successfully carried out. This bunker tanker was torn from its anchor during a storm and pulled onto the Odesa beach. The ship actually sank, completely grounded to the seabed on its starboard. The main requirement for lifting the vessel was to save its hull unbroken. The idea of cutting the hull into several blocks and transporting them separately was rejected due to the risk of significant environmental pollution. Two main scenarios for lifting the vessel were considered: 1. Engaging a floating crane with large lifting capacity, which would allow the vessel to be lifted and transported without heeling and restoring buoyancy. 2. Vessel's heeling, restoring buoyancy, using floating cranes of lower lifting capacity and tugs for further transportation.*
**Keywords:** *bunker tanker, residual strength, damaged hull.*

## INTRODUCTION

On the night of November 22, 2019, the bunker tanker "DELFI" (prj. 585), was torn from its anchor during a storm and pulled onto on the Odesa beach. The ship was thrown over a rock ridge by the waves, damaging its starboard side. As a result, the ship, having received a damage, grounded with a list of 90° to the starboard side in the coastal area, where there is a breakwater on one side of the ship, and a rock ridge on the other. Accordingly, the main question was: how to get the ship off the ground from a "rock trap".

## AIM OF THE PAPER

To describe the features of strength calculations when lifting and towing a wrecked bunker tanker.

## MAIN TEXT

The grounded vessel is a single-hull (single side and bottom) twin-screw motor ship, with a superstructure and engine room located aft, with the cargo area divided into 3 compartments along the breadth. Year of construction - 1974, hull material is steel with a yield strength of 235 MPa. The framing system is mixed: the ends of the vessel, side, deck and bottom in the area of the side compartments are transverse, the deck and bottom in the area of the central compartments are longitudinal. The frame spacing along the entire length of the vessel is 575 mm, the web frame spacing is 2.30 m, the distance between the longitudinal stiffeners is 0.650 m. The thickness of the shell plating: bottom and bilge - 9 mm, sides - 8 and 9 mm, deck plating - 8 mm. The overall length is 60.55 m, the length between perpendiculars is 58.90 m, the breadth is 10.50 m, the depth is 5.50 m, the light weight of the vessel is 638 tons.

By analogy with the three main problems of ship structural mechanics, we formulate three main features of the calculations performed:

**The first feature** ("external forces") is the location of the vessel and the atypical loads acting on the hull that accompany the salvage operation. The vessel lies on the ground with its starboard side, it is "trapped" between the breakwater and the rock ridge (see Fig. 1), which, in turn, does not allow the vessel to be put

*** Marine Engineering Bureau (Odessa, Ukraine), PhD, FRINA, general director, senior lecturer**
**** Marine Engineering Bureau (Odessa, Ukraine), PhD, FRINA, chief researcher**
***** Marine Engineering Bureau (Odessa, Ukraine), head of strength calculation department, senior researcher**
****** Marine Engineering Bureau (Odessa, Ukraine), AMRINA, deputy head of strength calculation department, senior researcher**

on an even keel and turned without additional damage. Damage to the port side plating leads to flooding of the left group of cargo compartments, which causes the flooding of the entire vessel [1]. Bending moments in the initial position are absent, since the vessel is statically supported by the ground along its entire length. Wave action during the salvage operation is minimal, due to the selected season for the work - August / early September. The situation will change as soon as the vessel begins to heel over and restore buoyancy.

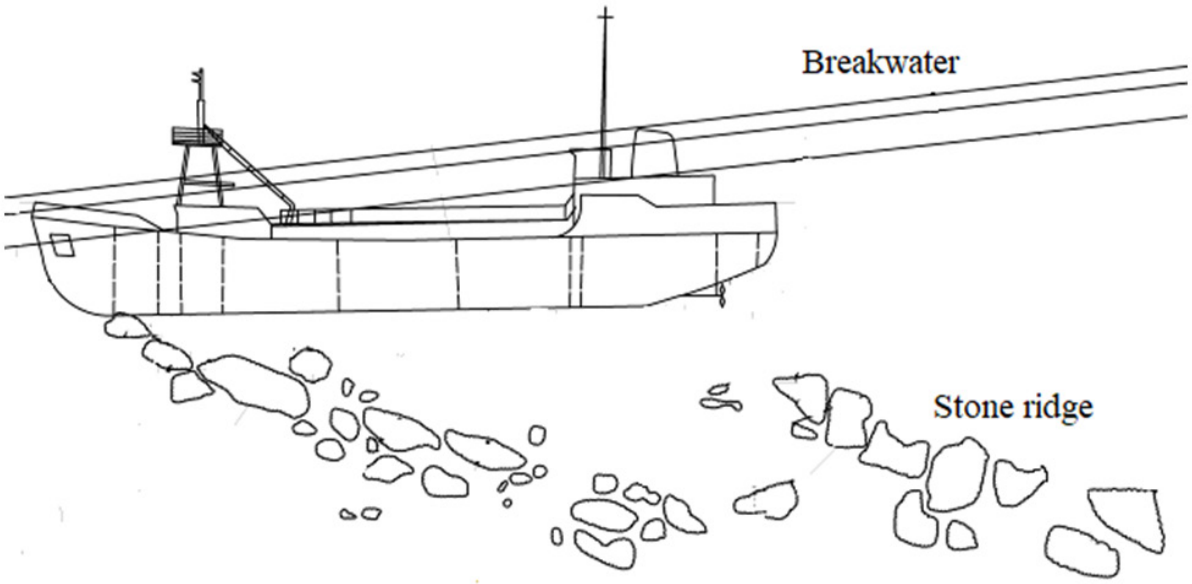


**Figure 1.**
**Ship's location between the breakwater and the stone ridge**

**The second feature** ("internal forces") is the condition of the vessel, its damage, flooded and undamaged compartments, cracks and holes, whether it is possible to seal the damaged compartments and pump water out of them. In essence, this feature is more concerned with the "response" of the vessel structure to external influences: normal stresses from general bending, shear stresses from torsional loads. Both of these parameters are directly affected by the final appearance of the damaged contour of the vessel's cross-section and the reduction of compressed hull elements. According to the diving inspection of the vessel, damage to the bottom and starboard side plating (holes and cracks, see Fig. 2), cracks in the deck were found. Preliminary diagrams of the hull girder (based on the results of the diving inspection) are shown in Fig. 3. Already in the course of the salvage operation, after the vessel was heeled over, it became clear that in the middle part the side and the bottom plating of the StB cargo tank were completely damaged, i.e. the calculated cross-section in the middle part is 2 closed contours of cargo compartments (PS and central). In conditions of insufficient information on the wear of hull structures, 40% wear for the outer contour and 20% for the inner one were adopted as calculated values.

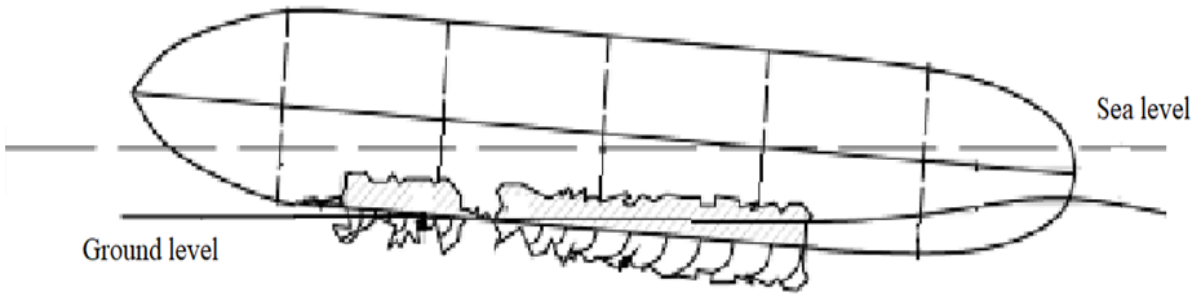


**Figure 2.**
**View from a seaside. Hull damage**

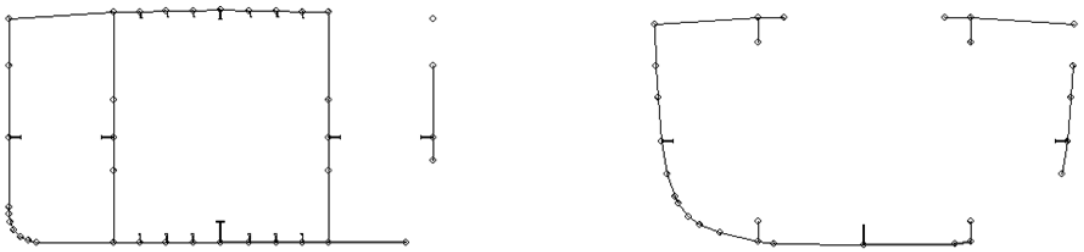

**Figure 3.**
**Transverse section schemes of damaged ship. Midship section, fr.52 (to the left), fore ER bulkhead, fr.73 (to the right).**

**The third feature** ("stress regulation"). The regulation itself when performing calculations is standard for rescue operations - the reduced stresses are compared with the yield point (235 MPa for the tanker "DELFI"). The use of a safety factor of 1.05-1.10 is considered separately for each stage, but, often, this criterion is rarely decisive. The current stresses in the vessel structures either significantly exceed the yield point, or are noticeably lower than this value.

Let us dwell in more detail on the type of **damaged cross-section**. When the hull is damaged, a group of elements is excluded from the hull girder scheme. In this case, the center of gravity of the damaged section shifts toward the undamaged remaining elements, and the main symmetry axes of the cross-section receive a rotation angle, which increases the distance from the neutral axis to the extreme elements of the hull.

For "open" cross-sections - hold-type vessels - rotation angle can reach 20-23 degrees in case of side damage along the entire depth, the area of which includes the outer side elements and longitudinal bulkhead with coaming [2]. As a consequence of such a rotation of the main axes for a damaged open cross-section, the normal stresses in the deck structures increase by 60%, compared to symmetrical damage with a similar area, which would not lead to a rotation of the axes. A completely different nature of the "response" to side damage, including double side damage, along the entire depth is observed for "closed" cross-sections - tanker-type vessels. For such damage, the angle of rotation of the main axes is up to 3 degrees, thus, there is no significant "additional" loss of strength due to the asymmetric nature of the damaged section.

The tanker "DELFI" suffered similar damage to the side construction (the rotation angle of the main axes of the damaged cross-section in the middle part was 6 degrees). A significant advantage of this type of vessel is the division of the hull in the cargo area into three compartments along the breadth (side compartments 2.6 m wide and a central one - 5.3 m). It was because of this division into compartments, even after having suffered serious damage to the side, that the vessel retained three longitudinal bulkheads. On the other hand, another design feature of project 585 vessels (the transverse framing system of side compartments) significantly reduces the strength of the vessel due to the reduction of compressed hull elements.

**In total**, the preliminary strength assessment based on the diving inspection results showed a loss of the strength for the unreduced hull by 10% / 18% for the deck / bottom, respectively (from 0.4693 / 0.5032 cubic meters to 0.3863 / 0.4528 cubic meters). For the "hogging" ship condition, the reduced section modulus of the damaged cross-section for the bottom drops by 42% (from 0.4528 cubic meters to 0.2647 cubic meters).

This article considers two scenarios for the lifting of the tanker "DELFI", one of which **was successfully implemented** in September 2020 [1].

## SCENARIO No 1. LIFTING THE TANKER WITH A FLOATING CRANE.

For these purposes, the floating crane "ZAKHARIY" with a lifting capacity of 680 tons was considered (the estimated lifting weight of "DELFI" was 645 tons according to a preliminary estimate, taking into account the loss of part of the side structures and the presence of residual reserves in the tanks).

Three options for the wrecked tanker (WT) lifting were considered:

1. Without preliminary heeling (heeling is carried out during the main lift as one operation).
2. With preliminary heeling up to 20 degrees' angle (until the bottom of the ship hits the rock).
3. With preliminary heeling up to 0 degrees' heel angle and laying the vessel on the ground with its entire bottom surface or without it (keeping the fore end afloat).

The result of all 3 options was the same, but with different intermediate actions, so we will dwell in

more detail on the option “without preliminary heeling” as an example of operational actions with a vessel. Sequence of actions:

1. «ZAKHARIY» is deployed with the aft anchors dropped opposite the WT forepeak at a safe distance from the rocky ridge.
2. Using the guide ropes, a short lifting sling with a lifting capacity of 170 t is inserted through the anchor hawses of the WT. The fore end of the WT is lifted up to height of 1-2 m.
3. A steel rope is placed under the raised fore end in the area of the aft bulkhead of the pump room (frame 25). The same operation is performed in the area of the forward bulkhead of the ER (frame 73).
4. The WT fore end is placed on the ground. Ship-lifting towels made of strip steel are pulled along the installed guides.
5. The main hooks are lifted. In this case, the ship-lifting slings on the starboard side and the locking slings on the port side are tensioned. The ship-lifting slings on the port side are sagging. The starboard side of the WT is raised, the port side is lowered, and the ship is heeled on the slings.
6. Elimination of trim is achieved by coordinated operation of the right and left main lift hooks.
7. The WT is lifted until it reaches an average draft of 1.5 m.

Lifting the vessel at an average draft of 1.5 m is a necessary condition for **towing** to the destination port of Chernomorsk. Strength calculations of the damaged vessel were made for partial lifting from the water and for complete drainage of the hull. Fig. 4-7 show a diagram of the weight distribution and buoyancy forces, the deflection of the vessel, the shear force and bending moment diagrams for the “vessel in the water” condition. The maximum equivalent stresses are **221 MPa** (94% of the yield strength). However, to **escape the “rock trap”** it was necessary to lift the vessel completely out of the water. Fig. 8-10 show a diagram of the weight distribution, the shear force and bending moment diagrams for the “dry vessel” condition. And in this case, with the absence of buoyancy forces, the equivalent stresses were **294 MPa** (125% of the yield strength), which meant a broken hull of the vessel in the area of the forward bulkhead of the ER. Therefore, based on the calculation results, scenario No. 1 **was not accepted**.

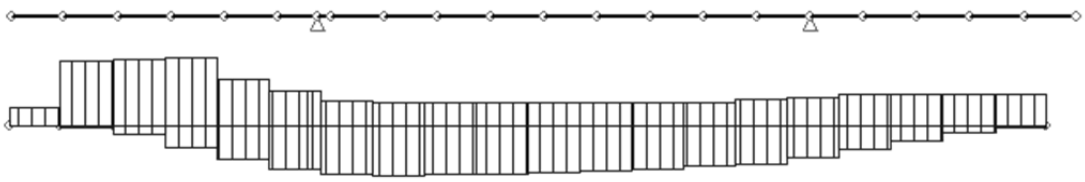

**Figure 4.**
**Ship lifting points at frames 73 and 25.**
**Reaction at frame 73 - 113 t, at frame 25 - 65 t.**

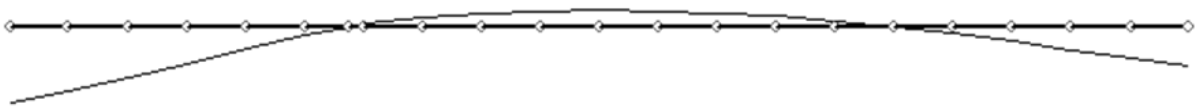

**Figure 5.**
**Movement of structural nodes. $w_{max}$ = 55 mm**

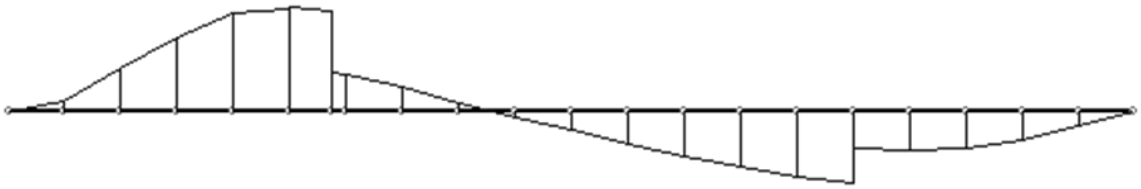

**Figure 6.**
**Shear force diagram. $Q_{max}$ = 1858 kN**

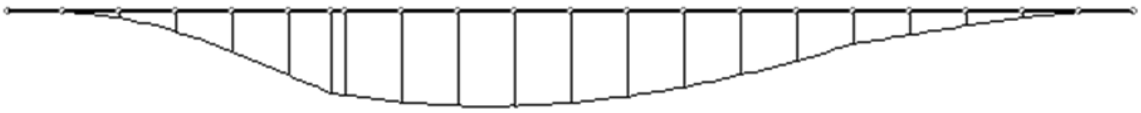

**Figure 7.**
**Bending moments diagram. $M_{max}$ = 21511 kNm**

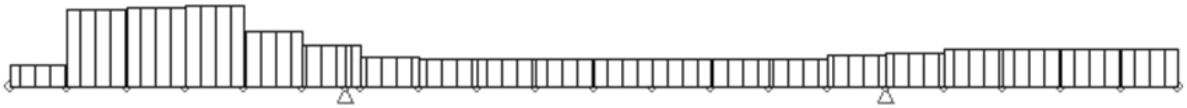

**Figure 8.**
**Ship lifting points at frames 73 and 25.**
**Reaction at frame 73 - 431 t, at frame 25 - 213 t.**

**Figure 9.**
**Shear force diagram. $Q_{max}$ = 2755 kN**

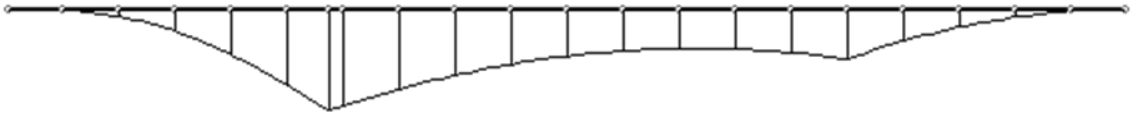

**Figure 10.**
**Bending moments diagram. $M_{max}$ = 22646 kNm**

**SCENARIO No 2. HEELING / EMERGING / TOWING.**

This scenario involved the use of two floating cranes with a lower lifting capacity than the "ZAKHARIY" and two tugs. The five main stages of this scenario [1]:

1. Preparation.

1.1. Clearing a rock ridge with a grab and a special chisel of the floating crane «Atlas 4»;

1.2. Smoothing the surface of the seabed area on which the tanker's bottom grounded after straightening using the Atlas 4 floating crane, digging a trench to shift the Delphi's turning axis in order to reduce the forces required to roll over;

1.3. A set of works to reduce the weight of the tanker (pumping out silt and sand from compartments, dismantling metal structures and mechanisms)

1.4. Sealing the vessel's hull;

1.5. Mounting of triangular supports in the area of PS sheerstrake for straightening the vessel using tugs.

2. Heeling is the vessel straightening by placing her on an even keel, with the stern of the vessel supporting by the ground.

2.1. Heeling with tugs allowed to decrease list from 90 down to 30 degrees;

2.2. A works' set of water pumping out of some compartments with subsequent pumping of air into others - the list decreased to 18 degrees.

3. Stern emersion and trimming.

3.1. Mooring of the floating crane "Atlas 4" to the tanker "DELFI", which provided additional buoyancy to the emergency vessel.

3.2. Additional pumping of water from the compartments. As a result, the stern floated up.

3.3. Trimming the tanker using the floating crane “PK-4”», which lifted the starboard side in the ER area.

4. Towing of a convoy (tanker “DELFI” and two non-self-propelled floating cranes “Atlas 4” and “PK-48”) by two tugs “Topaz N” and “Diamond N” to the port of Chernomorsk.

5. Lifting the tanker onto the slipway using ground-based winches.

All work related to the impact on the hull of the damaged vessel was accompanied by verification calculations of strength and stability. This article presents the most significant of the strength calculations.

**Local strength check of triangular support during vessel’s heeling**

The maximum tug thrust of 600 kN was adopted as the design force. The design scheme of the support, bending moment and shear forces diagrams are shown in Fig. 8. The maximum equivalent stresses arising in elements 1 and 8 are 59 MPa and 94 MPa (yield strength of the material is 315 MPa). The compressive forces in elements 1 and 8 are -634 kN and +575 kN, respectively. The compressive stresses directly perceived by the support brackets are 176 MPa or 57% of the critical stresses, which are equal to 311 MPa. **Conclusion**: the strength of the triangular support is ensured with a significant reserve under the action of the maximum design load.

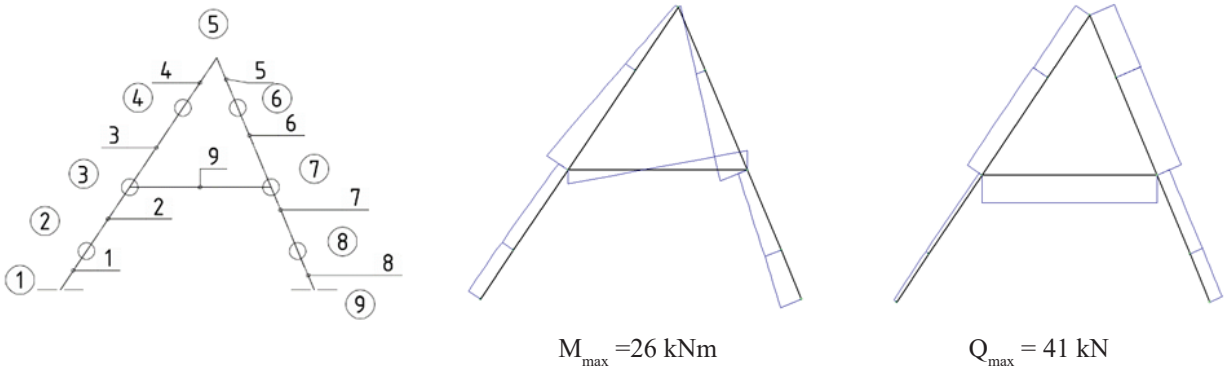


**Figure 8.**
**Calculation scheme. Bending moments diagram. Shear force diagram**

**Check of shear stresses in cross-sectional elements under torsion loads**

The effect of the torsional moment on the ship’s hull during heeling was estimated using the formula:

$$\tau = M / [2 \cdot b \cdot c \cdot t],$$

where

τ - shear stresses in the walls of a prismatic compartment during free warping, M - torsional moment, b - compartment’s breadth, c - compartment’s height, t - thickness of the element, in which the stresses determined. Shear stresses are calculated in table 1.

**Table 1. Shear stresses arising in tanker’s longitudinal bulkheads and side shell**

| $t_{new}$, mm | $t_{cor}$, mm | $t_{cor}$, m | b, m | c, m | P, t | P, MN | l, m | M, MNm | τ, MPa |
|---|---|---|---|---|---|---|---|---|---|
| 6.0 | 4.8 | 0.0048 | 7.9 | 5.5 | 60.0 | 0.589 | 10.5 | 6.180 | 14.8 |
| 7.0 | 5.6 | 0.0056 | 7.9 | 5.5 | | | | 6.180 | 12.7 |
| 8.0 | 6.4 | 0.0064 | 7.9 | 5.5 | | | | 6.180 | 11.1 |
| 9.0 | 7.2 | 0.0072 | 7.9 | 5.5 | | | | 6.180 | 9.9 |

**Conclusion**: the shear stresses that arise in tanker’s longitudinal bulkheads and side shell are insignificant during the vessel heeling.

**Assessment of the longitudinal strength of the damaged vessel**

The following vessel conditions were considered:

1. Tanker is afloat ($M_{sw\ max}$ = 17 948 kNm). Cargo tanks No.9, 10, 13 and ballast tanks No.1, 2, 3 are filled.
2. Tanker is afloat with stern crane support. ($M_{sw\ max}$ = 15 309 kNm). Cargo tanks No.9, 10, 13 and ballast tanks No.1, 2, 3 are filled. The force of the crane slings is 50.0 t (applied in the area of fr.92).
3. Tanker's towage with stern crane support. ($M_{sw\ max}$ = 17 801 kNm). Cargo tanks No.9, 10, 13 and ballast tanks No.1, 2, 3 and pump room are filled. The force of the crane slings is 50.0 t (applied in the area of fr.92).
4. Preparation for lifting the vessel onto the slipway. ($M_{sw\ max}$ = 14 946 kNm). Cargo tank No. 13 and ballast tanks No. 2, 3 are filled.
5. Lifting the vessel onto the slipway with crane support for the fore hawses. ($M_{sw\ max}$ = 10 500 kNm). Cargo tank No. 13 and ballast tanks No. 2, 3 are filled. The force of the crane slings is 55.0 t (applied in the area of fr.3). The reaction of the ground was not taken into account, since it reduces the "hogging" still water bending moment.

Among the options considered, case No. 3 "Tanker's towage with stern crane support" was selected as the calculation case ($M_{sw}$ = 17 801 kNm) as a case with the maximum value of the bending moment on still water and the simultaneous action of an additional wave bending moment during the operation. The additional wave bending moment was determined for wave heights that were obviously greater ($h_{3\%}$ = 3.5 m) than the actual wave heights during tanker towing.

$$M_w = 11\ 808 \text{ kNm for «hogging» condition.}$$

Minimum required ultimate hull bending moment:

$$[M_{ult}] = 1.1\ (0.92\ M_w + M_{sw}) = 1.1\ (0.92\ 11\ 808 + 17\ 801) = 31\ 530 \text{ kNm}$$

Actual ultimate hull bending moment for «hogging» condition is 59 760 kNm.

**Conclusion**: the longitudinal strength requirements are met with a noticeable margin.

## CONCLUSIONS

This article has considered the related strength calculations for two main scenarios of lifting of the emergency tanker "DELFI". The second scenario was successfully implemented in September 2020.

## REFERENCES

[1] E g o r o v, G.V., Gubankov, Yu.P., Ivanov, A.I., Golodnitskiy, A.G. «SAVING «DELFI» - UNIQUE OPERATION». Shipping, No. 10 (189), October 2020 (in Russian).

[2] N i l v a, V.A. Analytic method of definition of geometric characteristics of inland or river-sea navigation dry-cargo vessel after receiving damage. ONMU Reporter. - Odessa: ONMU, 2015. - Vol. 2 (44). - pp. 60 - 69 (in Russian).

[3] N i l v a, V.A. Assessment of load-carrying strength of river-sea going tanker's hull with the loss of the part of longitudinals. ONMU Reporter. - Odessa: ONMU, 2014. - Vol. 1 (40). - pp. 72 - 82 (in Russian).


# DECARBONIZATION IN SHIPPING

# OPPORTUNITIES TO INCREASE ENERGY EFFICIENCY THROUGH THE SHIP SUPERSTRUCTURE

**Gergana PENCHEVA***

**Abstract**. *The activities of the International Maritime Organization (IMO), as the UN agency responsible for safe, secure and efficient shipping and the prevention of pollution from ships, started 20 years ago with Resolution A.963 (23). A MEPC.203(62) [3] resolution from 2011 introduced requirements for the energy efficiency of new ships, so-called Energy Efficiency Design Index (EEDI). Ship superstructure can affect the EEDI through the size, shape and location to reduce air resistance and by using lightweight materials for the construction, to increase the cargo capacity of the ship. This paper analyses published results of the research of these two opportunities in the design and construction of the ship superstructure.*
**Keywords:** *air resistance, composites with natural fiber, energy efficiency, light materials, ship superstructure.*

## INTRODUCTION

The activities of the International Maritime Organization (IMO), as the UN agency responsible for safe, secure and efficient shipping and the prevention of pollution from ships, started 20 years ago with Resolution A.963 (23) [1]. Large-scale development of new legislation began with the adoption of Annex VI to MARPOL, which entered into force on 19 May 2005. Annex VI aims to reduce air emissions including sulphur oxides (SOx), nitrogen oxides (NOx), ozone-depleting substances (ODS), Volatile organic compounds (VOCs) and combustion emissions on board ships. The aim is to significantly reduce the carbon intensity of global shipping, ultimately eliminating its impact on both local and global air pollution as well as human health.

The most recent report from the International Maritime Organization (IMO) in 2020 [2] reveals alarming levels of greenhouse gas emissions, specifically carbon dioxide, methane, and nitrous oxide. These emissions have experienced a 9.6% increase, going from 977 million tonnes in 2012 to 1,076 million tonnes in 2018. Carbon dioxide emissions alone accounted for 962 million tonnes in 2012 and rose to 1,056 million tonnes in 2018, an increase of 9.3%. During the period from 2012 to 2018, shipping emissions contributed a greater share of global human-caused emissions, rising from 2.76% to 2.89%. These emissions are expected to continue growing based on possible long-term economic and energy scenarios. By 2050, emissions could be anywhere from 90% to 130% higher than the levels recorded in 2008.

A MEPC.203(62) [3] resolution from 2011 introduced requirements for the energy efficiency of new ships, so-called Energy Efficiency Design Index (EEDI). Despite the complex formula for EEDI index in the rules, its meaning can be represented as follows.

(1) $$EEDI = \frac{CO_2\ emission}{Transport\ work}$$

The attained EEDI for the ship must be below the 'Required EEDI' limit prescribed in MARPOL. To calculate CO2 emissions, the carbon content of the fuel is considered alongside the fuel consumption. Fuel consumption is figured out by measuring the power used for propulsion and auxiliary power under specific design conditions. To calculate the transport work, you multiply the ship's designated capacity (DWT or GT) by its speed, which is measured at maximum summer load draft and at 75% of its rated installed power.

Ship superstructure can affect the EEDI in two ways. Through the size, shape and location to reduce air resistance. This is considerably less than water resistance (about 2% of the total resistance [4] ) but will generally

* **Technical University of Varna, Bulgaria**

lead to a reduction in power and hence fuel consumption and $CO_2$ emissions. The use of lightweight materials for the construction, on the other hand, will increase the cargo ability of the ship while preserving the main dimensions of the ship. Thus, decreasing the value in the numerator and increasing that in the denominator of Eq. (1) will result in a decrease in the EEDI.

This paper analyses published results of the research of the two opportunities in the design and construction of the ship superstructure.

## LIGHT MATERIALS FOR SHIP SUPERSTRUCTURE

### Why lightweight structures?

Reasons for using lightweight materials and structural arrangements in ships (as in other types of transportation vehicles) include the following:

- They allow a greater payload for a given size or weight of vessel.
- They allow higher speeds to be achieved.
- They reduce fuel consumption and environmental emissions for a given payload and distance travelled.

For ships with more decks (such as cruise vessels) the use of lightweight solutions in the upper decks helps to lower the centre of gravity, thus improving stability and allowing larger height/breadth ratios. In addition, lightweight solutions (e.g. closed aluminium extrusions and sandwich configurations) are also compact, giving reduced space requirements and leading to smaller overall vertical distances between decks.

### The main lightweight materials

The main lightweight materials used in ships are fibre reinforced plastic (FRP) composites and aluminium alloys. FRP is used in both single-skin and sandwich configurations; in single-skin applications there is usually a system of stiffeners, but unstiffened monocoque solutions are also to be found. (Here we use the term “FRP” to include the special case of glass- reinforced plastics - GRP).

Aluminium alloys are commonly found in welded, stiffened plate configurations and in the form of extruded sections (both open and closed), but sandwich arrangements are also possible.

Although not normally considered to be lightweight materials, high strength steels may also be used to reduce weight; these are to be found in stiffened plates and, recently, some sandwich configurations. There is increasing use of mixed solutions in which various materials are combined in one ship or superstructure.

Current and potential applications of lightweight materials in ships are mainly related to high-speed passenger and car ferries, patrol and rescue craft, smaller naval ships (e.g. mine countermeasure vessels), pleasure craft and sailing yachts. However, they are also used in superstructures of cruise ships and of larger naval ships (e.g. frigates). Furthermore, they are used extensively in secondary structures and components for all types of ships, from masts and casings to moveable vehicle ramps and decks.

As a rough guide, in the main hull structure, FRP is used for craft with length up to about 50 m, and aluminium for vessels up to about 120 m, while high-strength steel is mainly used for larger vessels. In recent years composites have been rarely used in hulls of new ferries; their use has been mainly confined to patrol/rescue craft, pleasure craft, yachts and naval vessels. The main reason for this is the severe restriction on the use of combustible materials that was introduced in the IMO Code of Safety for High-Speed Craft in the 1990s. With new, approved fire protection systems now available, FRP has once more become a practical and safe alternative to aluminium for ferry applications.

### Materials and manufacturing methods for FRP composites

FRP composites for marine applications are generally laminated composites. These consist of an ore layers of reinforcement fabric in a polymer resin matrix. In the case of sandwich construction there are two skin laminates with a core between that keeps the laminates in place and provides a shear connection between them.

In reinforcement fabrics the main fibre materials are glass (E-glass, R-glass, S-glass), aramids (Kevlar, Twaron), carbon, polyester, high performance polyethylene (HPPE), and various hybrids/combinations. Various fabric formats are used, including chopped strand mat, continuous strand mat (randomly placed fibres), woven roving (plain weave, satin, twill), uniaxial, and “multiaxial” configurations (layers of uniaxial stitched together, also known as non-crimp fabrics).

Matrix materials (resins) include polyesters, vinyl esters, epoxies, various modifications of these resins (e.g. rubber-modified vinyl ester), and phenolics. In a pre-preg, layers of fabric are pre-impregnated with partially cured resin that will completely cure on being heated. Sandwich core materials (Fig. 1) include polymer foams, end-grain balsa wood, honeycombs and corrugated FRP cores. The main foams in use are PVC (diverse types), polymethacrylimide (PMI), polyetherimide (PEI) and phenolic. Honeycombs are normally metal (mainly aluminium) or aramid paper ("Nomex").

About manufacturing methods, the most common *contact moulding* method is hand lay-up, but automated lay-up systems are used for larger production, and spray lay-up in some cases when short fibres are being used. Greater compaction can be achieved by applying pressure, e.g. by vacuum bagging, or (for relatively small items) an autoclave. High fibre content can also be achieved by resin transfer moulding (RTM) or by vacuum-assisted resin infusion (e.g. the SCRIMP process). These compression and injection/infusion methods have also the advantage of being closed processes, so that emission of solvent vapours is much reduced. For cylindrical and similar shapes, filament winding is a convenient and economical production method.

One choice for manufacturing sandwich structures (Figure 1) is to produce the skin laminates separately and then bond them to the core. However, a frequent practice for hulls is to first build up the core on a simple wooden framework and then laminate directly onto one side of the core. The framework is then removed, and the other side is laminated. Alternatively, if resin infusion techniques are used, it is possible to infuse sandwich panels with face laminates on both sides in one step and then assemble the panels to create a larger structure. In some cases, the entire sandwich structure or part can even be infused in one step.

**Advantages and disadvantages of the application of sandwich panels**

***Advantages***

Sandwich panels currently consist of two steel or aluminium skins separated by a lightweight core made of the same material or plastic. These panels have a higher sectional modulus to sectional area ratio compared to traditional plates due to the distance between the skins. In dredging ships [5], the strength of the ship structure is largely influenced by local bending moments caused by loads or water pressures. By using sandwich panels, the structural weight of certain parts, such as decks, can be reduced by 39%. This enables ship owners to buy lighter ships with a higher deadweight-displacement ratio, leading to reduced operational costs. Additionally, shipyards receive help from reduced production time and material costs.

Laser welding machines are used to produce steel cored sandwich panels because they allow for plate welding, which is necessary for this type of production. Using this method reduces the amount of manual labour needed in the manufacturing process. Suppliers provide large semi-finished sandwich panel areas, which significantly decreases production time at the shipyard. By using sandwich panels, the number of panel stiffeners that need to be installed by the shipyard is reduced, thanks to the higher sectional modulus of these panels compared to single plate panels. This shift to sandwich panels can lower production costs at a shipyard by reducing the need for panel stiffeners, as well as brackets, cut-outs, collar plates, and buckling stiffeners.

By applying sandwich panels instead of conventional stiffened panels production costs will shift from the shipyard to the supplier of sandwich panels. Most of the welding work at the shipyard during section assembly is done manually, but the assembly of the sandwich panels is done semi-automatically, which is relatively cheap. Therefore, in most cases total production costs (production of panels and assembly of the section) will be reduced when applying sandwich panels in (ship) structures. Generally, the application of sandwich panels will reduce the total production costs (material, panel and section assembly) by 25% [5].

Due to the reduction in parts not only the assembly costs for the specific sandwich application be reduced, but also the throughput time of the assembly. Transport, handling, welding, surface treating, and inspection work will be reduced by applying sandwich panels. In case of the Switch Board Room the throughput time of the section assembly is reduced with 70% [5].

Additional benefits of the application of sandwich panels are improved fatigue and corrosion characteristics. It is difficult to judge these benefits in a quantitative way. But the number of parts will reduce the risk of fatigue cracks and the number of corrosion sensitive details. Finally, the use of sandwich panels can result in more available space for non-structural parts, which is particularly interesting in accommodation areas.

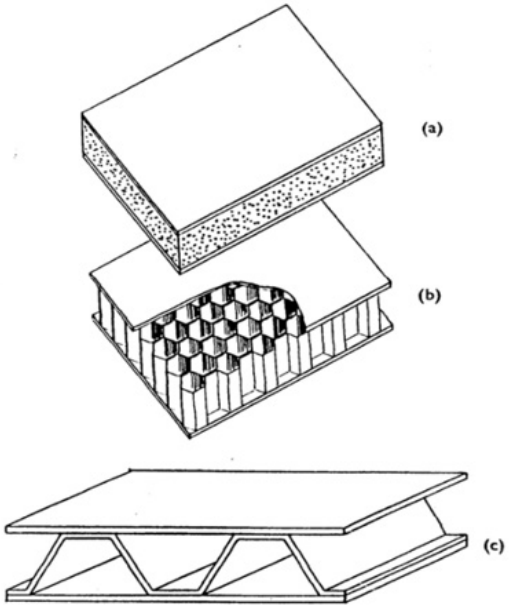


**Figure 1.**
**Sandwich core materials a) polymer foam core b) honeycomb core c) corrugated core [6]**

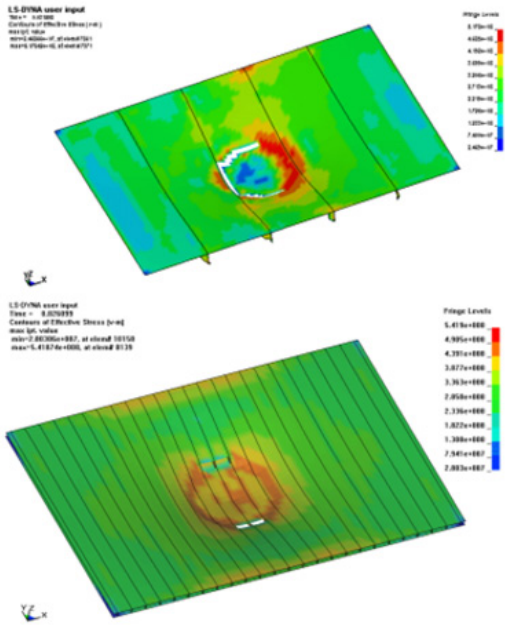

**Figure 2.**
**Finite element results for conventional and I-core® sandwich panel under impact loads [5]**

***Disadvantages***

Compared to conventional stiffened panels, sandwich panels have certain disadvantages. These include the shell plates in sandwich panels having low resistance to impact loads and local (point) loads, the core (metal or polymer) of the sandwich panel having low shear strength, and the panel joints also having low shear strength. Additionally, there is limited freedom in the structural design of sandwich panels.

One of the main concerns is the potential decrease in impact resistance (Figure 2). This is especially true when using 2.5 mm shell plates or thinner for the sandwich panel, as it reduces the local impact strength of the metal core panels. However, when using polymer cores, the local impact strength is greatly improved compared to traditional stiffened panels.

## IMPLEMENTATION OF LIGHT MATERIALS FOR SHIP SUPERSTRUCTURE

The use of aluminium sandwich panels for ship structures above the waterline is not new. In [5] is presented the use of such panels for tier of superstructure (Figure 3) and Switch Board Room (SBR) and of a trailing suction hopper dredger (TSHD) (Figure 4).

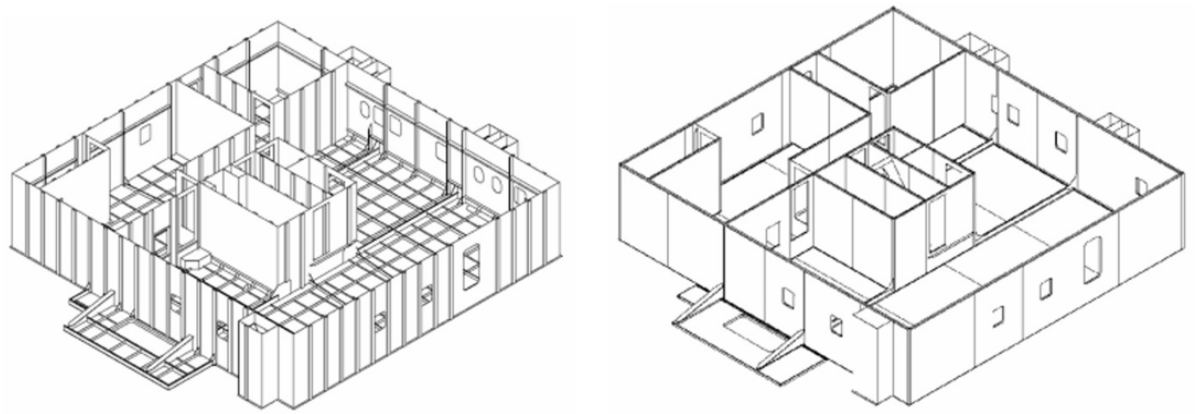

**Figure 3.**
**Conventional stiffened tier of a superstructure (left) and an all-steel sandwich tier (right) of 3500 m$^3$ TSHD [5]**

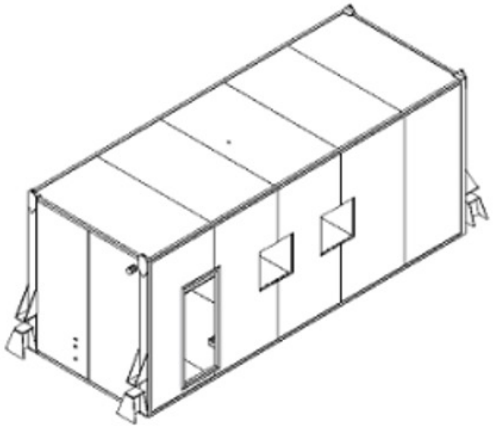

**Figure 4.**
**Structural design of a sandwich SBR of 6000 m³ TSHD [5]**

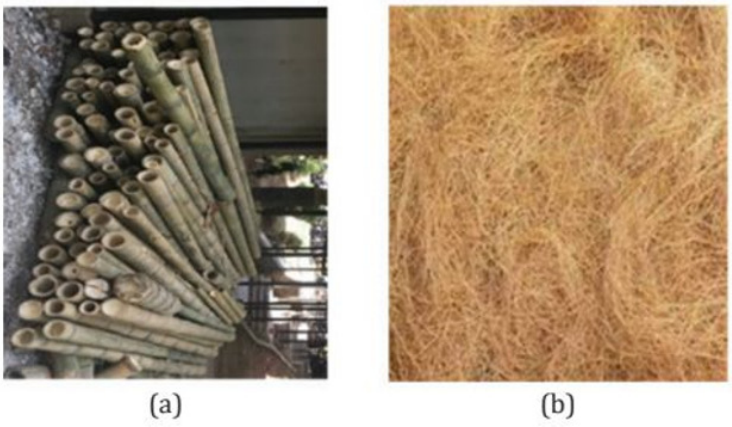


**Figure 5.**
**Materials a) Petung bamboo, b) coconut coir fibre [7]**

The findings of the study for the superstructure showed that while the decrease in structural weight and overall production costs was not significant, there was a notable 50% reduction in both steel building hours and throughput time. For SBR first calculations showed a decrease in overall expenses (including material and production costs) by 34%. Additionally, there was a reduction in weight by 20% and a substantial decrease in production time by 63%.

Nowadays, there is a growing trend towards using inexpensive and environmentally friendly materials, also known as natural materials. To address this issue, researchers have been exploring new alternative materials such as bamboo and coconut fibre [[7] (Figure 5). In this study, the focus was on investigating how the arrangement of laminated Petung bamboo (*Dendrocalamus asper*) affects the strength of ship construction. Specifically, the researchers examined the compressive and flexural strength of laminated bamboo with two different fibre arrangements: 0° unidirectional and 90° unidirectional.

The findings revealed that laminated bamboo could be effectively used in ship components that require different strength levels, depending on the fibre direction. For example, if prominent levels of strength are needed, laminated bamboo with a fibre direction of 0° would be recommended for components like keels, machine foundations, web frames, and hull plates. On the other hand, laminated bamboo with a fibre direction of 90° would be more suitable for ship components like the ship deck, deck plate, and construction parts above the waterline, where lower strength levels are needed. In conclusion, this study highlights the potential applications of laminated bamboo in ship construction, offering a versatile and sustainable alternative to traditional materials.

Another study [8] investigated possibilities to implement laminated bamboo composites (LBC) in structures of fishing vessels. It has been determined that only specimens with 7 layers (Figure 6) meet the bending and tensile strength requirements set by the Indonesian Bureau Classification. The layer configuration of LBC includes 7 layers with 45°/-45°/45°/-45°/ 45°/-45°/45° orientation, 1 mm of thickness, with 35% epoxy resin and 65% bamboo lamina and total thickness of 10 mm.


**Figure 6.**
**7 layers laminated bamboo - fibreglass boards [8]**

In review paper [9] is concluded that the bamboo is a rapidly expanding plant that has the capacity to not just substitute wood in specific uses, but also serve as a greener alternative to unfriendly and non-recyclable materials like fiberglass and polyurethane in composite applications.

The researchers behind [10] have created a material known as a bamboo-plastic composite, which they suggest could be used as a substitute material for ship superstructures. In terms of compressive strength, the bamboo composite is about 42% stronger than plywood and 20 times stronger than steel. However, when it comes to bending strength, the bamboo composite is roughly 62% weaker than plywood and five times than steel. The authors believe that the findings from this study could offer valuable insights for future designs and experiments involving the combination of bamboo culms and other materials.

Composite materials have also been used to retrofit the part of the superstructure of a passenger ship (Figure 7). The weight of the composite structure was approximately 71% less than that of an equivalent steel structure. Additionally, the lightship of the vessel was reduced by 4.8%. Furthermore, the newly added composite part accounted for 2.1% of the new lightship weight [11].

The findings also prove that the use of composite materials in a part of the superstructure results in a 12.9% increase in GM value. Furthermore, as expected, the GZ values also experience an increase. The maximum GZ value is boosted by 24% [12]. The retrofitting also has an impact on fuel consumption, due to less water resistance at reduced draught. This reduction is not remarkable and is estimated at 1.5% per year [12].

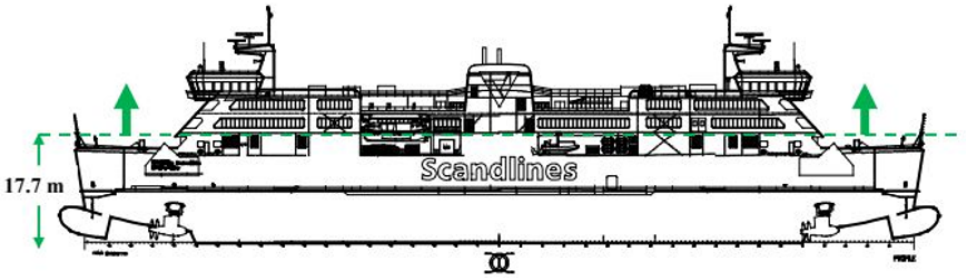


**Figure 7.**
**Part of the superstructure above 17.7 m retrofitted [11]**

Despite the growing trend of utilizing marine-grade aluminium composite in commercial vessels and surface warships over the past three decades, particularly for decks and superstructures, the authors in [13] have reported a significant decline in its usage in recent warship construction. This decline can be attributed to issues such as thermal softening during fire incidents and frequent cracking in superstructures connected to steel hulls. The proposea solution is combining carbon fibers, plastic fibers, and aluminum nano powder to enhance strength, stability, and fire resistance of structures.

Materials that contain impermeable two-dimensional substances, known as nanocomposites, are of particular interest for protecting metals from corrosion. Authors of recently published papers **Error! Reference source not found.** propose to add 3-(m-aminophenoxy) propyltrimethoxysilane (APPMS) functionalized hafnium nitride (HfN) to a coating matrix to enhance its ability to act as a barrier against harmful elements due to the superior chemical and thermal stability of APPMS. By incorporating functionalized HfN into graphitic carbon nitride (GCN) within a polyurethane (PU) material, the resulting composite offers improved corrosion resistance and fire-retardant properties. When applied to aluminum alloy surfaces immersed in seawater, novel nanocomposites - PU-HfN, PU-APPMS/HfN, PU-GCN/HfN, and PU-GCN-APPMS/HfN - provide superior surface protection, water repellency, flame retardancy, and mechanical properties.

## AIR RESISTANCE OF SHIP SUPERSTRUCTURE

Wind resistance is significantly less than that of water, but nevertheless, its reduction has a positive effect on the energy efficiency of the ship with overall reduction of fuel consumption. The study [14] presents the results of testing various concepts and devices on the superstructure of a container ship in a wind tunnel to estimate the reduction in air drag. The design concepts are shown in Figure 8 -Figure 10.

The effects of studied design concepts are shown in Table 1( y is the angle of wind direction). The most effective methods for reducing drag were found to be the use of gap-protectors between containers and the

installation of a visor in front of the upper deck. It's important to note that the computation results indicate a similar trend in drag reduction as observed in the experiment for small heading angles only.

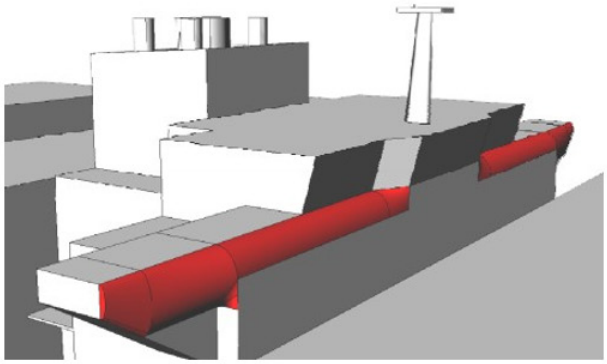

**Figure 8.**
**Design concept of slanted appendage around the wheelhouse [14]**

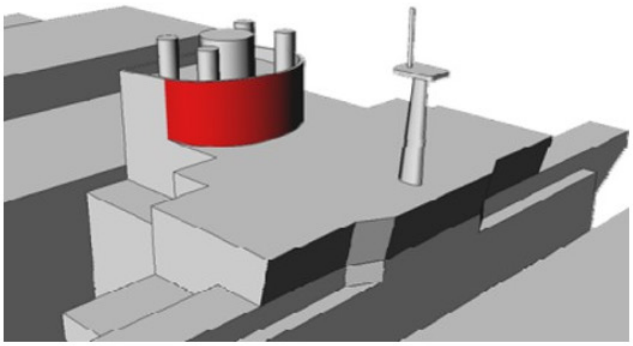

**Figure 9.**
**Design concept of rounded funnel [14]**

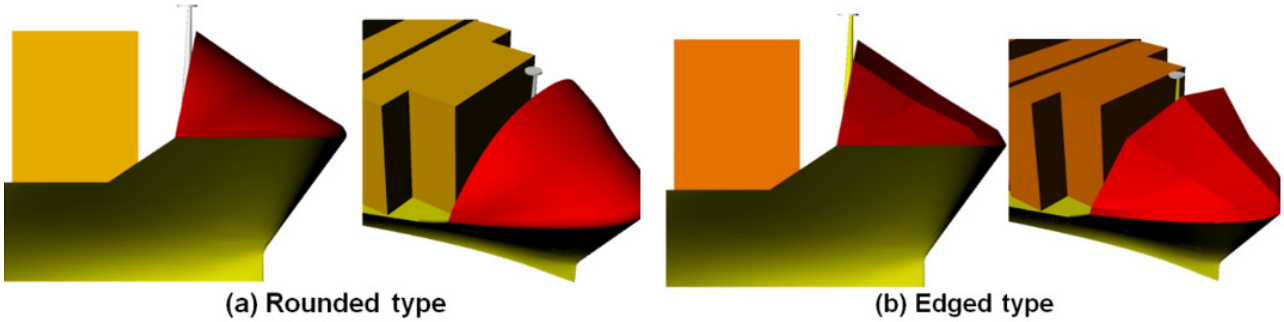


**Figure 10.**
**Design concept of a visor: a) Rounded type; b) Edged type [14]**

**Table 1. Air drag reduction of each design concept**

| Design Concept | ψ=0 | Mean values | |
|---|---|---|---|
| | | ψ = 0 ~ 30° | ψ = 0 ~ 50° |
| Gap protectors | 13.4% | 25.9% | 53.4% |
| Rounded Visor | 13.2% | 6.2% | 7.2% |
| Edged Visor | 14.7% | 6.8% | 7.3% |
| Slanted appendage | 0.6% | 1.2% | 0.4% |
| Rounded Funnel | 1.2% | 1.1% | 1.0% |

## CONCLUSIONS

Today, reducing fuel oil consumption and the resulting greenhouse gas emissions from ships is a significant concern in ship design and the shipping industry. Research is conducted in different directions -technological improvement and innovations, operational measures, alternative fuels. Substantial efforts are made to reduce the water and air resistance of the ship to reduce fuel consumption and hence the emissions. The paper reviews the possibilities for influencing the energy efficiency of the ship through the ship superstructure. Studies are analysed and presented in two directions: use of lightweight materials for superstructure construction and different shapes to reduce air resistance.

Along with the widely used aluminium composite materials, natural raw materials such as bamboo and coconut fibres are used to meet the environmental requirements of reducing carbon emissions from shipping. Notwithstanding the relatively small impact of the ship's superstructure mass on some types of ship, the reduction and lowering of the centre of gravity may have an impact on the energy and economic efficiency of

the ship. The analysis of this impact shall consider the entire life cycle of the ship. For example, recycling a ship's superstructure from aluminium is much more profitable than the same from steel.

This paper starts an in-depth study of the possibilities for increasing the energy efficiency of ships through modification and innovative design solutions of the ship superstructure of modern ships.

**REFERENCES**


[1] IMO (2004) Resolution A.963(23). IMO policies and practices related to the reduction of greenhouse gas emissions from ship. IN IMO (Ed. A 23/Res.963. London.

[2] IMO (2020). Fourth IMO GHG Study 2020. Available online: https://www.imo.org/en/ourwork/Environment/Pages/Fourth-IMO-Greenhouse-Gas-Study-2020.aspx (accessed on 12 August 2024).

[3] MEPC.203(62),2011, Inclusion of regulations on energy efficiency for ships in MARPOL Annex VI, London.

[4] WÄRTSILÄ. Encyclopedia of Marine and Energy Technology. Available online: https://www.wartsila.com/encyclopedia/term/ship-resistance (accessed on 22 August 2024).

[5] K o r t e n o e v e n, J., Boon, B. de Bruijn, A. Application of Sandwich Panels in Design and Building of Dredging Ships. J Ship Prod 24 (03): 125-134. Paper Number: SNAME-JSP-2008-24-3-125 https://doi.org/10.5957/jsp.2008.24.3.125.

[6] N o u r y, P., Hayman, B., Weitzenböck, J. Lightweight Construction for Advanced Shipbuilding -recent Development Selection of Design Performance Improvement Options Weapon Induced Loads and Load Effects Use of Adhesive Bonding on Superstructures of High-speed Craft and Passenger Ships Background, Engineering, Materials Science, Published 2005.

[7] M a n i k, P. Tuswan, T., Rahardjo, F. A. O., Misbahudin, S. Mechanical Properties Evaluation of Laminated Composites of Petung Bamboo (*Dendrocalamus asper*) and Coconut Coir Fiber as Ship Construction Components. Scientific Journal of Maritime Research 37 (2023) 75-85, Faculty of Maritime Studies Rijeka, 2023.

[8] M a n i k, P., Samuel, S., Tuswan, T. Jokosisworo, S., Nada dap, R.K. Mechanical properties of laminated bamboo composite as a sustainable green material for fishing vessel: Correlation of layer configuration in various mechanical tests. Journal of the Mechanical Behaviour of Materials 2022; 31: 673-690.

[9] P o p a t, T.V., Patil, A.Y. A Review on Bamboo Fiber Composites. IRE Journals, Volume 1, Issue 2, ISSN: 2456-8880, August 2017.

[10] H u a, J., Luo, J. S. Experimental Study of Bamboo Composite Materials Proposed for Application in Ship Superstructure. Proceedings of the 4 World Congress on New Technologies (NewTech'18), Madrid, Spain, August 19 - 21, 2018 Paper No. ICEPR 187, DOI: 10.11159/icepr18.187.

[11] K a r a t z a s , V., Hjørnet, N., Berggreen C., Jensen, J.J. Retrofitting the superstructure of a large passenger ship using composites - a demonstration. 20 International Conference on Composite Materials, Copenhagen, 19-24 July 2015.

[12] K a r a t z a s, V., Hjørnet, N., Berggreen C., Jensen, J.J. The effects on the operating condition of a passenger ship retrofitted with a composite superstructure. Proceedings of PRADS2016, 4 -8 September 2016, Copenhagen, Denmark.

[13] D e v Anand, M., Janardhanan, K.A., Rajesh, R., Ramachandran, D. Fibre Reinforced Plastic Material with Aluminum Filling Used for Ship Superstructure. Journal of Chemical and Pharmaceutical Sciences, JCPS Volume 9 Issue 1, January-March 2016, pp 351-355.

[14] K i m, Y., Kim, K-S., Jeong, S-W., Jeong, S-G., Van, S-H., Kim, J. Design and Performance Evaluation of Superstructure Modification for Air Drag Reduction of a Container Ship. Journal of the Society of Naval Architects of Korea. Vol. 52, No. 1, pp. 8-18, February 2015, http://dx.doi.org/10.3744/SNAK.2015.52.1.8.

# ENERGY EFFICIENCY OF SHIPS AT VARNA ANCHORAGE

**Ivet FUCHEDZIEVA***

**Abstract**. *The study deals with statistics of ships anchored in front of the port of Varna. The research is in two directions - statistics of the technical ship characteristics and their energy efficiency. The presented results are based on the analysed 256 ships anchored in a period of 7 months. The data for emission are taken from EU-MRV database for 5 consecutive years 2018-2022. To analyse the results better, relative intensity and efficiency indicators have been defined. Conclusions has been drawn on the energy efficiency of the observed ships.*
**Keywords:** *anchorage, efficiency, energy efficiency, EU - MRV, intensity.*

## INTRODUCTION

Over the past 20 years, the International Maritime Organization (IMO) has been actively working on the decarbonisation of maritime transport. In July 2023, the initial strategy was revised. Now the goal is to achieve zero levels of greenhouse gas emissions from shipping by 2050. In this activity, ports also have an important role, which are called to organize power supply of ships from the shore in an ecological and efficient way.

In the Varna Bay there are two anchorages for the Port of Varna (Figure 1). Summer (A) is used from May 1 to September 30, and Winter (C) from October 1 to April 30.

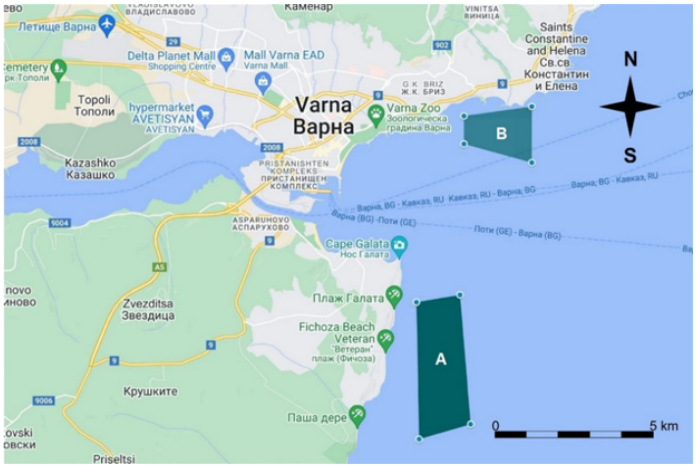


**Figure 1.**
**Two anchorages in Varna Bay [1]**

It has been found [1] that NOx emissions from ships anchored at 1000 m from the source can exceed the norms by approx. 10% at a period of return of 12-15 weeks. These results are obtained from data for ships in berth (B).

In the period 01.05. 2022 - 4.12. 2022, data on ships in berth (A) were collected through the MarineTraffic website (https://www.marinetraffic.com). Despite the definition of summer and winter anchorage, it is clear from practice that this is not a hard rule to be observed.

This study deals with the statistical description of ship characteristics. This will give an idea of the type, size and age of the ships visiting the port of Varna, as well as their characteristics in terms of current energy efficiency.

## VESSEL CHARACTERISTICS STATISTICS

During this period, a total of 395 ships were at anchor, or about 14 ships per week. The percentage state of their load is presented in Figure 2. The loading states according to the site MarineTraffic are laden, ballast,

* **Technical University of Varna, Bulgaria**

partly laden, and 'n/a'. The number of ships under ballast is approximately equal to that with full or partial load. It can be thought that the import and export of cargo from the port of Varna is approximately the same if judged by the condition of the ships serviced in the port.

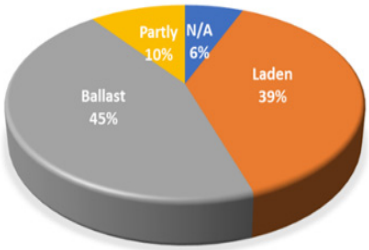


**Figure 2.**
**Percentage of vessel load at anchor in summer anchorage**

**Table 1. Statistical description of 'Stay' time, hours**

| Summary statistics: | | | | | | | |
|---|---|---|---|---|---|---|---|
| Variable | Observations | Obs. with missing | Obs. without | Minimum | Maximum | Mean | Std. deviation |
| Stay,h | 395 | 0 | 395 | 1.100 | 654.770 | 57.975 | 77.503 |

The total stay in hours of these ships is 22900.3 hours, which is 954 days. Statistical description of the 'Stay' time is presented in Table 1. The average duration is ab. 58 hours or a little more than 2 days. These data can also be analysed in terms of the productivity of loading and unloading activities in the port of Varna and the time for this. One of the directions for reducing emissions from shipping is the concept of "Just in Time". The goal is to coordinate the actions of the ship and the port so that the ship arrives at the port just in time-without having to stop.

The distribution of the stay by hours is presented in Figure 3. The highest percentage -71% is the time of stay on the ship up to 66 hours (2 ¾ days).

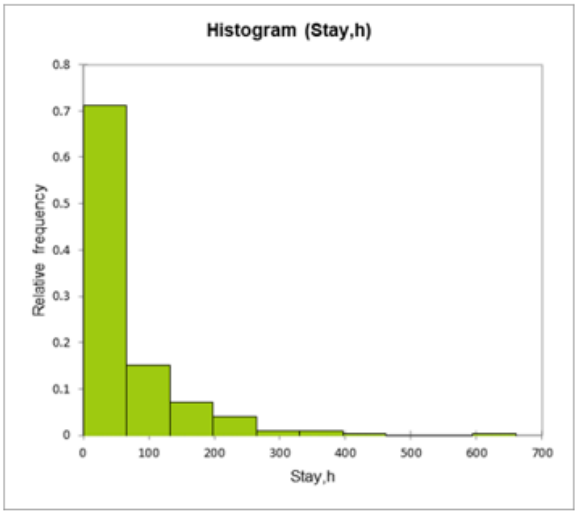


| Lower bound | Upper bound | Frequency | Relative frequency |
|---|---|---|---|
| 0.000 | 66.000 | 281 | 0.711 |
| 66.000 | 132.000 | 60 | 0.152 |
| 132.000 | 198.000 | 28 | 0.071 |
| 198.000 | 264.000 | 16 | 0.041 |
| 264.000 | 330.000 | 4 | 0.010 |
| 330.000 | 396.000 | 4 | 0.010 |
| 396.000 | 462.000 | 1 | 0.003 |
| 462.000 | 528.000 | 0 | 0.000 |
| 528.000 | 594.000 | 0 | 0.000 |
| 594.000 | 660.000 | 1 | 0.003 |

**Figure 3.**
**Distribution of the stay by hours: histogram(left), relative frequency (right)**

A total of 395 stays were made by 256 different ships. In many cases, the same ship makes periodic trips to and from the port of Varna.

Figure 4 shows the distribution of ships by type. More than half (56.4%) are general cargo ships. "Others" includes container ship -2.3%, Ro-Ro -1.2% and Ro/Pax, Heavy Load Carrier, Vehicles Carrier, LPG tanker- each with less than 1%. It is interesting to note the small number of container ships. Probably, the organization of work of the container terminals in the port is such that no downtime is necessary.

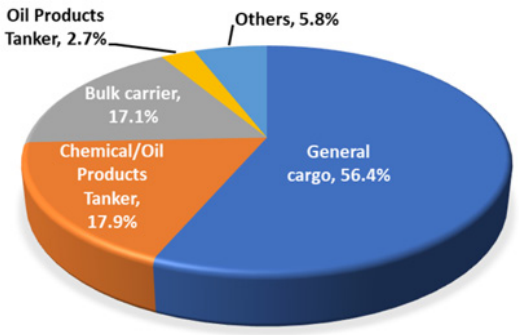


**Figure 4.**
**Distribution of vessels by type**

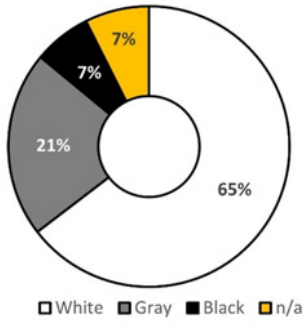


**Figure 5.**
**Distribution of ships by type of administration according to the Paris Memorandum**

For the ships at anchor from the database Equasis [2] are extracted data on the main dimensions, the age of the ships and the maritime administration to which the ship belongs (the flag of the ship). According to the Paris Memorandum, flag administrations are arranged in three lists: White, Grey and Black.

The "White, Grey and Black (WGB) list" [3] categorizes flags based on their performance, ranging from flags of high quality to those with poor performance that are considered high or very high risk. The list is determined by the number of inspections and detentions a flag has had over a period of three years, with a minimum requirement of 30 inspections within that timeframe. The Paris MoU Annual Report publishes a new White, Grey, and Black list every year. Figure 5 shows the distribution of the vessels according to the respective lists.

Most of the half (65%) of the ships are on the "white" list, but nearly 30% are on the "grey" and "black" list. Belonging to an administration is related in some way to the age of the ships. The total statistics for the age of ships as of 2023 are presented in Figure 6. The average age of the ships is 24.2 years, with the largest percentage -25.4% being between the ages of 15 and 20. Only 6.3% of the ships are under 10 years old.

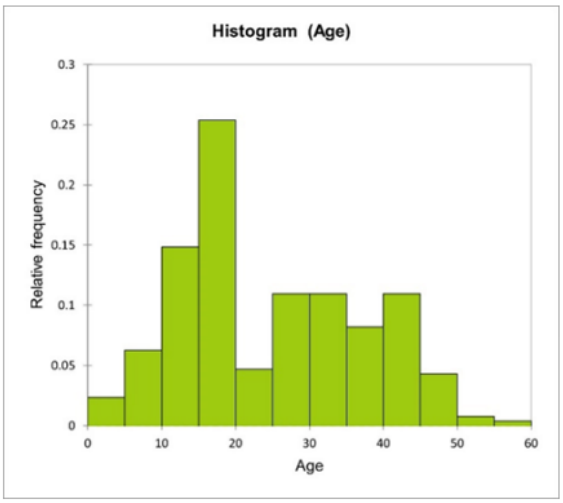


| Lower bound | Upper bound | Frequency | Relative frequency |
|---|---|---|---|
| 0.000 | 5.000 | 6 | 0.023 |
| 5.000 | 10.000 | 16 | 0.063 |
| 10.000 | 15.000 | 38 | 0.148 |
| 15.000 | 20.000 | 65 | 0.254 |
| 20.000 | 25.000 | 12 | 0.047 |
| 25.000 | 30.000 | 28 | 0.109 |
| 30.000 | 35.000 | 28 | 0.109 |
| 35.000 | 40.000 | 21 | 0.082 |
| 40.000 | 45.000 | 28 | 0.109 |
| 45.000 | 50.000 | 11 | 0.043 |
| 50.000 | 55.000 | 2 | 0.008 |
| 55.000 | 60.000 | 1 | 0.004 |

**Figure 6.**
**Distribution of the age of ships: histogram(left), relative frequency (right)**

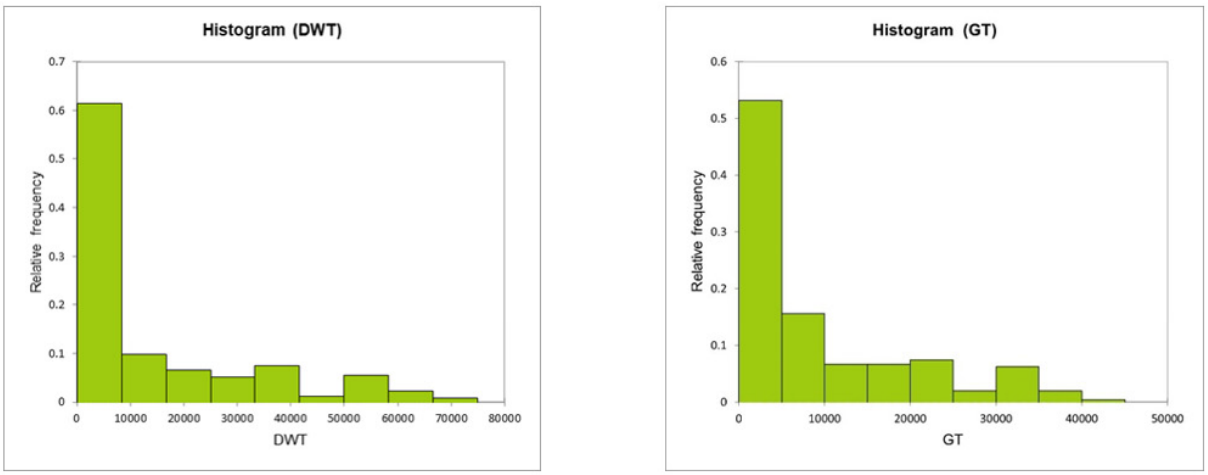


**Figure 7.**
**Distribution of the DWT (left) and GT (right)**

Figure 7 includes distribution of DWT and GT of the ships Hight percentage 61.3% belongs to the ships with DWT up to 8333 t DWT and in the range 8333-16666 t DWT there are 9.8%. It can be concluded that the size of ships visiting the port of Varna is typical for Short Sea Shipping.

The gross tonnage (GT) of the ships is important for the economic benefits of the port activity, but here attention is drawn to another important fact. The largest percentage (53.1%) are ships with GT < 5000. This limit is important because according to the latest requirements, ships with a GT > 5000 are required to carry out a year-round monitoring of $CO_2$ emissions, which is reported and approved by an authorised institution. This is the so-called. MRV - Monitoring, Reporting and Verification procedure [4]-[6]. In practice, for most of the half of the ships anchored in front of the port of Varna there is no information on emissions and consequently cannot be controlled.

## ENERGY EFFICIENCY OF SHIPS

For the analysed ships, data were extracted from the EMSA\THETIS-MRV [7] for the parameters related to $CO_2$ emissions for the last 5 years: 2018-2022. Data available for most ships include: Total fuel consumption [m tonnes]; Total $CO_2$ emissions [m tonnes]; $CO_2$ emissions from all voyages between ports under a MS jurisdiction [m tonnes]; $CO_2$ emissions from all voyages which departed from ports under a MS jurisdiction [m tonnes]; $CO_2$ emissions from all voyages to ports under a MS jurisdiction [m tonnes]; $CO_2$ emissions which occurred within ports under a MS jurisdiction at berth [m tonnes]; Annual Total time spent at sea [hours]; Annual average Fuel consumption per distance [kg / n mile]; Annual average $CO_2$ emissions per distance [kg $CO_2$ / n mile].

For a further in-depth study of the relationship between ship size and annual emissions, the following relative characteristics, most generally related to environmental efficiency and transport efficiency, were statistically examined. A similar analysis of another group of ships is presented in [8]. There are several relative characteristics considered:

**Fuel consumption intensity**

$$FC_{int\ i,j} = \frac{FC_{i,j}}{Time_{i,j}} \quad (1)$$

where

$FC_{i,j}$ is the average fuel consumption in (t) of the ship $i$ in the $j$ year and $Time_{i,j}$ is the time (days), spent in one year of operation of the ship $i$ in the year $j$.

The five-year indicator is presented in Table 2. From the results the indicator has increased over the last two years, increasing the standard deviation, i.e. the values are more scattered than the average.

**Table 2. Descriptive statistics on fuel consumption intensity (t/h) by years**

| Year | Observations | Obs. with missing data | Obs. without missing data | Min | Max | Mean | Std. deviation |
|---|---|---|---|---|---|---|---|
| 2018 | 78 | 0 | 78 | 0.123 | 1.427 | 0.675 | 0.317 |
| 2019 | 79 | 0 | 79 | 0.065 | 1.381 | 0.669 | 0.307 |
| 2020 | 90 | 0 | 90 | 0.119 | 1.670 | 0.717 | 0.347 |
| 2021 | 90 | 0 | 90 | 0.154 | 2.982 | 0.774 | 0.399 |
| 2022 | 110 | 0 | 110 | 0.157 | 3.238 | 0.777 | 0.421 |

**Shipping intensity**

This intensity is measured by the ratio of deadweight of the ship $DWT_i$ to time at sea for the respective ship in different years $Time_{i,j}$ .

$$Shipping_{int\ i,j} = \frac{DWT_i}{Time_{i,j}} \quad (2)$$

In Table 3 is a description of the statistics for the magnitude by years, and in Figure 8 the mean values and the standard deviation are compared. It can be noted that the indicator for the analysed ships has been increasing over the last 2 years, and the standard deviation, i.e. the dispersion of the indicator values relative to the average value has increased. This activity is partly due to the over COVID crisis.

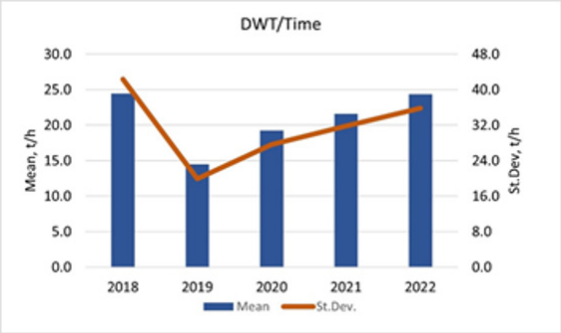


**Figure 8.**
**Mean and standard deviation of shipping intensity by years**

**Table 3. Statistical description of shipping intensity (t/h)**

| Variable | Observations | Obs. with missing data | Obs. without missing data | Minimum | Maximum | Mean | Std. deviation |
|---|---|---|---|---|---|---|---|
| 2018 | 79 | 1 | 78 | 0.952 | 222.008 | 24.452 | 42.353 |
| 2019 | 80 | 1 | 79 | 0.837 | 127.138 | 14.507 | 19.933 |
| 2020 | 90 | 0 | 90 | 1.059 | 180.315 | 19.220 | 27.653 |
| 2021 | 92 | 2 | 90 | 1.055 | 217.957 | 21.608 | 31.829 |
| 2022 | 110 | 0 | 110 | 0.000 | 187.470 | 24.343 | 35.859 |

**$CO_2$ intensity**

The $CO_2$ intensity is defined as the average $CO_{2\ i,j}$ emissions (t) generated per ship *i*, at the time spent in the sea during the year *j*.

$$CO_{2int\ i,j} = \frac{CO_{2i,j}}{Time_{i,j}} \quad (3)$$

Table 4 presents the description of the statistics for the indicator by years, and Figure 9 shows mean values and standard deviation. The indicator for the analysed ships has increased in the last 2 years, increasing the standard deviation too. The increase in this indicator is negative -for a unit of time at sea, ships emit more $CO_2$. These data need further analysis regarding the reasons for this.

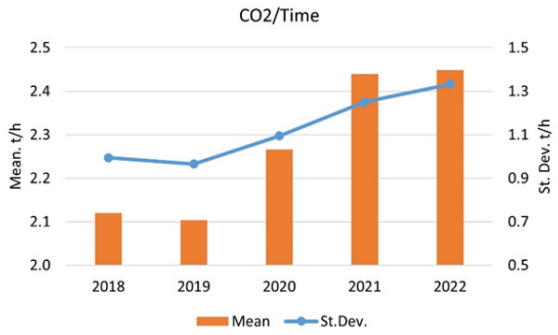


**Figure 9.**
**Mean and standard deviation of $CO_2$ intensity by years**

**Table 4. Statistical description of $CO_2$ intensity (t/h)**

| Variable | Observations | Obs. with missing data | Obs. without missing data | Min | Max | Mean | Std. deviation |
|---|---|---|---|---|---|---|---|
| 2018 | 79 | 1 | 78 | 0.393 | 4.479 | 2.120 | 0.995 |
| 2019 | 80 | 1 | 79 | 0.207 | 4.352 | 2.103 | 0.965 |
| 2020 | 90 | 0 | 90 | 0.375 | 5.235 | 2.266 | 1.094 |
| 2021 | 92 | 2 | 90 | 0.494 | 9.305 | 2.439 | 1.250 |
| 2022 | 110 | 0 | 110 | 0.503 | 10.294 | 2.449 | 1.332 |

**Eco-efficiency**

The Eco-efficiency is defined as the average $CO_{2\,i,j}$ emissions (t) generated per ship $i$, at the year $j$ related to the DWT if the ship.

$$Eco_{eff\,i,j} = \frac{CO_{2_{i,j}}}{DWT_i} \quad (4)$$

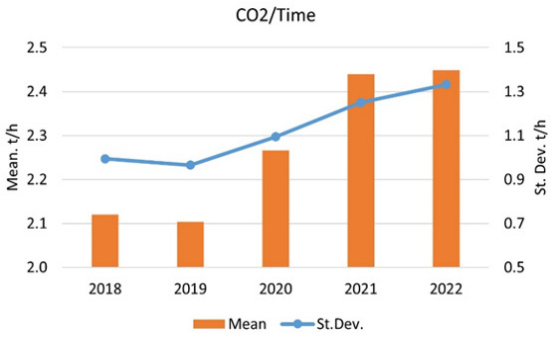


**Figure 10.**
**Mean and standard deviation of eco-efficiency**

**Table 5. Statistical description of eco-efficiency**

| Variable | Observations | Obs. with missing data | Obs. without missing data | Min | Max | Mean | Std. deviation |
|---|---|---|---|---|---|---|---|
| 2018 | 79 | 1 | 78 | 0.393 | 4.479 | 2.120 | 0.995 |
| 2019 | 80 | 1 | 79 | 0.207 | 4.352 | 2.103 | 0.965 |
| 2020 | 90 | 0 | 90 | 0.375 | 5.235 | 2.266 | 1.094 |
| 2021 | 92 | 2 | 90 | 0.494 | 9.305 | 2.439 | 1.250 |
| 2022 | 110 | 0 | 110 | 0.503 | 10.294 | 2.449 | 1.332 |

Table 5 includes description of the statistics for the eco-efficiency by years, and Figure 10 presents the mean and the standard deviation. For the average value, the trend of reduction over the years is also shown, which is a positive circumstance, i.e. for transporting 1 ton of deadweight from the ship less $CO_2$ is emitted. The values for 2021 differ from the trend shown and this circumstance should be further analysed.

**Fuel consumption efficiency**

Fuel consumption efficiency is defined as the fuel consumption of ship $i$ needed for transporting a unit of DWT in during year $j$,

$$FC_{eff\,i,j} = \frac{FC_{i,j}}{DWT_i} \quad (5)$$

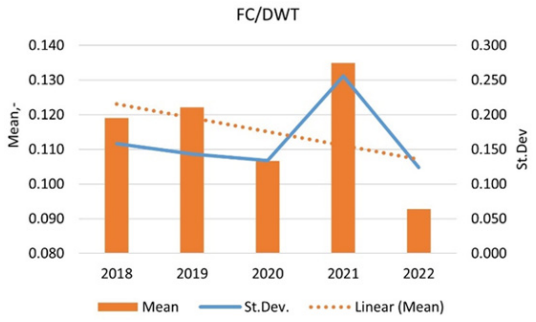


**Figure 11.**
**Mean and standard deviation of fuel consumption efficiency by years**

**Table 6. Statistical description of fuel consumption efficiency**

| Variable | Observations | Obs. with missing data | Obs. without missing data | Min | Max | Mean | Std. deviation |
|---|---|---|---|---|---|---|---|
| 2018 | 79 | 0 | 79 | 0.002 | 1.130 | 0.119 | 0.158 |
| 2019 | 80 | 1 | 79 | 0.007 | 0.902 | 0.122 | 0.143 |
| 2020 | 90 | 0 | 90 | 0.006 | 1.035 | 0.107 | 0.134 |
| 2021 | 92 | 2 | 90 | 0.005 | 2.018 | 0.135 | 0.256 |
| 2022 | 110 | 0 | 110 | 0.004 | 0.988 | 0.093 | 0.124 |

The comparison between years shows a positive trend in the mean value of indicator (Figure 11), i.e. for transporting 1 ton of deadweight from the ship less fuel is consumed. The values for 2021 differ from the trend shown similarly in the previous indicator and should be analysed further. From the histograms (not presented in the paper) for about 90% of the ships, the value of this efficiency is within 0.25 and we can take the value typical for this indicator.

## CONCLUSIONS

Considering the importance of emissions from ships in coastal areas for the quality of life of people, a study of the characteristics of ships anchored in front of the port of Varna was made. The research is in two directions-the technical characteristics of the ships and their energy efficiency. The presented results are based on the analysed 256 ships anchored in a period of 7 months.

About the characteristics of the vessels, the following conclusions were drawn:

- By vessel type, more than half (56.4%) were general cargo vessels. Container ships are only 2.3%, which supports the concept of container transportation-no waiting and fast cargo handling.
- The average age of the ships is 24.2 years, with the largest percentage-25.4% being between the ages of 15 and 20. Only 6.3% of the ships are under 10 years old.
- Most of the half (65%) of the ships are from the "white" list of the flag administrations, but nearly 30% are from the "grey" and "black". Belonging to an administration is related in some way to the age of the ships.
- In the range up to 8333 t DWT there are 61.3% of all ships and in the range from 8333-16666 t DWT -9.8%. The size of ships visiting the port of Varna is typical for Short Sea Shipping.
- The largest percentage (53.1%) are ships with GT < 5000. This limit is important because according to the IMO requirements, for ships with a GT > 5000, year-round monitoring of $CO_2$ emissions is required, which is reported and approved by an authorised institution (MRV).

Conclusions regarding the defined relative intensity and efficiency are:

- In terms of intensity, there is an increase in fuel consumption and $CO_2$ emissions per unit time at sea in recent years, which is negative, and an increase in deadweight per unit time, which is a positive trend. It should not be forgotten that these indicators refer to a heterogeneous group of ships anchored in front of the port of Varna.
- For the last two years analysed in the study (2021-2022), the efficiency has improved, i.e. for transporting a ton of deadweight, fewer emissions and less fuel consumption are emitted. For the latter value, a typical value of 0.25 can be assumed.

## ACKNOWLEDGEMENTS

Part of the presented results were obtained during the development of the master's thesis of Beatris Todorova that was successfully defended in 2024 under the supervision of the author of this paper.

**REFERENCES**

[1] G a r b a t o v, Y, Georgiev P, Fuchedzhieva, I. Extreme Value Analysis of NOx Air Pollution in the Winter Seaport of Varna. Atmosphere. 2022; 13(11):1921. doi.org/10.3390/atmos13111921.
[2] E q u a s i s. https://www.equasis.org/EquasisWeb/public/HomePage (last assessed on 15 September 2024).
[3] Paris MoU. White, Grey and Black List. https://parismou.org/Statistics%26Current-Lists/white-grey-and-black-list (assessed on 1 September 2024).
[4] EU 2015/757. Regulation on the monitoring, reporting and verification of greenhouse gas emissions from maritime transport, and amending Directive 2009/16/EC, OJ L 123 19.5.2015, p. 55.
[5] EU 2003/87/EC. Regulation of the Establishing a system for greenhouse gas emission allowance trading within the Union and amending Council Directive 96/61/EC, OJ L 275, 25.10.2003, p.32.
[6] EU 2023/1805. Regulation of the use of renewable and low-carbon fuels in maritime transport, and amending Directive 2009/16/EC, OJ L 234, 22.9.2023, p. 48.
[7] EMSA\THETIS - MRV. (https://mrv.emsa.europa.eu/#public/emission-report).
[8] G a r b a t o v, Y., Georgiev, P. (2023). Principal component analysis of containership traffic in the Black Sea. Brodogradnja, 74 (4), 73-87. https://doi.org/10.21278/brod74404.

# BENEFITS AND HAZARDS OF ALTERNATIVE FUELS IN ENERGY EFFICIENT SHIPS

**Aleksandar ENEV***

**Abstract**. *The decision made by the International Maritime Organization (IMO) to globally limit the sulphur content of ship fuel to 0.5 per cent starting from 1 January 2020, along with the recently adopted resolution to achieve a 50 per cent reduction in greenhouse gas (GHG) emissions by 2050, will have a profound impact on the future composition of ship fuels. This paper analyses the status of production and use of alternative fuels, existing legislation and possible hazards.*
**Keywords:** *alternative fuels, GHG, LNG, ammonia, methanol hydrogen.*

## INTRODUCTION

In 2011, IMO adopted amendments to MARPOL Annex VI to mandate technical and operational energy efficiency measures to reduce the amount of $CO_2$ emissions from international shipping [1]. The Energy Efficiency Design Index (EEDI) and the Ship Energy Efficiency Management Plan (SEEMP) entered into force on 1 January 2013. Those measures represent the first global mandatory GHG-reduction regime for an international industry sector and have been driving energy efficiency improvements across the global fleet for more than a decade. Goal-based and technology-neutral regulations have incentivized the use of energy-efficient technologies such as hull air lubrication, wind assisted propulsion, waste heat recovery, etc. [1]. The requirements for new ships are implemented to existing ships as well according to Energy Efficiency Existing Ship Index (EEXI).

The decision made by the International Maritime Organization (IMO) to globally limit the sulphur content of ship fuel to 0.50 % starting from 1 January 2020, trying to achieve goals of initial IMO GHG strategy. IMO established even stricter limit of 0.10% m/m in emission control areas (ECAs) [2]. In addition to the four existing ECAs in 2022, MEPC 79 adopted amendments to designate the entire Mediterranean Sea as an emission control area for Sulphur Oxides (SOx-ECA) and particulate matter, meaning that ships will have to comply with more stringent controls on sulphur oxide emissions from 1 May 2025 [3].

The initial GHG strategy was revised in 2023, and new objective is to rapidly reduce greenhouse gas emissions from international shipping and achieve near-zero emissions by or around the year 2050 [4].

One of the ways to achieve these goals is the use of alternative fuels. DNV has identified LNG, LPG, methanol, biofuel, and hydrogen as the most promising alternative fuels for shipping. Additionally, they believe that battery systems, fuel cells, and wind-assisted propulsion hold potential for use in ships as new technologies [5].

The article examines the state of use of alternative fuels, the existing rules, implemented projects and some hazards associated with them.

## CURRENT STATUS OF ALTERNATIVE FUELS USED

Alternative marine fuels are divided into 3 categories [6]: Fossil fuels, Carbon neutral and Carbon free (Figure 1).

### Liquefied natural gas (LNG)

Liquefied natural gas is classified as a non-renewable energy source and is still considered a carbon-based fuel. Although after-treatment methods can help decrease the emission of methane from exhaust gas, there are still unresolved technical issues surrounding this. It is important to pay special attention to the impact of storing and arranging the required gas onboard, as these factors can influence the design of vessels. As a result, using LNG as fuel for new ship constructions is generally associated with higher costs. This is particularly relevant

* **Technical University of Varna, Bulgaria**

for projects involving container vessels, car carriers, gas carriers, chemical tankers, very large crude carriers (VLCC), ro-ro vessels, and bulk carriers above Capesize.

Many ship owners and operators are considering LNG as a retrofitting option. This is because LNG can be a cost-effective solution that allows existing vessels to be used for a longer period while also meeting the energy efficiency requirements set by the IMO, specifically the Energy Efficiency Existing Ship Index (EEXI) and Carbon Intensity Indicator (CII). Furthermore, retrofitting with LNG can enhance the performance of the vessels taking also into account still higher prices [7].

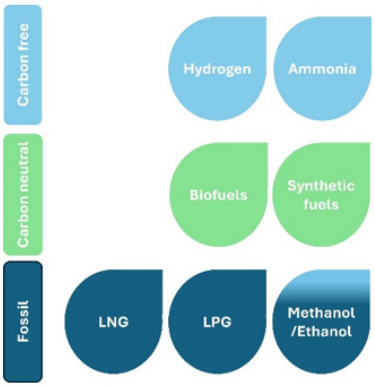


**Figure 1.**
**Alternative marine fuels (based on [6])**

**Liquefied petroleum gas (LPG)**

LPG, a well-established propellant, boasts a noteworthy decrease in $CO_2$ emissions. While it demands less initial investment compared to LNG as fuel, it does pose a hazard due to its high flammability, especially in the case of leaks. It is important to mention that marine four-stroke engines powered by LPG have not yet entered the market.

**Methanol**

Methanol is a hazardous chemical that requires safety precautions due to its flammability and toxicity. After gaining experience from several years on methanol carriers, using methanol as a fuel on merchant ships can be achieved in the short to mid-term. It is environmentally friendly, can dissolve in water, and can be stored as a liquid at regular temperatures. When produced from fossil sources, it may not offer a significant reduction in $CO_2$ emissions compared to traditional fuel oils. However, it could be competitively produced as a biofuel or from renewable sources and low carbon hydrogen as an e-fuel. Nevertheless, there are challenges associated with methanol, such as its low energy content, low flashpoint, and toxicity with prolonged exposure.

**Biofuels**

The Biofuels are made by biomass (plant and/or animal materials or used cooking oils). All vessel types - large or small, deep-sea or short-sea trading, gas-fuelled or traditionally liquid fuelled - could use biofuels without requiring major technical, safety or design adjustments. They can also be mixed with fossil fuels, to reduce emissions without needing full dependency on biofuels. However, the resources for producing second- and third-generation biofuels, must be developed to supply the volumes needed. Blended or unblended biodiesels are an achievable mid-term solution in the global CO2 reduction chain. They are both simple and safe to use, and characteristically close to standard fuel oil, with a flashpoint above 60°C. It would require minimal investment to keep in line with evolving regulations and ensure crew safety.

**Ammonia**

Ammonia has the potential to contribute to marine decarbonization as it produces zero carbon emissions. Currently, there are efforts underway to develop ammonia-powered two-stroke engines for use as a fuel. However, there are several safety challenges associated with using ammonia as a fuel that need to be addressed before it can be used on ships. These challenges include its toxicity at low concentrations and its corrosive

nature. Furthermore, even small amounts of released ammonia can cause discomfort due to its pungent smell. Additionally, the combustion of ammonia should be carefully controlled to minimize the release of nitrous oxide ($N_2O$), a greenhouse gas with 273 times the global warming potential of $CO_2$. Furthermore, ammonia has a lower energy density compared to conventional fuel oils, which significantly reduces the available space onboard for cargo transportation.

**Hydrogen**

Hydrogen can be produced from renewable electricity and is considered a zero-carbon fuel. It is currently being tested on inland navigation vessels and short-sea ships. However, hydrogen is a highly flammable and explosive molecule, requiring safety precautions to prevent hazards and minimize risks. It also has a low volumetric density, meaning that ships need to store large quantities of hydrogen or adapt their operations accordingly. Advantages Hydrogen is another promising option, as a potentially zero-carbon fuel (when sourced from renewable electricity via electrolysis). The technology to integrate fuel cells on larger vessels, such as cruise ships and containerships, is being developed and adapted to their needs rapidly. For the moment, fuel cells are mainly envisioned for powering the auxiliary systems of larger vessels, offering a zero-emissions solution for ships idling at port or using auxiliary power. The next major technological push will entail scaling up to fully power ships' primary propulsion systems.

Table 1 summarises the characteristics of alternative fuels [6].

**Table 1. Typical characteristics of alternative fuels**

| | LNG | LPG | Methanol | Bio-Diesel | Ammonia | Hydrogen |
|---|---|---|---|---|---|---|
| Physical properties for storage | Liquid at -162°C | Liquid at 18 bar or at -42°C or semi -20°C at 7 bar | Liquid (up to 65°C) | Liquid | Liquid at -33°C | Compressed gas at > 250 bar or liquid at -253°C |
| Fuel tank size for same energy content as MDO | 1.8 times | 1.5 times | 2.5 times | 1 time | 3 times | 5-7 times |
| Fuel Containment System (Cryo/ conventional) | CRYO | COLD | CONV | CONV | COLD | CRYO |
| Flammability limits in air (%V/V) | 5% - 15% (Methane) | 1% - 11% | 6% - 36.5% | / | 15% - 28% | 4 - 75% |
| Minimum Ignition Energy (mJ) | 0.3 (Methane) | 0.25 | 0.14 | / | 8 to 680 | 0.017 |
| Flashpoint (°C) | -188 | -104 | 12 | > 61 | 132 | ---- |
| Density of liquid phase (kg/m$^3$) | 450 | 493 | 790 | 900 | 696 | 71 |
| LCV* (MJ/kg) | 50 | 46.4 | 19.9 | 42.7 | 18.6 | 120 |
| Energy density (MJ/L) | 21.2 | 26.5 | 15.7 | 35.7 | 12.7 | 8.5 |

* The lower calorific value LCV measures the released energy when a fuel is burnt.

Table 2 summarises the current (September 2024) number of ships using alternative fuels [8] and Figure 2 presents the growth of alternative fuel uptake by number of ships. Above the bars is the total number of vessels.

**Table 2. Number of ships using alternative fuels**

| Project | LNG | LPG | Methanol | $H_2$ Fuel Cell | $H_2$ ICE | Ammonia |
|---|---|---|---|---|---|---|
| In Operation | 590 | 142 | 53 | 1 | 3 | 2 |
| In order | 564 | 116 | 294 | 20 | 10 | 28 |
| Total | 1154 | 258 | 347 | 21 | 13 | 30 |

ICE = internal combustion engine

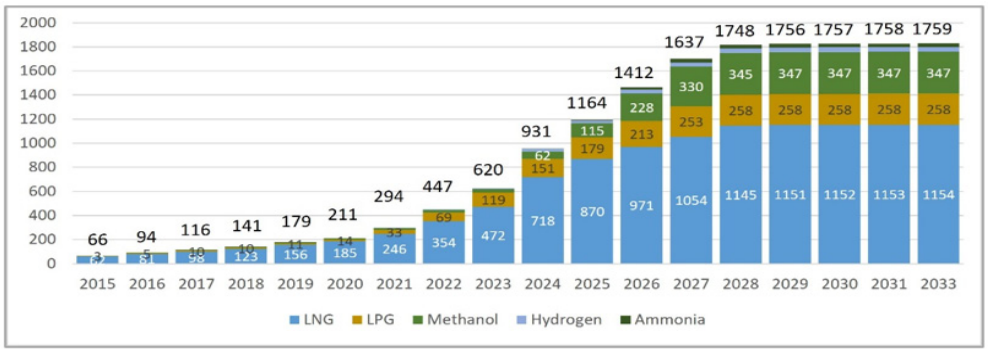


**Figure 2.**
**Growth of alternative fuel uptake by number of ships (based on [8])**

## FUEL PRODUCTION

In addition to technological solutions for the use of alternative fuel, an important circumstance for their use is the availability. Information will be provided regarding the production of certain alternative fuels.

### Ammonia

Two low-emissions pathways exist for producing ammonia today by combination of hydrogen and nitrogen from air using the Haber-Bosh process. The Haber-Bosch[1] process involves the direct combination of nitrogen from the air with hydrogen under immense pressure and relatively high temperatures to obtain ammonia. By utilizing a catalyst predominantly composed of iron, the reaction can occur at a lower temperature. Depending on the method of obtaining hydrogen, we have two options: Blue ammonia and Electro-ammonia (Figure 3).

For the first option blue hydrogen is obtained by conventional methane reforming, combined with CO2 capture and storage. In the second option, hydrogen is the result of electrolysis of water powered by renewable sources. The ratio between the produced quantities of the two types of ammonia is 84.86% against 15.14% in favour of E-ammonia [8]. The production capacity of the leading countries is presented in Figure 1.

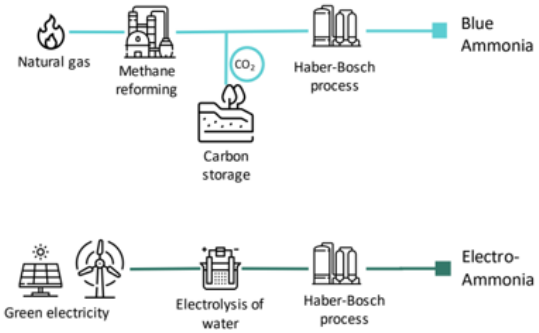


**Figure 3.**
**Options for ammonia production [9]**

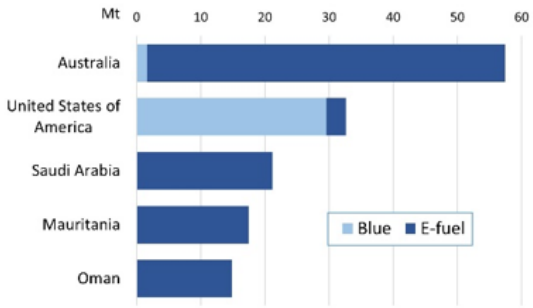


**Figure 4.**
**Production capacity of the leading countries**

### Biofuel

DNV statistics include four biofuels: Blank, Bio_MGO, Bioethanol, Biokerosene. The share in production if everyone is presented in Figure 5 and the capacity of leading countries in Figure 6.

[1] https://www.britannica.com/technology/Haber-Bosch-process

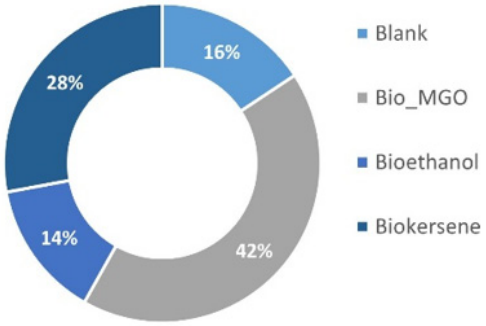


**Figure 5.**
**Share in the production for Biofuels [8]**

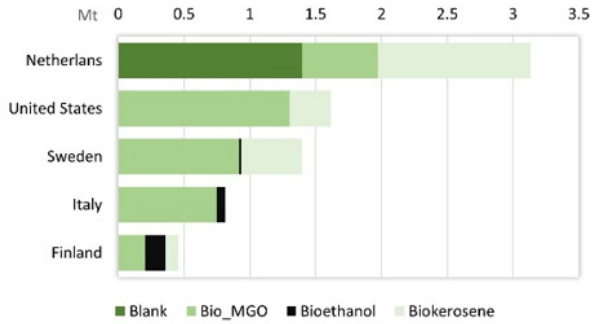


**Figure 6.**
**Production capacity for Biofuels of the leading countries [8]**

**Methanol**

Bio-methanol is derived from renewable sources such as landfill gas, sewage plants, and animal manure farms. It can also be produced from biomass feedstock, including forestry and agricultural waste, municipal solid waste, and black liquor from the pulp and paper industry [10]. Green methanol, also known as e-methanol, is derived from the combination of green hydrogen and $CO_2$ captured from renewable sources. Green hydrogen refers to hydrogen produced using renewable electricity, while $CO_2$ is obtained via bioenergy with Carbon Capture and Storage or Direct Air Capture. The share of production capacity between the two types is 63.6% and 36.4% in favour of e-methanol. Country leader is China with 3.14 Mt Bio methanol and 3.73 Mt E-ethanol yearly production.

**Hydrogen**

At present, hydrogen production relies primarily on fossil fuels such as natural gas (blue hydrogen) [11]. The process of blue hydrogen involves separating natural gas into hydrogen and CO2 through Steam Methane Reforming (SMR) or Auto Thermal Reforming (ATR), followed by capturing and storing the CO2. However, in the future, there is potential for hydrogen to be produced on a larger scale using renewable energy sources. There are several pathways for producing green hydrogen: electrolysis (e-fuel), direct solar production, biomass fermentation, and thermochemical biomass conversion (bio-based). Among these, electrolysis using renewable electricity is currently considered the most suitable due to technological advancements and limited availability of sustainable biomass.

Currently, global e-fuel production capacity is 72 MT or 87.93% of the total capacity [8]. The leading countries by capacity are represented in Figure 7.

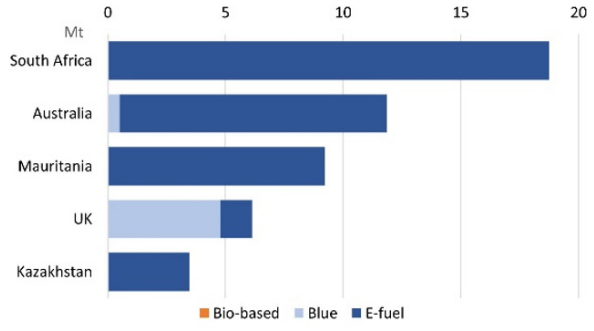


**Figure 7.**
**Production capacity for hydrogen of the leading countries [8]**

The demand for hydrogen for producing ammonia for shipping could represent 3.7%-7 % of the expected total global hydrogen demand in 2030 and reach 8.3%-17.5 % by 2050. This poses pressure to scale hydrogen infrastructure to meet increasing demand from the shipping industry at the required pace.

## RULES AND REQUIREMENTS FOR ALTERNATIVE FUELLED SHIPS

The International Code of the Construction and Equipment of Ships Carrying Liquefied Gases in Bulk is mandatory since 1986 - adopted by MSC.5(48), SOLAS chapter VII [12] amended by Resolution MSC. MSC.370(93) [13]. The Code regulates LNG fuelled ships prior to adoption of IGF Code. It includes stringent requirements for fuel piping, fuel tank location, Emergency Shut Down (ESD) engine room, etc. (Figure 8).

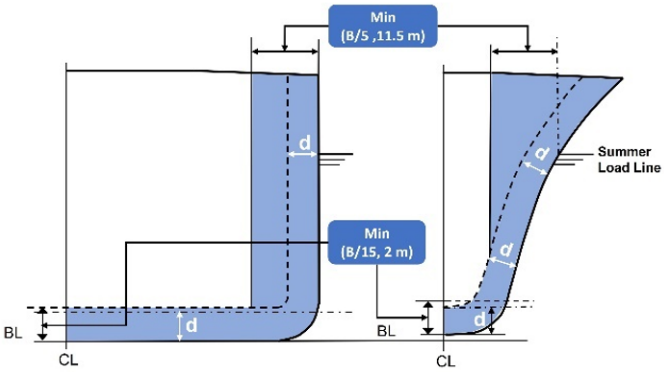


**Figure 8.**
**Limits for tank location [7]**

The International Code of Safety for Ship Using Gases or Other Low-flashpoint Fuels (IGF Code) entered into force in 2017 was adopted by MSC 391.95 [14]. It applies to all ships, other than those covered by IGC Code, operating with gas or low-flashpoint liquids. The Code provides industry standards for ships that use fuels with a flashpoint of less than 60°C.

The boundary of the fuel tank should not be located closer than distance *d* to the shell depending on the 100% of the gross design volume of the individual fuel tank at 20°C, including domes and appendages $V_C$.

$$V_c \leq 1{,}000 m^3 \qquad d = 0.80\ m$$

$$1{,}000\ m^3 < V_c < 5{,}000 m^3 \qquad d = 0.75 + \frac{V_c 0.2}{1{,}000}\ m$$

$$5{,}000\ m^3 \leq V_c < 30{,}000 m^3 \qquad d = 0.80 + \frac{V_c}{25{,}000} m$$

$$30{,}000\ m^3 \leq V_c \qquad d = 2.00\ m$$

The possible location of the fuel tanks is shown in Figure 9 - Figure 14.

In addition to these Codes, the Classification societies issued own rules and guidelines for ships using alternative fuels (Table 3).

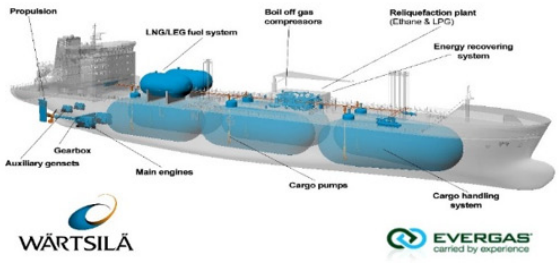


**Figure 9.**
**Scheme of the 27,500 cbm multi-gas carrier (https://www.wartsila.com)**

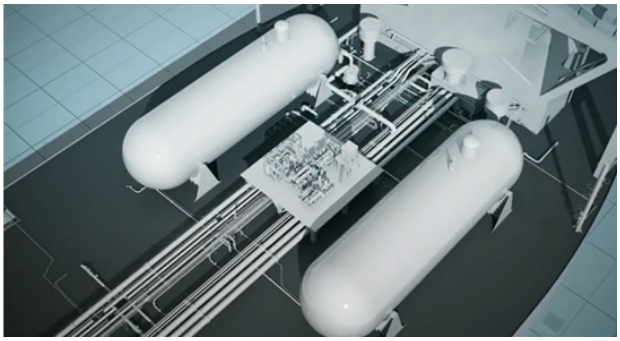

**Figure 10.**
**LNG Fuel Gas Supply Systems (FGSS) (https://www.mhi.com/)**

**Figure 11.**
**Aft ward location of the fuel tanks**
**(http://en.gh-lgm.com)**

**Figure 12.**
**LNG fuel tank and the foundation**
**(https://www.jcnnewswire.co)**

**Figure 13.**
**Forward location of the fuel tanks**
**(http://en.gh-lgm.com)**

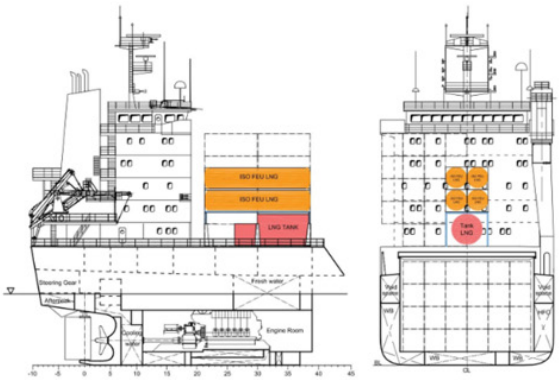

**Figure 14.**
**Retrofitted multipurpose ship for LNG as fuel**
**(project) [7]**

**Table 3. Rules and guidelines of some Classification Societies**

| Classification Society | Rules (Guidelines) | Source |
|---|---|---|
| ABS | Advisory on gas and other low flashpoint fuels | [15] |
| BV | NR678 Hydrogen-Fuelled Ships<br>NR467 Rules for the classification of steel ships<br>NR529 Gas fuelled ships<br>NR670 Methyl/ethyl alcohol fuelled ships<br>NR671 Ammonia-fuelled ships - tentative rules<br>NI647 LPG-fuelled ships<br>NR547 Ships using fuel cells | [16] |
| ClassNK | Guidelines for Ships Using Alternative Fuels (Edition 3.0)" | [17] |

## HAZARDS AND SAFETY CONSIDERATIONS

Review and analysis of fire and explosion accidents in maritime transport finds that in 48% of cases the cause is human error [18]. Research has indicated that a significant portion, specifically 31%, of fire and explosion incidents occur due to unintentional fuel or lubricating oil spillages in the engine room. To mitigate the risk of ignition during such accidental leaks, it is recommended to replace these highly flammable substances with alternative fuels that are less prone to catching fire.

**Table 4. Ignition and combustion properties of some alternative fuels [18]**

| Material | Gas Calorific Value (MJ/kg) | Octane number | Flash point (°C) | Flammable limits (%, v/v) | Auto ignition temperature (°C) | Resistivity (Ωm) | Minimum Ignition Energy (mJ) |
|---|---|---|---|---|---|---|---|
| Ethanol | 29.73 | 100 | 13 | 3.3-19 | 363 | 7.4 x 10 $^{6}$ | f |
| Methanol | 22.72 | 99 | 11 | 6-36 | 385 | 3 x 10 $^{3}$ | 0.14 |
| LNG | 19.98 | > 100 | -188 | 5-15 | 537 | Gas | 0.28 |
| CrNG | 19.98 | 120 | Gas | 5-15 | 537 | N/A | 0.28 |
| LPG propane | 50.49 | 4 | Gas | 2.1-9.5 | 450 | Gas | 0.25 |
| LH2 | 158.9 | f | Gas | 4-75 | 500 | $10^{17}$ | 0.017 |
| Hydrogen | 158.9 | f | Gas | 4-75 | 500 | N/A | 0.017 |

*f = No data available.

A review of explosion accident calculation on LNG-fuelled ships is presented in [19]. The potential harm or loss caused by the cryogenic impact (effects on the skin like a thermal burn), the extremely high temperature of the jet fire (a high temperature flame of burning fuel), or Vapor Cloud Explosion (VCE) is considered. These consequences, known as the "Domino Effect," could occur sequentially.

It was found that a greater extent of the use of alternative fuels exists in the bunkering of a ship. In a survey [20] , the likelihood of fuel release during bunkering of liquefied natural gas (LNG), liquid hydrogen (LH2), and liquid ammonia (LNH3) was analysed. There were two scenarios considered for the release of fuel: one involving a release of 0.3 $m^3$ and the other a release of 100 kilograms. In both scenarios, LH2 completes the evaporation process first, followed by LNG. However, it is worth noting that the evaporation rate of LNH3 is significantly slower compared to LH2 and LNG. Detailed descriptions of the distribution of individual fuels are made considering the wind and the dimensions of the ship. When it comes to post-release safety, both LNG and LH2 present a similar level of danger considering evaporation and dispersion outcomes. However, compared to LNG and LH2, LNH3 poses a significantly higher level of danger.

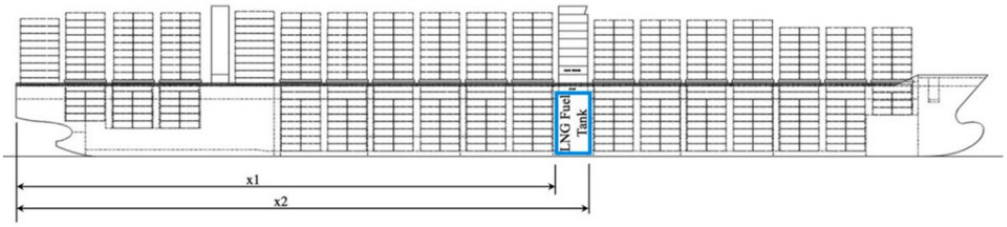


**Figure 15.**
**LNG fuelled containership and tank location [21]**

Recently published paper [21] presents a safety analysis of a hypothetical 9,000 TEU LNG-fuelled containership (Fig) in ship-ship collisions. The analysis uses LS-DYNA nonlinear finite element methods to evaluate the crashworthiness of the vessel's structure. A total of 12 collision scenarios were examined, considering different loading conditions and collision speeds of the striking ship, while the struck ship was stationary. The main conclusions are:

- The inner hull plates surrounding the LNG fuel tank in the struck ship can be damaged when colliding with a ship of the same size. The collision speed required for this damage to occur is 3.3, 3.6, 4.0 knots or higher at full load, 50% partially load and in the ballast load condition.

- Given that containerships typically operate at speeds exceeding 20 knots, there exists a significant potential for damage to the LNG fuel tank in the event of ship-ship collisions. This could result in leaks of LNG fuel, ultimately leading to severe and catastrophic consequences.

## CONCLUSIONS

One way to reduce emissions from shipping is to use alternative fuels. The main activities are related to both improving the technologies for their use and ensuring sufficient production to meet the rapid building of new ships. The study provides up-to-date information on the characteristics and production of prospective alternative

fuels- ammonia, biofuel, methanol, hydrogen, describes the basic rules of Classification Societies for their use, and highlights some problems and current research on the hazards and safety of shipping.

To achieve the goal of a larger scale study of the strength of ship structures after a modification of the propulsion system powered by alternative fuel, a more thorough analysis of accident cases both on the shore and on board the ship is necessary.

**REFERENCES**


[1] I m p r o v i n g the energy efficiency of ships. Available online: https://www.imo.org/en/OurWork/Environment/Pages/Improving%20the%20energy%20efficiency%20of%20ships.aspx.

[2] IMO 2020 - cutting sulphur oxide emissions. Available online: https://www.imo.org/en/MediaCentre/HotTopics/Pages/Sulphur-2020.aspx.

[3] E a s o n, C. IMO approves plans for whole Med Sea SOx ECA in 2025. https://fathom.world/imo-approves-plans-for-whole-med-sea-sox-eca-in-2025/ (Accessed online 12 March 2024).

[4] MEPC. Resolution MEPC.377(80). 2023 IMO strategy on reduction of GHG emissions from ships. London, 7 July 2023.

[5] DNV.2018. Alternative fuels: the options. Available online: https://www.dnv.com/expert-story/maritime-impact/alternative-fuels/ (accessed August 2024).

[6] BV. White Paper. Alternative Fuels Outlook for Shipping, September 2022.

[7] Y a l a m o v, D., Georgiev, P., & Garbatov, Y. (2023, June 30). Retrofitting measure of an ageing multi-purpose ship exposed to short-sea LNG operation. ANNUAL JOURNAL OF TECHNICAL UNIVERSITY OF VARNA, BULGARIA, 7(1), 68-87. https://doi.org/10.29114/ajtuv.vol7.iss1.293.

[8] V e r a c i t y DNV. Alternative Fuels Insight Platform (accessed on 10 September 2024).

[9] M a e r s k Mc-Kinney Moller Center. Ammonia as a marine fuel. Prospects for the shipping industry. February 2022.

[10] M e t a n e x. Methanol Types and Production Methods. https://www.methanex.com/about-methanol/how-methanol-is-produced/.

[11] EMSA.2023. Potential of hydrogen as fuel for shipping.31 August 2023.

[12] MSC. Resolution MSC.5(48). Adoption of the international code for the construction and equipment of ships carrying liquefied gases in bulk (IGC code).17 June 1983, London.

[13] MSC. Resolution MSC.370(93). Amendments to the international code for the construction and equipment of ships carrying liquefied gases in bulk (IGC code). 22 May 2014, London.

[14] MSC. Resolution MSC.391(95). Adoption of the International Code of Safety for Ships using Gases or other Low-flashpoint Fuels (IGF Code). 11 June 2015, London.

[15] ABS. Advisory on gas and other low flashpoint fuels.

[16] BV. https://marine-offshore.bureauveritas.com/rules-guidelines.

[17] ClassNK. https://www.classnk.or.jp/hp/en/hp_news.aspx?id=11502&type=press_release&layout=1.

[18] B a a l i s a m p a n g, T., Abbassi, R. Garaniya, V., Khan, F., Dadashzadeh, M. Review and analysis of fire and explosion accidents in maritime transportation, Ocean Engineering, Volume 158, 2018, Pages 350-366, ISSN 0029-8018, https://doi.org/10.1016/j.oceaneng.2018.04.022.

[19] N u b l i, H., Fajri, A., Prabowo, A.R., Khaeroman, Sohn, J.M. CFD implementation to mitigate the LNG leakage consequences: A review of explosion accident calculation on LNG-fueled ships, Procedia Structural Integrity, Volume 41, 2022, Pages 343-350, ISSN 2452-3216, https://doi.org/10.1016/j.prostr.2022.05.040.

[20] F a n, H., Xu, X., Abdussamie, N., Chen, P. Sh-L., Harris, A. Comparative study of LNG, liquid hydrogen, and liquid ammonia post-release evaporation and dispersion during bunkering, International Journal of Hydrogen Energy, Volume 65, 2024, Pages 526-539, ISSN 0360-3199, https://doi.org/10.1016/j.ijhydene.2024.04.039.

[21] K i m, S. K, Park, S-In, Paik, J.K. 2022. Collision-accidental limit states-based safety studies for a LNG-fuelled containership, Ocean Engineering, Volume 257, 2022, 111571, ISSN 0029-8018, https://doi.org/10.1016/ j.oceaneng.2022.111571.

# HYDROGEN AS THE FUTURE OF SUSTAINABLE MARITIME ENERGY: A COMPARATIVE ANALYSIS OF HYDROGEN-BASED FUEL CELLS FOR MARINE APPLICATIONS

**Kaloyan VANGELOV***

**Abstract**. *The maritime industry faces increasing pressure to reduce its greenhouse gas emissions and meet the decarbonization targets set by the International Maritime Organization. Hydrogen-based fuel cells have appeared as a promising solution to help this transition by offering zero-emission energy sources for ships. This paper explores the potential of hydrogen fuel cells, in maritime applications. A comparative analysis is conducted to assess the efficiency, emissions, cost, and safety of these technologies in contrast to other alternative marine fuels like LNG and battery-electric solutions. The paper highlights key challenges in hydrogen production, storage, and bunkering at ports, while also outlining opportunities for innovation and policy support to accelerate the integration of hydrogen fuel cells into the global maritime fuel supply chain.*
**Keywords:** *fuel-cells, hydrogen, maritime energy, GHG.*

## INTRODUCTION

The maritime industry oversees approximately 2.5% of global greenhouse gas (GHG) emissions, making it a significant contributor to climate change [1]. This contribution is expected to increase with the growing demand for global trade and shipping. According to the International Maritime Organization (IMO), without significant intervention, maritime emissions could increase by up to 50% by 2050 due to the expansion of international trade routes and the rising number of vessels in operation [2]. The initial GHG strategy was revised in 2023, and new objective is to rapidly reduce greenhouse gas emissions from international shipping and achieve near-zero emissions by or around the year 2050 [3].

Traditional marine fuels, such as heavy fuel oil (HFO) and marine diesel oil (MDO), are major sources of carbon dioxide ($CO_2$), nitrogen oxides ($NO_x$), and sulphur oxides ($SO_x$) emissions, which not only contribute to global warming but also cause air pollution, acid rain, and respiratory health problems in coastal communities [4]. These pollutants contribute to the environmental degradation of both the atmosphere and ocean ecosystems, further driving the urgency for cleaner energy solutions in the shipping industry.

Moreover, the introduction of new regulations, such as the IMO‘s sulphur cap, highlights the urgent need for alternative, low-carbon fuels to reduce the maritime industry‘s environmental footprint. Hydrogen, alongside other sustainable energy sources, offers a promising solution to significantly reduce GHG emissions and align the maritime sector with global climate targets [5]

### Importance of the IMO Regulations

To combat the growing environmental challenges posed by the shipping industry, IMO has introduced stringent regulations aimed at reducing the industry’s carbon footprint. One of the most ambitious initiatives (so cold initial strategy) is the IMO’s 2050 decarbonization strategy, which seeks to reduce GHG emissions by at least 50% compared to 2008 levels by mid-century [6]. This long-term strategy is designed to align with the global climate targets set by the Paris Agreement, aiming for the complete phase-out of GHG emissions in shipping by the end of the century.

The IMO’s initial GHG strategy, adopted in 2018, requires member states to implement both short-term and long-term measures to reduce emissions. These include technical and operational improvements, such as energy efficiency measures and speed reductions, as well as the adoption of low- and zero-emission fuels [2]. Hydrogen is emerging as a key solution in this transition due to its ability to power ships without emitting $CO_2$, $NO_x$, $SO_x$, or particulate matter, making it a promising candidate for achieving the IMO’s ambitious decarbonization goals [7]

*** Technical University of Varna, Bulgaria**

Hydrogen fuel cells are seen as a front-runner in the race to decarbonize maritime transport. By offering zero-emission operations, hydrogen has the potential to drive the industry toward a sustainable future while meeting the stringent regulatory requirements imposed by the IMO. As the shipping industry moves closer to the 2050 target, investment in hydrogen infrastructure and technologies will be essential to ensure a successful transition to cleaner energy sources [8]

**Hydrogen as a clean energy alternative**

Hydrogen stands out as a versatile and clean energy carrier with the potential to significantly reduce maritime emissions. When used in fuel cells, hydrogen generates electricity through an electrochemical process, producing only water vapor as a by-product and emitting no $CO_2$ or other harmful pollutants [7]. This makes hydrogen an attractive choice for decarbonizing the shipping industry, particularly considering international efforts to curb GHG emissions.

One of hydrogen's key advantages is its ability to be produced through renewable energy sources, such as wind, solar, or hydropower, creating what is known as "green hydrogen" [5]. This process ensures that hydrogen's lifecycle stays fully sustainable, from production to consumption. By using renewable electricity to split water into hydrogen and oxygen via electrolysis, green hydrogen offers a zero-emission alternative to traditional marine fuels like HFO and MDO, which are responsible for significant $CO_2$, $NO_x$, and $SO_x$ emissions [1].

In addition to its environmental benefits, hydrogen's adaptability allows it to be used across a variety of vessel types, from small ferries to large cargo ships. Its application in fuel cells, provides flexible and scalable solutions for the maritime industry [9]. As the shipping industry looks to follow increasingly stringent environmental regulations, hydrogen's potential to enable a fully decarbonized supply chain positions it as a key player in the future of sustainable maritime energy.

**Purpose of the paper**

This paper aims to evaluate hydrogen-based fuel cells for marine applications and analyse their potential to contribute to the maritime industry's decarbonization goals. Through a comparative analysis of different hydrogen fuel cell technologies, their advantages, challenges, and market potential will be discussed the contrast with other alternative marine fuels [9]. Furthermore, the paper will explore the environmental, economic, and logistical factors that will shape the future of hydrogen-powered ships and assess how hydrogen technology can align with the IMO revised strategy to reduce GHG emissions.

This evaluation includes an information of hydrogen production methods, such as green hydrogen from renewable sources, storage solutions. The paper also addresses the economic feasibility of hydrogen fuel cells, focusing on capital expenditures (CAPEX) and operating expenses (OPEX), as well as the emerging market potential for hydrogen in the global shipping industry.

## LITERATURE REVIEW

**Earlier studies on hydrogen fuel cells for maritime applications**

Hydrogen fuel cells have been explored for several decades as a practical alternative to fossil fuels across various industries, including the maritime sector. Early research has consistently proved the potential of hydrogen to serve as a clean fuel for both small-scale and large-scale shipping operations. For example, Gilchrist and Maggs [10]showed that hydrogen fuel cells could significantly reduce GHG emissions compared to traditional marine fuels. Additionally, Smith et al. [10] highlighted the efficiency improvements and emission reductions achievable through the deployment of hydrogen fuel cells in marine vessels, emphasizing their potential in long-distance shipping applications.

However, despite these promising results, the large-scale adoption of hydrogen fuel cells in the maritime industry has been hindered by economic and infrastructural challenges. The excessive cost of hydrogen production, particularly green hydrogen, is still a significant barrier [5]. Additionally, the lack of hydrogen bunkering infrastructure at major ports globally complicates the logistical feasibility of widespread hydrogen use in shipping [12].

**Types of hydrogen fuel cells**

Several types of hydrogen fuel cells are applicable in maritime contexts, each offering unique advantages and challenges: These types are Proton Exchange Membrane Fuel Cells (PEMFC) [8], Solid Oxide Fuel Cells (SOFC) [12]and Molten Carbonate Fuel Cells (MCFC) [11]. The comparison of characteristics of fuel cells is shown in Hydrogen storage and bunkering present significant challenges for maritime applications. Due to its low energy density compared to traditional marine fuels, hydrogen requires advanced storage solutions to meet the energy demands of long-distance shipping.

Hydrogen storage and bunkering present significant challenges for maritime applications. Due to its low energy density compared to traditional marine fuels, hydrogen requires advanced storage solutions to meet the energy demands of long-distance shipping.

The primary methods for hydrogen storage include compressed gas [5], liquefaction [8]and chemical carriers (e.g., ammonia) [13], each of which presents unique logistical and safety challenges. A comparison of storage methods is presented in Table 2.

**Table 1. Comparison of characteristics of hydrogen fuel cells**

| Parameter | Proton Exchange Membrane (PEMFC) | Solid Oxide Fuel Cell (SOFC) | Molten Carbonate Fuel Cell (MCFC) |
|---|---|---|---|
| Operating Temperature | 60 - 100°C | 700 - 1000°C | 600 - 650°C |
| Efficiency | 40% - 60% | 50% - 65% | 45% - 55% |
| Start-up Time | Fast | Slow | Moderate |
| Suitable Applications | Small vessels, ferries | Large ships, cruise liners | Long-distance vessels, tankers |
| Main Advantages | High efficiency, fast start-up | High heat efficiency | Fuel flexibility, potential for long-distance shipping |
| Main Disadvantages | Expensive materials (platinum) | High-temperature wear and tear | Experimental application, slower response time |

**Table 2. Comparison of methods for hydrogen storage**

| Storage Method | Description | Advantages | Disadvantages |
|---|---|---|---|
| Compressed Hydrogen | Stored at high pressure (350 - 700 bar) | Mature technology, easier integration | Bulky, heavy tanks assume significant space on ships |
| Liquefied Hydrogen ($LH_2$) | Stored at cryogenic temperatures (-253°C) | Higher energy density than compressed hydrogen | Requires advanced cryogenic systems, risk of boil-off |
| Hydrogen Carriers (Ammonia) | Hydrogen stored chemically as ammonia | Easier to store, existing bunkering infrastructure | Requires conversion back to hydrogen, lowering efficiency |

In addition to these storage challenges, hydrogen bunkering infrastructure at ports is still in its infancy. The global maritime industry currently lacks the widespread infrastructure necessary to support hydrogen refuelling. Developing hydrogen bunkering facilities at key international ports would require significant investments in new infrastructure, including storage tanks, pipelines, and safety systems designed to handle high-pressure or cryogenic hydrogen [7]. Ensuring consistent standards for hydrogen bunkering across regions and addressing safety concerns related to hydrogen's flammability are critical hurdles that must be addressed for the large-scale adoption of hydrogen in maritime shipping.

**Case studies of hydrogen fuel cell deployment in ships**

T pioneering projects have successfully deployed hydrogen fuel cells in real-world marine environments, highlighting the potential of hydrogen as a practical alternative to conventional marine fuels. Two notable examples are the *Energy Observer* and the *Hydroville* ferry (Figure 1).

- **The *Energy Observer*** is a unique ship that runs on hydrogen and combines various renewable energy sources like solar, wind, and hydrogen fuel cells to generate sustainable power for long journeys. It was launched in 2017 and has successfully travelled across several continents, proving that hydrogen can be used as a clean energy solution for maritime purposes. The ship's fuel cell system is fuelled by

hydrogen created on board through electrolysis, which is powered by the renewable energy harnessed by its solar panels and wind turbines.

- ***Hydroville***: The *Hydroville* ferry runs in Belgium for short-distance passenger transport. Launched in 2017 it is the world's first certified passenger shuttle running on hydrogen. It uses a dual-fuel combustion engine that allows it to work on both hydrogen and diesel, ensuring flexibility in areas with not developed infrastructure. The vessel proves the practicality of hydrogen fuel cells in ferries and short-distance marine applications, offering a cleaner alternative to diesel without compromising operational reliability [7].

## ENVIRONMENTAL IMPACT AND EMISSION REDUCTION POTENTIAL

The environmental impact of hydrogen as a maritime fuel lies in its ability to virtually cut harmful emissions from shipping.


**Figure 1.**
**Vessels with hydrogen fuel cell *Energy Observer* [14] (left) and *Hydroville* [15] (right)**

### Comparison of hydrogen with traditional marine fuels

Hydrogen-powered fuel cells produce electricity through an electrochemical process that generates only water vapor as a by-product, resulting in zero emissions of $CO_2$, $NO_x$, $SO_x$, or PM in contrast to conventional marine fuels. Release of $NO_x$ and $SO_x$, contributes to acid rain and respiratory health issues, and PM negatively affects air quality in coastal areas [2]. Table 3 summarise the characteristics of considered marine fuels.

**Table 3. Comparison of hydrogen with traditional marine fuels**

| Fuel Type | $CO_2$ Emissions | $NO_x$ Emissions | $SO_x$ Emissions | Particulate Matter (PM) | Global Warming Potential (GWP) |
|---|---|---|---|---|---|
| Hydrogen ($H_2$) | 0 | 0 | 0 | 0 | Zero emissions |
| Liquefied Natural Gas | ~20% lower than HFO | Reduced | Extremely low | Reduced | Methane slip (25 times more potent than $CO_2$) |
| Heavy Fuel Oil (HFO) | High | High | High | High | High |
| Diesel | High | High | High | High | High |
| Ammonia | 0 ($CO_2$) | High | Low | 0 | Potential $NO_x$ emissions |

### Hydrogen's role in achieving global climate goals

Hydrogen's potential to drastically reduce emissions positions it as a key enabler of the maritime industry's transition to sustainability. Hydrogen fuel cells offer a pathway to meet these targets, particularly for long-distance shipping, where battery-electric propulsion systems are not possible due to range limitations.

By adopting hydrogen as a primary fuel, the maritime industry could contribute to achieving broader global climate goals, such as those outlined in the Paris Agreement. Additionally, hydrogen can contribute to the IMO's strategy to reduce shipping-related $NO_x$ and $SO_x$ emissions in Emission Control Areas (ECAs), where stricter pollution limits are in place [7].

The zero-emission capabilities of hydrogen fuel cells make them a crucial part of the industry's long-term decarbonization strategy. As hydrogen production becomes more cost-effective - particularly through green hydrogen, produced via electrolysis powered by renewable energy sources -the environmental benefits of adopting hydrogen in shipping will only increase, accelerating the transition toward zero-emission shipping [5].

**Comparative analysis of hydrogen vs. LNG and other alternative fuels**

When comparing hydrogen with other alternative marine fuels, it is important to assess both the direct emissions (those released during operation) and the lifecycle emissions (those produced from the fuel's extraction, production, and transportation).

***Hydrogen***

Hydrogen can be produced through multiple pathways:

- **Green hydrogen**, produced via electrolysis using renewable energy, results in zero lifecycle $CO_2$ emissions, making it the cleanest available choice [5].
- **Blue hydrogen,** produced from natural gas with carbon capture and storage (CCS), can reduce lifecycle $CO_2$ emissions significantly but still has some carbon footprint compared to green hydrogen [2]
- The scalability of hydrogen depends on infrastructure development and cost reductions in hydrogen production, especially for green hydrogen, which stays more expensive than other fuels [7].

***Liquefied Natural Gas (LNG)***

Liquefied natural gas (LNG) has been promoted as a cleaner alternative to traditional marine fuels, offering reductions in $CO_2$, $NO_x$, $SO_x$, and PM emissions. However, LNG is not a zero-emission fuel:

- **$CO_2$ emissions**: LNG reduces $CO_2$ emissions by about 20% compared to HFO [12].
- **Methane slip**: LNG introduces the issue of methane slip, where unburned methane is released into the atmosphere during fuel combustion. Methane is a potent greenhouse gas, with a global warming potential (GWP) more than 25 times higher than $CO_2$, which undermines LNG's environmental benefits if not properly mitigated [11].
- **Lifecycle emissions**: The extraction, liquefaction, and transportation of LNG contribute additional lifecycle $CO_2$ emissions, making LNG less sustainable than green hydrogen in the long run [13].

***Biofuels and Ammonia***

- **Biofuels**: Derived from organic materials, they are often considered a lower-carbon alternative to fossil fuels. While they offer reduction in lifecycle $CO_2$ emissions, they still release $NO_x$ and PM during combustion, and their sustainability depends on feedstock availability and land-use impacts.
- **Ammonia**: Ammonia is a carbon-free fuel that can be used as a hydrogen carrier or directly combusted in engines. It produces no $CO_2$ during combustion, but it releases $NO_x$, which requires mitigation through after-treatment systems. Ammonia also has energy-intensive production processes that contribute to its lifecycle emissions unless it is produced using green hydrogen [13].

**Impact on climate goals and IMO's decarbonization strategies**

Hydrogen fuel cells have the potential to make a substantial contribution to global climate goals, particularly in the shipping sector, which has been slower than other industries in transitioning to low-carbon energy sources. By cutting emissions at the point of use, hydrogen enables ships to run in compliance with future IMO regulations that may require increasingly stringent GHG reductions.

Achieving the goals of revised IMO strategy will require the large-scale adoption of zero-emission technologies such as hydrogen fuel cells. Hydrogen, when used in fuel cells, produces only water vapor as a by-product, meaning it emits zero $CO_2$, $NO_x$, $SO_x$, or PM during operation, unlike traditional marine fuels [7]

**Importance for coastal and port cities**

In addition to reducing GHG emissions, hydrogen-powered ships would cut air pollutants such as $SO_x$, $NO_x$, and PM, which are harmful to both human health and the environment. These pollutants are particularly problematic in coastal and port cities, where shipping emissions contribute significantly to air quality degradation. Shipping-related pollution is linked to respiratory illnesses and other health problems, especially in urban areas

where ships dock and refuel. By adopting hydrogen fuel cells, the maritime industry can significantly reduce these localized emissions, contributing to cleaner air and improved public health in port communities.

The elimination of $NO_x$ and $SO_x$ emissions is especially important for compliance with regulations in Emission Control Areas (ECAs), where limits on these pollutants are more stringent. Hydrogen fuel cells offer a direct solution for ships operating in ECAs, allowing them to meet these regional environmental requirements without relying on additional exhaust treatment systems, such as scrubbers [8]

## ECONOMIC FEASIBILITY AND MARKET POTENTIAL

The economic feasibility of hydrogen as a maritime fuel hinges on key factors, including the cost of hydrogen production, CAPEX and OPEX of hydrogen fuel cell systems, and the development of supporting infrastructure for hydrogen storage and bunkering. While hydrogen fuel cells offer clear environmental advantages, their widespread adoption in the maritime industry will depend on their ability to compete with traditional and alternative marine fuels on a cost basis.

### Cost of hydrogen production

The cost of hydrogen production is one of the main barriers to its large-scale adoption in the maritime industry. Hydrogen can be produced through electrolysis using renewable energy being the cleanest but also the most expensive choice. The cost of green hydrogen production currently ranges from $3 to $6 per kilogram, depending on the availability of renewable energy sources and electrolysis technology [5]. In contrast, blue hydrogen (produced from natural gas with carbon capture) is less expensive but still emits some $CO_2$ during production, making it less environmentally attractive [7]

Advances in electrolysis technology and economies of scale are expected to reduce the cost of green hydrogen significantly over the coming decade. The International Renewable Energy Agency (IRENA) projects that the cost of green hydrogen could fall to between $1.50 and $2.50 per kilogram by 2050, making it more competitive with conventional marine fuels.

### CAPEX and OPEX for hydrogen fuel cell systems

CAPEX for hydrogen fuel cell systems is currently higher than for traditional marine engines due to the need for specialized equipment such as fuel cells, hydrogen storage tanks, and refuelling infrastructure. For example, PEMFCs and SOFCs cells rely on expensive materials, including platinum for PEMFCs and ceramic components for SOFCs, which drive up the initial investment [8]

However, the OPEX for hydrogen-powered ships is expected to be lower than for traditional vessels due to fewer moving parts and less maintenance compared to internal combustion engines, which suffer from wear and tear over time. Additionally, hydrogen fuel cells can achieve higher energy efficiency, reducing fuel consumption for the same amount of energy output [11].

The combined effect of lower OPEX and falling hydrogen production costs could make hydrogen-powered ships economically practical over the long term, particularly as fuel cell technology continues to improve.

### Infrastructure development and hydrogen bunkering

The development of bunkering infrastructure is critical to supporting the widespread adoption of hydrogen-powered ships. As of today, the global network of hydrogen refuelling stations is limited, and the infrastructure needed to support large-scale maritime hydrogen bunkering is still in its first stages. Ports will need to invest in new hydrogen storage facilities, pipelines, and safety protocols to accommodate hydrogen refuelling. Building this infrastructure will require significant upfront investment, but it also presents an opportunity for public-private partnerships and government subsidies to drive the transition [12].

### Market potential for hydrogen-powered shipping

The market potential for hydrogen-powered shipping is significant, especially as regulatory pressure to reduce GHG emissions increases. According to a report by DNV GL, hydrogen could supply up to 20% of the global shipping energy demand by 2050, particularly in sectors such as container shipping, ferries, and cruise liners where emissions regulations are more stringent [2].

The maritime industry's transition to hydrogen will likely follow a phased approach, with short-distance and

regional routes adopting hydrogen first, while long-distance routes rely on hybrid solutions or transitional fuels such as LNG or biofuels. As hydrogen production costs decrease and infrastructure expands, hydrogen could play a central role in achieving the IMO's 2050 decarbonization targets and contributing to global climate goals [3].

## CHALLENGES AND OPPORTUNITIES

While hydrogen holds great promise for decarbonizing the shipping industry, technological, regulatory, and operational challenges must be addressed before it can be widely adopted.

### Technological challenges

One of the main technological barriers to the widespread adoption of hydrogen in maritime shipping is the lack of mature hydrogen fuel cell technology. Although PEMFC and SOFC cells have been proven in various applications, they still face challenges related to durability, energy efficiency, and cost.

Another significant challenge is hydrogen storage. Storing hydrogen efficiently and safely on-board ships is complex due to its low energy density and the need for either high-pressure tanks or cryogenic systems for liquefied hydrogen. These storage methods increase the weight and cost of ships and require advanced insulation and safety measures to prevent leaks and explosions [8]. Additionally, converting hydrogen into liquid ammonia or methanol as an energy carrier introduces further complexity, as these carriers must be converted back to hydrogen for use in fuel cells, reducing overall energy efficiency [12].

### Regulatory and safety challenges

Regulatory challenges also pose barriers to hydrogen adoption in the shipping industry. Currently, there are no unified international standards for hydrogen bunkering or storage at ports. The development of consistent and clear regulations for hydrogen handling, storage, and refuelling across global ports is critical to enabling the widespread adoption of hydrogen-powered ships [6].

Safety concerns surrounding hydrogen use are also significant. Hydrogen is highly flammable, and its safe storage and use on ships require specialized materials and equipment to minimize the risk of leaks or explosions. Ensuring that ship crews and port personnel are trained in handling hydrogen will be crucial for the safe deployment of hydrogen bunkering infrastructure [7]

### Operational challenges

From an operational standpoint, hydrogen-powered ships face challenges related to range limitations. Hydrogen has a lower energy density compared to traditional marine fuels, meaning that more frequent refuelling stops are needed for long-distance voyages. This presents logistical challenges for global shipping routes, where hydrogen refuelling infrastructure is not yet widely available [2].

In addition, the current lack of hydrogen bunkering infrastructure is a major obstacle. Most ports around the world are not equipped to manage hydrogen refuelling, and significant investments will be needed to build this infrastructure. The industry will need to rely on the coordinated efforts of governments, port authorities, and private-sector stakeholders to develop a network of hydrogen refuelling stations [5]

### Opportunities: Policy incentives and international collaboration

Despite these challenges, there are significant opportunities for advancing hydrogen adoption in the maritime sector. Policy incentives will play a key role in accelerating the transition. Governments can provide subsidies, tax breaks, or grants to shipping companies that invest in hydrogen technologies and infrastructure. Additionally, carbon pricing mechanisms, such as carbon taxes or emissions trading systems, can incentivize shipowners to adopt low-emission fuels like hydrogen over conventional fossil fuels.

Technological innovation also presents significant opportunities. Advances in electrolysis technology for green hydrogen production, as well as breakthroughs in fuel cell design, could reduce costs and improve the efficiency of hydrogen as a maritime fuel. Moreover, innovations in hydrogen storage, such as solid-state hydrogen storage or advancements in liquid hydrogen handling, could make hydrogen more practical for long-distance shipping. The challenges and opportunities are summarised in Table 6.

**Table 4. Challenges and opportunities for hydrogen as fuel**

| Category | Challenges | Opportunities |
|---|---|---|
| Technology | Excessive cost of fuel cells, storage difficulties | Development of new storage technologies, efficiency improvements |
| Infrastructure | Lack of hydrogen refuelling stations at ports | Public-private partnerships for infrastructure expansion |
| Regulations | No global standards for hydrogen use in ships | International regulations and collaboration via IMO |
| Financial | High initial investment costs | Government subsidies, carbon pricing incentives |

## OUTLOOK AND POLICY RECOMMENDATIONS

As the shipping industry transitions towards decarbonization, hydrogen fuel cells are expected to play a crucial role in meeting the sector's long-term climate goals. Hydrogen-powered ships offer a practical solution for reducing GHG emissions and addressing air pollution, particularly in the context of global regulatory efforts like the IMO 2050 decarbonization targets.

### Outlook for hydrogen in maritime applications

Hydrogen fuel cells are set to become a major contributor to the maritime industry's decarbonization strategy, especially as regulatory frameworks tighten around GHG emissions. In the near term, hydrogen adoption is expected to grow in short-distance shipping, such as ferries, coastal vessels, and inland waterway transport, where refuelling infrastructure can be more easily developed. As the technology matures and hydrogen production costs decline, hydrogen fuel cells will likely play a greater role in long-distance and deep-sea shipping, particularly for large cargo ships and tankers, where the need for zero-emission solutions is most pressing [2].

The development of green hydrogen, produced through renewable energy, will be key to ensuring the sustainability of hydrogen-powered shipping. By 2050, it is anticipated that green hydrogen will become cost-competitive with fossil fuels, driven by technological advancements in electrolysis and the scaling up of renewable energy capacity [5].

### Policy recommendations for accelerating hydrogen fuel cell adoption

To accelerate the adoption of hydrogen fuel cells in the shipping industry, a coordinated approach involving government policies, industry collaboration, and international standards will be necessary. The following policy recommendations aim to help the transition:

- **Subsidies and financial incentives for hydrogen production and use**: Governments should provide subsidies and financial incentives to reduce the cost of hydrogen production and encourage investment in hydrogen-powered vessels. Tax credits for shipowners who retrofit their fleets with hydrogen fuel cells or buy new hydrogen-powered ships could accelerate the transition. Additionally, subsidies to produce green hydrogen through renewable energy sources would help lower the cost of this zero-emission fuel [7]
- **Investment in hydrogen infrastructure and bunkering facilities**: The development of hydrogen bunkering infrastructure is critical to the widespread adoption of hydrogen-powered ships. Governments, in collaboration with port authorities and private companies, should invest in the construction of hydrogen refuelling stations at key ports. International ports must be equipped with the necessary storage and safety systems to manage hydrogen refuelling safely and efficiently.
- **Development of international hydrogen standards and safety regulations**: To help global hydrogen adoption, international standards must be set up for hydrogen storage, handling, and refuelling. Regulatory bodies such as the IMO, along with national governments, should work to create unified safety protocols and certification systems for hydrogen-powered vessels [8].
- **Research and development (R&D) funding for hydrogen technology:** Increased funding for R&D into hydrogen fuel cells, hydrogen storage systems, and electrolysis technologies is essential to overcoming the current technological barriers to hydrogen adoption. Governments and private-sector stakeholders should collaborate to accelerate innovation in hydrogen production, storage, and distribution. Advances in solid-state hydrogen storage and improvements in the efficiency and durability of fuel cells could make hydrogen more cost-effective and practical for maritime applications.

- **Carbon pricing and emissions Regulations**: Governments can incentivize the adoption of hydrogen by implementing carbon pricing mechanisms that make high-emission fuels less economically attractive. This can include carbon taxes or emissions trading systems (ETS), which would encourage shipowners to switch to zero-emission fuels like hydrogen to avoid financial penalties. Strict emissions regulations from international bodies like the IMO will also play a crucial role in driving the industry toward cleaner fuels [11].

**Roadmap for integrating hydrogen into global maritime fuel supply chain**

To ensure the successful integration of hydrogen into the global maritime fuel supply chain, a phased approach should be adopted, Table 5 gives information for the roadmap for integrating hydrogen into global maritime fuel supply chain [12].

**Table 5. Roadmap for integrating hydrogen into global maritime fuel supply chain**

| Phase | Period | Main Goals | Expected Outcomes |
|---|---|---|---|
| Phase 1: Short Routes | 2020 - 2030 | Develop hydrogen infrastructure for ferries and coastal vessels | Initial deployment of hydrogen on short marine routes |
| Phase 2: Expansion | 2030 - 2040 | Increase hydrogen refuelling stations for long-distance shipping | Widespread use of hydrogen for international shipping routes |
| Phase 3: Full Adoption | 2040 - 2050 | Full integration of hydrogen as a primary fuel | Hydrogen becomes competitive with fossil fuels in the maritime industry |

## CONCLUSIONS

Hydrogen-based fuel cells are a promising solution for achieving the maritime industry's decarbonization goals. By offering a zero-emission alternative to traditional marine fuels, hydrogen has the potential to significantly reduce the shipping's environmental impact while also providing a pathway to compliance with future emissions regulations, such as those set by the IMO. Hydrogen fuel cells can drastically cut GHG emissions and eliminate harmful pollutants like $SO_x$, $NO_x$, and PM, making them an attractive option for the decarbonization of the global shipping fleet [6].

The excessive cost of hydrogen production, particularly for green hydrogen, limits its competitiveness with conventional fuels. The lack of a global hydrogen supply chain and the infrastructure needed for hydrogen storage and bunkering further complicate its adoption in the maritime sector. Additionally, safety concerns related to the storage, handling, and transportation of hydrogen must be addressed to ensure the safe and scalable use of hydrogen on ships[8]

This paper has explored the 3 types of hydrogen fuel cells, outlining their respective advantages, challenges, and applications in maritime contexts. A comparative analysis of hydrogen production methods, such as electrolysis for green hydrogen and steam methane reforming (SMR) for blue hydrogen, has highlighted the environmental and economic impacts of hydrogen as a marine fuel. Despite the obstacles, hydrogen is a promising candidate for the future of zero-emission shipping, especially when supported by policy incentives, technological innovation, and international collaboration [7].

To ensure the successful adoption of hydrogen in the maritime sector, future research and investment should focus on:

- Improving the efficiency and cost-effectiveness of hydrogen fuel cells.
- Developing scalable hydrogen production methods, particularly for green hydrogen, to reduce production costs.
- Addressing the logistical challenges of hydrogen bunkering and storage, with an emphasis on expanding the global hydrogen supply chain [5].

With the right investments, technological advancements, and policy support, hydrogen fuel cells could become a key technology in the transition to a sustainable, zero-emission shipping industry, helping the sector meet its IMO 2050 decarbonization targets and contributing to global climate goals.

**REFERENCES**

[1] IMO, “GHG Emissions Report,” 2020.
[2] DNV GL, “Maritime Forecast to 2050,” 2021.
[3] MEPC. Resolution MEPC.377(80). 2023 IMO strategy on reduction of GHG emissions from ships. London, 7 July 2023.
[4] S m i t h, T. et al., “The Future of Maritime Fuels,” Journal of Marine Engineering, 2022.
[5] IRENA, “Green Hydrogen: A Guide to Policy Making,” 2020.
[6] I n t e r n a t i o n a l Maritime Organization (IMO), “IMO Strategy on Reduction of GHG Emissions from Ships,” 2018.
[7] H y d r o g e n Council, “Scaling Up: Hydrogen in Maritime,” 2020.
[8] W a r t s i l a Corporation, “Hydrogen as a Fuel for Marine Applications,” White Paper, 2021.
[9] P u t h i y a p u r a, V.K., et al., “PEM Fuel Cells for Marine Applications,” Renewable Energy, 2021.
[10] G i l c h r i s t, J., & Maggs, L., “Hydrogen and LNG in Marine Transport,” Energy Policy, 2020.
[11] S m i t h, T., et al., “Hydrogen Fuel Cells in Maritime Applications,” Journal of Marine Technology, 2021.
[12] B a l c o m b e, P. et al., “Hydrogen Fuel Cells in Shipping,” Applied Energy, 2021.
[13] A m a d i, K., & Zhang, W., “Hydrogen Bunkering Challenges,” Maritime Technology Journal, 2021.
[14] https://www.yachtingworld.com/extraordinary-boats/energy-observer-from-ocean-racer-to-tech-wonder-132195.
[15] https://www.marinetraffic.com/en/photos/of/ships/shipid:5295253/shipname:HYDROVILLE.

# DYNAMICS OF THE CARBON INTENSITY INDICATOR FOR VEHICLE CARRIERS VISITED EUROPEAN PORTS

**Dimitar YALAMOV***

**Abstract**. *The study examines the Carbon Intensity Indicator transformation for vehicle carriers listed in the EU-MRV database due to input data for 2022 and 2023. BLACK SEA 2024. Based on the results, conclusions were drawn about the changes in the CII rating of 379 ships of this type visiting European ports. The total amount of $CO_2$ emitted decreases by 1.4% in 2023 compared to 2022, with 50% of ships keeping their CII rating until 2026.*
**Keywords:** *carbon intensity indicator, vehicle carrier, EU-MRV.*

## INTRODUCTION

Annex VI to the MARPOL Convention entered into force about 20 years ago (19 May 2005) [1]. The Annex places restrictions on the amount of sulphur oxides (SOx), nitrogen oxides (NOx) and particulate matter released into the air from ships. It also forbids intentional emissions of ozone depleting substances. Additionally, specific areas have been chosen as emission control zones, where even stricter standards are set. Moreover, a chapter that was approved in 2011 focuses on obligatory measures related to the technical aspects and operation of ships to improve energy efficiency and decrease greenhouse gas emissions. Over the years, organisational and technical measures have been imposed to reduce emissions in both new and existing ships.

Amendments to the MARPOL Convention Annex VI entered into force on 1 November 2022. They were developed under the framework of the Initial IMO Strategy on Reduction of GHG Emissions from Ships agreed upon in 2018. Starting from 1 January 2023, it is compulsory for all ships to calculate their attained Energy Efficiency Existing Ship Index (EEXI) to assess their energy efficiency and begin collecting data for reporting their annual operational carbon intensity indicator (CII) and CII rating.

The study compares the results for the CII of vehicle carriers, based on the annual reports of their emissions included in the EU-NRC system for 2023, compared to those from 2022. The interest in this type of ship is dictated by the increased production of electric cars and the shortage and need of these ships for their transportation, as well as the increased fires on board caused by the car battery [2].

The following sections present the requirements for collecting information on ship emissions, the algorithm for calculating the achieved CII rating and the results for input data for the two consecutive years.

## REDUCTION OF EMISSIONS FROM EXISTING SHIPS

Requirements for energy efficiency of new ships are in force from 1 January 2013 [3]. The attained Energy Efficiency Design Index (EEDI) should be less than a reference value depending on ship type and size [4]. For existing ships, the same requirements for Energy Efficiency Existing Ship Index (EEXI) are valid. There are different methods for meeting these requirements for new ships, while for existing ships they are limited.

The first and natural reaction was to reduce the speed of the ship. This is at odds with the design philosophy of some types of ships-for example, the container ship. Another measure is the conversion of the ship to use alternative fuel. In Table 1 a status (by September 2024) of retrofitted ships for alternative fuels is shown [5]. The efficiency of retrofitting for using of LNG as fuel is investigated in [6].

Often the ships utilize Overridable Engine Power Limitation (EPL) and Overridable Shaft Power Limitation (SHaPoLi) as approaches to aid in meeting the EEXI. These systems are intentionally built to be overridable, enabling the use of power reserve during emergency circumstances [7].

In addition to technical measures, operational measures summarized as maintenance strategies can be considered. The evaluation of thrust efficiency, engine efficiency, and hydrodynamics to enhance the energy efficiency of ships was conducted a decade ago [2].

* **Technical University of Varna, Bulgaria**

**Table 1. The number of retrofitted ships using alternative fuel**

| LNG | LPG | Methanol | Ammonia | $H_2$, ICE | $H_2$, Fuel Cell |
|---|---|---|---|---|---|
| 27 | 19 | 17 | 2 | 3* | 1 |

**- Newbuild*

The EEXI is a one-time certification for existing ships targeting design parameters while the CII rating is intended to improve the operational carbon performance of ships.

**Carbon Intensity Indicator**

Regulation 28 of the revised MARPOL Convention outlines the applications and requirements of the Carbon Intensity Indicator (CII) for specific types of vessels with a gross tonnage (GT) of 5000 and above. This regulation mandates the calculation of the Required Annual Operational CII, which will be used as a reference point for finding the Operational Carbon Intensity Rating. Each ship will be assigned an annual rating, represented by one of five grades (A, B, C, D, or E), based on their Attained Annual Operational CII. These grades show different performance levels, ranging from major superior (A) to minor superior, moderate, minor inferior, and inferior (E). The guidelines for estimating the CII are included in the Resolution of MEPC [8]-[11].

According to [8], the simplest method to calculate the annual operational CII rates for individual ships is as follows:

$$\text{Attained CII}_{ship} = M / W \tag{1}$$

$$M = FC_j \cdot C_{Fj} \tag{2}$$

$$W = C \cdot D_t \tag{3}$$

where:

$M$ is the total mass of $CO_2$ emissions, $W$ is the transport work, $j$ is the fuel oil type, $FC_j$ is the total mass (in grams) of consumed fuel oil of type $j$, $FC_j$ is the fuel oil mass to $CO_2$ mass conversion factor for fuel oil type $j$, $C$ is the ship's capacity (for vehicle carriers, gross tonnage - GT), and $D_t$ is the total distance travelled (in nautical miles, nm).

According to [9], for a vehicle carrier, the reference line is formulated as follows:

$$\text{CII}_{ref} = a\text{GT}^{-c} \tag{4}$$

where:

$$a = 330;\ c = 0.329 \text{ for GT} < 30{,}000 \tag{5}$$

$$a = 3627;\ c = 0.59 \text{ for GT} \geq 30{,}000 \tag{6}$$

The required annual operational CII rate, according to [10], is:

$$\text{CII} = ( 1 - Z / 100 )\ \text{CII}_{ref} \tag{7}$$

where:

$Z$ is the general reference to the reduction factors for 2023-2030 compared to 2019. The reduction factor ($Z$ %) for 2023-2026 is 5%, 7%, 9%, and 11%, respectively. $Z$ factors for the years 2027-2030 will be further strengthened and developed considering the review of the short-term measures by 2026.

Finally, the corresponding rating depends on the relation between the attained and required CII is shown in Figure 1.

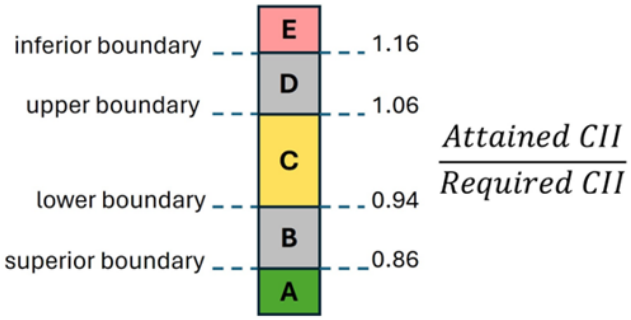


**Figure 1.**
**Boundaries between the CII ratings for vehicle carriers [2]**

**EU-MRV system**

The European Commission (EC) has started the process of including maritime emissions in the European Union's policy to decrease domestic greenhouse gas (GHG) emissions in June 2013. This policy's essential elements include the careful *monitoring*, comprehensive *reporting*, and diligent *verification* (MRV) of carbon emissions originating from ships. Additionally, it involves setting up greenhouse gas reduction targets specifically tailored for the maritime transport industry. The EU-MRV system is based on several EU Regulations [12]-[14]. Alongside this is being built an international system IMO DCS (Data Collection System) and separate UK- MRV system. The features of these systems are discussed in [15].

There are six (2018 - 2023) finished reporting periods for EU-MRV. The reports include information for $CO_2$ emission on about 12,000 ships of 17 types. The information is available from EMSA/THETIS-MRV database (https://mrv.emsa.europa.eu/#public/eumrv).

For estimation of CII rating the total $CO_2$ emissions [m tonnes] is taken directly from the database. the total distance travelled is calculated based on *Total fuel consumption [m tonnes]* and *Annual average Fuel consumption per distance [kg / n mile]* included in the database. The missing information for GT is taken from VesellFineder web site (https://www.vesselfinder.com/).

The CII rating based on the EU-MRV data from 2022 are used [2] to investigate the influence of different maintenance strategies. The report from this year includes 450 vehicle carriers (VC). The 2023 report includes information on emission for 456 ships, with 379 repeating ones. The calculations according to (1)-(7) are made for these 379 VC and compared with the results obtained with input data for 2022.

## CHANGES IN CII RATINGS OF VC FOR ONE YEAR

To compare the results for CII ratings, 25 combinations of two ratings were formed. For example, the combination AB means that for input data from 2022, the rating for the ship was A, while for input data from 2023 it is B. The other combinationd are fromed by analogy.

Ratings for three yaers - 2024, 2025 and 2026 are calualted and compared. The number of vehicle carriers belonging to each combination is shown in Figure 2- Figure 4. Combinations in which CII worsens using 2023 data are marked in red (negative change), in cases without change i.e. AA, BB, CC, etc. with yellow (constant), and when CII improves according to 2023 data-with green (positive change). 3D graph of the same result is shown in Figure 5- Figure 7.

| | | Data from 2023 | | | | |
|---|---|---|---|---|---|---|
| | | A | B | C | D | E |
| 2022 | A | 21 | 12 | 3 | 1 | 1 |
| | B | 5 | 9 | 8 | 4 | 0 |
| | C | 4 | 23 | 60 | 36 | 4 |
| | D | 1 | 1 | 27 | 42 | 18 |
| | E | 0 | 5 | 13 | 33 | 48 |

**Figure 2.**
**Change of CII rating for 2024**

| | | Data from 2023 | | | | |
|---|---|---|---|---|---|---|
| | | A | B | C | D | E |
| 2022 | A | 18 | 6 | 1 | 0 | 1 |
| | B | 3 | 12 | 9 | 4 | 0 |
| | C | 6 | 14 | 54 | 32 | 5 |
| | D | 1 | 3 | 32 | 41 | 18 |
| | E | 0 | 3 | 13 | 39 | 64 |

**Figure 3.**
**Change of CII rating for 2025**

| 2022 | Data from 2023 | | | | |
|---|---|---|---|---|---|
| | A | B | C | D | E |
| A | 15 | 5 | 0 | 1 | 1 |
| B | 4 | 9 | 11 | 1 | 1 |
| C | 2 | 7 | 45 | 23 | 10 |
| D | 2 | 3 | 33 | 44 | 22 |
| E | 0 | 2 | 13 | 38 | 87 |

**Figure 4.**
**Change of CII rating for 2026**

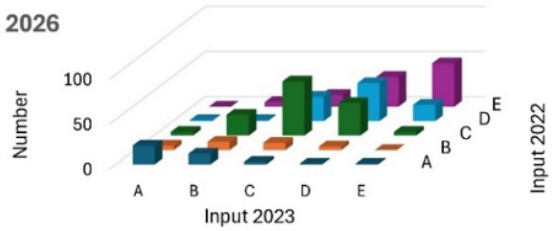


**Figure 5.**
**3D graph of CII changes for 2024**

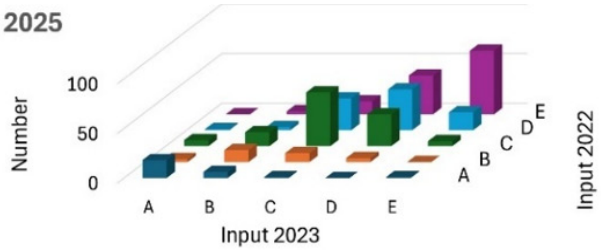


**Figure 6.**
**3D graph of CII changes for 2025**

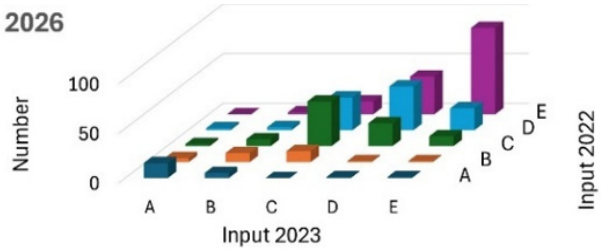


**Figure 7.**
**3D graph of CII changes for 2026**

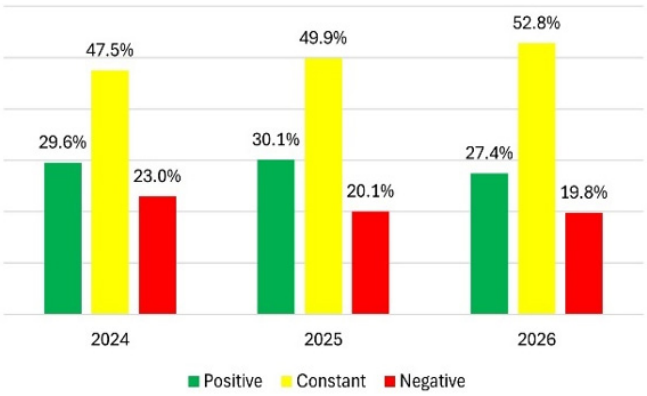


**Figure 8.**
**Rating change in percentage over the three years**

Figure 8 presents CII rating change in percentage over the three years. The data shows a slight (ab. 2%) decreasing of positive changes along with a slight decreasing (ab. 3%) of negative changes and an increased (ab. 5 %) percentage of ships keeping their CII rating. In the following lines, the main variables on which CII depends are analysed.

Two relative variables have been defined for the 2022 and 2023 EU-MRV database values.

(8) $$\overline{CO_2} = \frac{CO_2^{2023}}{CO_2^{2022}} \quad ; \quad \overline{D_t} = \frac{D_t^{2022}}{D_t^{2023}}$$

where:

$CO_2^{2022}$ and $CO_2^{2023}$ total mass of $CO_2$ emissions for both years respectively; $C_t^{2022}$ and $C_t^{2023}$ annual distance travelled in 2022 and 2023 respectively.

A positive change in variables for two years we have when $\overline{CO_2}$ and $\overline{D_t}$ are less than 1.0. Table 2 presents

the descriptive statistics of variables used for CII evaluation. Table 3 includes descriptive statistics of intervals for $CO_2$ emissions. One can see that the statistics for two years are practically the same. The distribution of values for annual distance travelled is presented in Figure 10.

**Table 2. Descriptive statistics of considered variables**

| Variable | Minimum | Maximum | Mean | Std. deviation |
|---|---|---|---|---|
| GT | 7314.000 | 76420.000 | 58162.485 | 12747.206 |
| $CO_2^{2022}$, mt | 19.880 | 32512.200 | 9585.514 | 5964.197 |
| $CO_2^{2023}$, mt | 95.800 | 30209.420 | 9446.249 | 6051.408 |
| $C_t^{2022}$, nm | 254.000 | 118852.900 | 30049.261 | 20383.611 |
| $C_t^{2023}$, nm | 320.200 | 109486.800 | 30530.985 | 21270.577 |

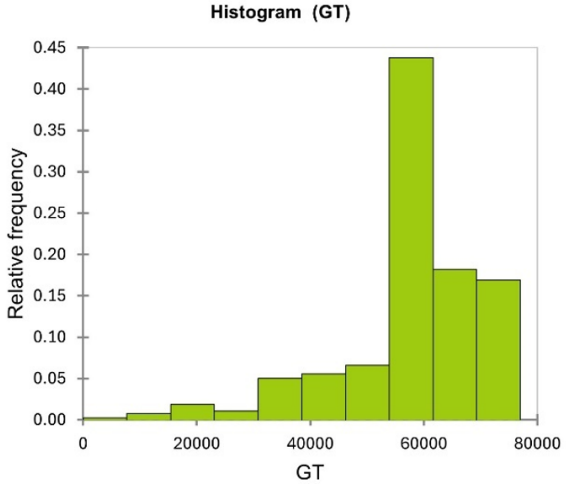


**Figure 9.**
**Histogram of GT of vehicle carriers used in the study**

**Table 3. Descriptive statistics for the intervals of $CO_2$ emission**

| | | $CO_2^{2022}$ | | $CO_2^{2023}$ | |
|---|---|---|---|---|---|
| Lower bound | Upper bound | Frequency | Relative frequency | Frequency | Relative frequency |
| 0.0 | 3300.0 | 54 | 0.142 | 58 | 0.153 |
| 3300.0 | 6600.0 | 81 | 0.214 | 82 | 0.216 |
| 6600.0 | 9900.0 | 88 | 0.232 | 87 | 0.230 |
| 9900.0 | 13200.0 | 60 | 0.158 | 57 | 0.150 |
| 13200.0 | 16500.0 | 46 | 0.121 | 45 | 0.119 |
| 16500.0 | 19800.0 | 23 | 0.061 | 25 | 0.066 |
| 19800.0 | 23100.0 | 21 | 0.055 | 12 | 0.032 |
| 23100.0 | 26400.0 | 4 | 0.011 | 7 | 0.018 |
| 26400.0 | 29700.0 | 1 | 0.003 | 5 | 0.013 |
| 29700.0 | 33000.0 | 1 | 0.003 | 1 | 0.003 |

The number of cases in which vehicle carriers have travelled a distance between 12,000 and 24,000 nm for 2023 is ab. 30% that is greater than the number for 2022. This is at the expense of neighbouring intervals.

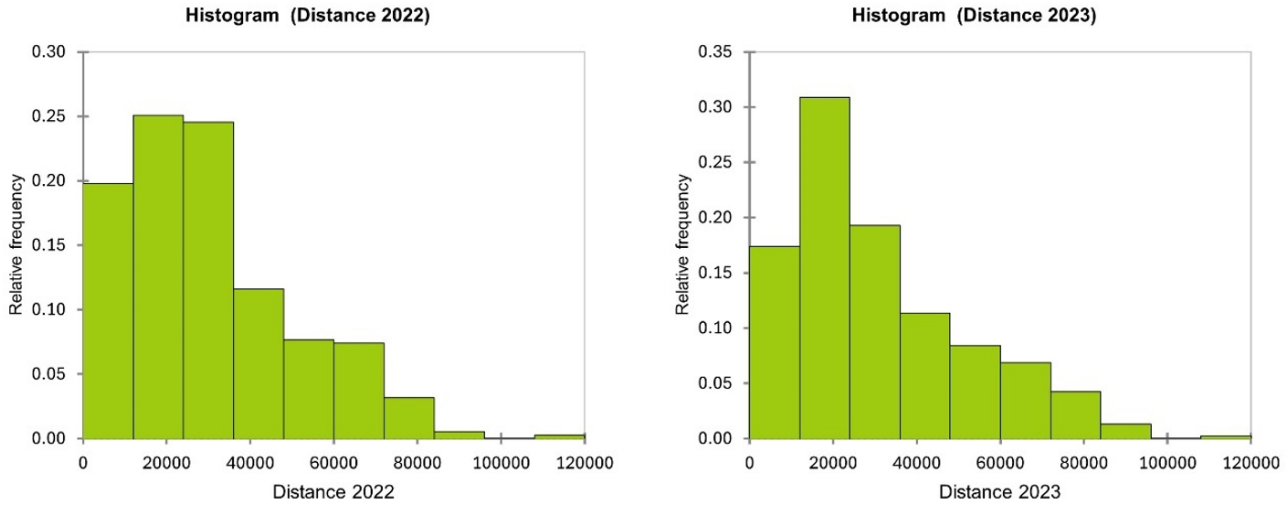


**Figure 10.**
**Histograms for annual distance of VC for 2022 (left) and 2023 (right)**

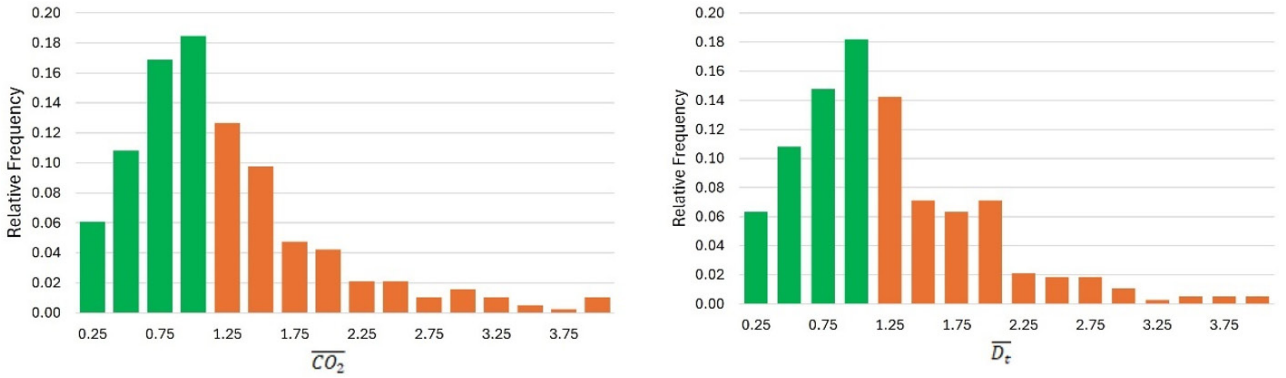


**Figure 11.**
**Histograms for relative values of $\overline{CO_2}$ (left) and $\overline{D_t}$ (right)**

For the relative variables, the confidence interval CI (95%) is for $\overline{CO_2}$ =2.057 ± 0.644 and $\overline{D_t}$ 1.967 ± 0.675. For both variables values close to 100 were obtained so, the histograms in Figure 11 are limited to 4. These are 93.4 % and 93.7 % from all 379 values of $\overline{CO_2}$ and $\overline{D_t}$ respectively.

The changes in the data for 2022 and 2023 lead to positive or negative influence on CII. A strictly positive shift is when $CO_2$ emissions are reduced, and distance $D_t$ is increased. Conversely, we have a strictly negative change in the carbon intensity indicator when emissions $CO_2$ increase and distance $D_t$ decrease. This information is summarised in Table 4. The information should be understood as follows: for 108 (28.5%) of the vessels the distance sailed has increased while the volume of $CO_2$ emissions has decreased. This leads to improvement of CII rating, but the specific rating will depend on the attitude towards the limit for a given year. For 99 (26.1%) of the ships, $CO_2$ emissions increased for less distance travelled. This means that the CII rating will deteriorate. For the remaining combinations, the corresponding mixed changes occurred and is hard to estimate overall change in CII.

**Table 4. Number of ships with positive or negative change in $CO_2$ emissions an $D_t$**

| | | $CO_2$ | |
|---|---|---|---|
| | Change | (+) | (−) |
| $D_t$ | (+) | 108<br>28.5% | 82<br>21.6% |
| | (−) | 90<br>23.7% | 99<br>26.1% |

**ACKNOWLEDGEMENTS**

This work has been performed within the Technical University of Varna Research Plan, funded by the State Budget under the contract PD14-2024.

**CONCLUSIONS**

In the described study, the change in the Carbon Intensity Indicator (CII) for vehicle carriers included in the EU- MRV database is analysed. The values of the indicator are calculated based on input data from 2022 and 2023. Based on the obtained results, estimates of the dynamics of the CII rating are made.

It is found that at the end of the target period 2026 there is an approximately equal reduction in both the improvement and the deterioration of the CII rating. At the same time, for this and the following years, the number of ships that will keep their rating for 2024 will increase twofold with different input data.

For 44% of the VC the GT is in the range 53,900 - 61,600. There are no considerable changes in the distribution of amount of $CO_2$ emissions in different ranges for the two years 2022 and 2023. Considering the annual distance travelled the greatest share ab. 30% for 2023 is in the range 12,000 - 24,000 nm.

To conduct the study, relative variables were introduced for emission values and distance travelled for the two years 2022 and 2023. These variables are defined in such a way that a relative value of less than one results in keeping or improving the CII rating of the vessel. For the $CO_2$ emissions this variable is less than one in 52.2% of the cases and for the distance 50.1%.

For 108 (28.5%) of the ships, there is a simultaneous reduction in $CO_2$ emissions and an increase in the distance travelled according to the data from 2022 and 2023, which is a positive trend. For another 99 (26.1%) ships, $CO_2$ emissions are increased and the distance sailed is reduced, leading to a deterioration in the CII rating.

The total amount of emitted $CO_2$ from VC visited EU ports for years 2022 and 2023 is 3,632,910 and 3,580,128 mt that means 1.45% reduction.

About half of the ships keep their CII rating over the years despite gradually increasing requirements, but for about 20% of ships this rating deteriorates. For 6% - 9% of the ships with CII rating E across the years will be necessary to develop a SEEMP Part III Corrective Actions Plan.

This first attempt to analyse the dynamics of the CII rating should be followed by a more in-depth analysis of the extent to which the objectives set in the IMO strategy will be fulfilled for the period up to 2026 and whether it is necessary to increase the requirements for the next period 2027-2030.

**REFERENCES**

[1] IMO. International Convention for the Prevention of Pollution from Ships (MARPOL).
[2] G a r b a t o v, Y.; Georgiev, P. Markovian Maintenance Planning of Ship Propulsion System Accounting for CII and System Degradation. Energies 2024, 17, 4123. https://doi.org/10.3390/en17164123.
[3] MEPC. Resolution MEPC.203(62). Amendments to the annex of the protocol of 1997 to amend the international convention for the prevention of pollution from ships, 1973, as modified by the protocol of 1978 relating thereto. (Inclusion of regulations on energy efficiency for ships in MARPOL Annex VI). IMO. July 2011, London.
[4] MEPC. Resolution MEPC.364(79). 2022 guidelines on the method of calculation of the attained energy efficiency design index (EEDI) for new ships. IMO, January 1st, 2023. London.
[5] V e r a c i t y DNV. Alternative Fuels Insight Platform (accessed on 10 September 2024).
[6] Y a l a m o v, D., Georgiev, P., & Garbatov, Y. (2023, June 30). Retrofitting measure of an ageing multi-purpose ship exposed to short-sea LNG operation. ANNUAL JOURNAL OF TECHNICAL UNIVERSITY OF VARNA, BULGARIA, 7(1), 68-87. https://doi.org/10.29114/ajtuv.vol7.iss1.293.
[7] MEPC. Resolution MEPC 335(76). 2021 guidelines on the shaft / engine power limitation system to comply with the EEXI requirements and use of a power reserve. IMO, 17 June 2021, London.
[8] MEPC.352(78); 2022 Guidelines on Operational Carbon Intensity Indicators and the Calculation Methods (CII Guidelines, G1). MEPC: London, UK, 2022.
[9] MEPC.353(78); 2022 Guidelines on the Reference Lines for Use with Operational Carbon Intensity Indicators (CII Reference Lines Guidelines, G2). IMO: Palo Alto, CAM USA, 2022.
[10] MEPC.338(76); 2021 Guidelines on the Operational Carbon Intensity Reduction Factors Relative to Reference Lines (CII Reduction Factors Guidelines, G3). MEPC: London, UK, 2022.

[11] MEPC.354(78); 2022 Guidelines on the Operational Carbon Intensity Rating of Ships (CII Rating Guidelines, G4). MEPC: London, UK, 2022.
[12] EU 2015/757. Regulation on the monitoring, reporting and verification of greenhouse gas emissions from maritime transport, and amending Directive 2009/16/EC, OJ L 123 19.5.2015, p. 55.
[13] EU 2003/87/EC. Regulation of the Establishing a system for greenhouse gas emission allowance trading within the Union and amending Council Directive 96/61/EC, OJ L 275, 25.10.2003, p.32.
[14] EU 2023/1805. Regulation of the use of renewable and low-carbon fuels in maritime transport, and amending Directive 2009/16/EC, OJ L 234, 22.9.2023, p. 48.
[15] G e o r g i e v, P, Garbatov Y. Carbon emissions statistical analysis for container shipping in the Black Sea. Proceedings of the Institution of Mechanical Engineers, Part M: Journal of Engineering for the Maritime Environment. 2024;238(2):395-405. doi:10.1177/14750902241228628.


# SHIP HYDRODYNAMICS

# THE BOW FLEXIBLE SKIRT BEHAVIOR OF AN AMPHIBIOUS HOVERCRAFT DURING ITS FORWARD MOTION ON CALM WATER

**Volodymyr ZAYTSEV*, Valeriy ZAYTSEV**,**
**Dmytro ZAYTSEV***, Victoria LUKASHOVA******

**Abstract.** *The paper presents a mathematical model of bow flexible skirt without diaphragm tightening under the hull of hovercrafts in the forward operation mode over calm water after the transition mode. Particular attention is paid to the stress-strain state of the shell of the bow flexible skirt when it is tightened under the hull after the transient mode. The developed complex of mathematical models allows to analyse in-depth the performance characteristics of hovercrafts before the completion of their design and before the beginning of construction.*
**Keywords:** *hovercraft, air cushion, bow flexible skirt, tightening, motion in operation mode, calm water, transition mode, mathematical model.*

## INTRODUCTION

During operation, the bow flexible skirt (BFS) of an amphibious air cushion vehicle (hovercraft) is subjected to various static and dynamic loads, which cause changes in its shape. Forces and moments of a wave nature act on the BFS during hovercraft operation over still water, due to the impact of the air cushion (AC) moving across the water surface. This leads to the flexible skirt being pulled under the hovercraft's hull. The phenomenon of skirt pulling plays a key role not only in solving issues related to the hovercraft's directional stability but also in determining the magnitude of speed reduction in rough water and the probability of losing stability due to skirt pulling.

While the hovercraft operates in forward motion over still water, the water surface deforms under the pressure of the air cushion. Therefore, during the design process of the flexible skirt, it is crucial to determine the moment when the skirt begins to be pulled under the hull. Identifying the influence of design factors of the receiver and the removable elements of the flexible skirt on the pulling under the hull is particularly important during the transition phase of the skirt operation - from the moment when only the removable elements contact the water to the point when the flexible receiver itself starts making contact with the water.

The main external hydrodynamic forces acting on the bow flexible skirt during its pulling under the hull in the transition mode while the hovercraft is moving are usually divided into two components: the first component is related to the excess air pressure in the vehicle's air cushion and the flexible receiver of the BFS, while the second is associated with water resistance. This resistance arises on the removable elements of the BFS as a result of their contact with water and is directed parallel to the water surface, both when the hovercraft is moving over still water and over a disturbed sea surface. Due to the impact of water resistance on the removable elements under certain conditions, the BFS is pulled under the hovercraft's hull.

The behavior of the BFS in the transition mode depends on its ability to resist being pulled under, which

*** Volodymyr ZAYTSEV, Prof., Doctor of Technical Sciences, Chief of department, Dept. of Marine Technology and Ocean Engineering, Shipbuilding Institute, Admiral Makarov National University of Shipbuilding (NUOS), Nikolaev, UKRAINE**

**** Valeriy ZAYTSEV, Docent, Doctor of Technical Sciences, Deputy Director of Science, Design Bureau IMT, LLC, Nikolaev, UKRAINE**

***** Dmytro ZAYTSEV, Docent, Candidate of Technical Sciences, Deputy Director of Design, Design Bureau IMT, LLC, Nikolaev, UKRAINE**

******Victoria LUKASHOVA, assistant, Dept. of Marine Technology and Ocean Engineering, Shipbuilding Institute, Admiral Makarov National University of Shipbuilding (NUOS), Nikolaev, UKRAINE**

is determined by the shape parameters of the flexible skirt, air pressure, and the presence of diaphragms that reduce the likelihood of the BFS being pulled under the hovercraft's hull.

Despite the fact that hovercraft have been in use for several decades and there is a significant amount of literature related to the theory of such vessels and the practice of their design, a number of unresolved issues remain concerning these vessels. Various methodologies, theories, and publications [1-4] exist, allowing for the calculation and design of various complexes and systems for hovercraft, ultimately leading to the creation of vessels that perform successfully in operation. However, questions regarding the pulling of the bow flexible skirt under the hull of the hovercraft remain unresolved.

In this regard, the purpose of this study is to determine the shape parameters of the BFS without diaphragms in hovercraft and its stress-strain state after transitioning to side-slip mode over still water, which affects the pulling of the single-layer receiver with removable elements, without BFS diaphragms, under the hovercraft's hull.

**NARRATION**

he study addresses the problem of accounting for the phenomenon of the flexible skirt (FS) of the bow flexible skirt being pulled under the hull of the vessel when determining the stress-strain state (SSS) of its receiver without diaphragms (Figure 1) and without considering the size of the air duct cutouts (pressure jump along the inner line $\boldsymbol{K_1}$ of the BFS internal section of the flexible receiver), as shown in Figure 2. The external view of the hovercraft "ACV-70" (designed by "Design Bureau IMT") is shown in Figure 3, while the direction of the external pulling force acting on its BFS during forward motion over still water in operational mode is shown in Figure 4.

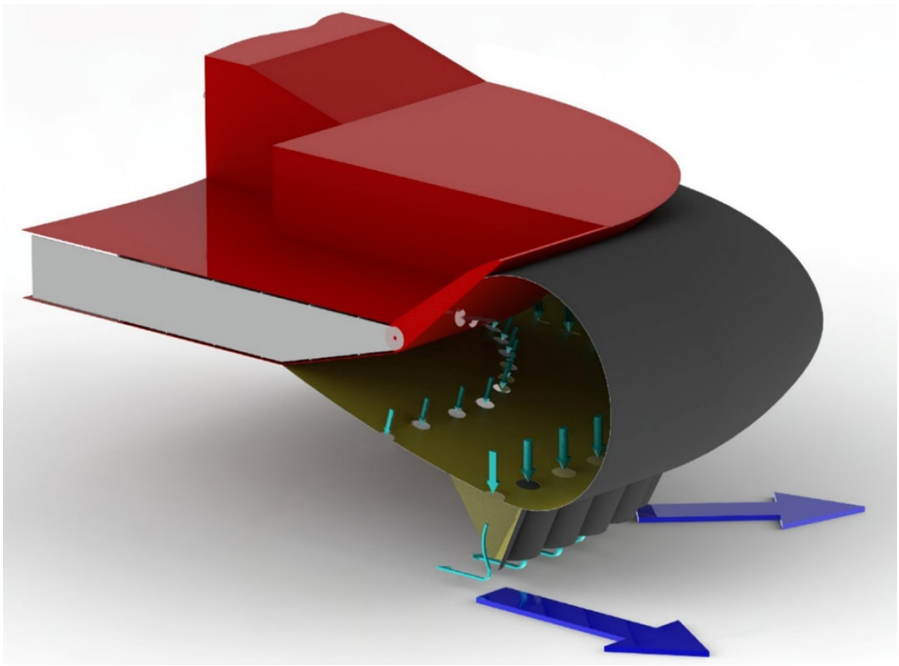

**Figure 1.**
**Bow flexible skirt of hovercraft "ACV-70"**

The shell of the BFS receiver is studied (see Figure 2), which consists of three sections $DK_2$, $K_2K_1$ and $K_1A$ made of isotropic, non-stretchable, and absolutely flexible material. Between these sections is the horizontal part $K_1K_2$, to which the removable element (RE) is attached.

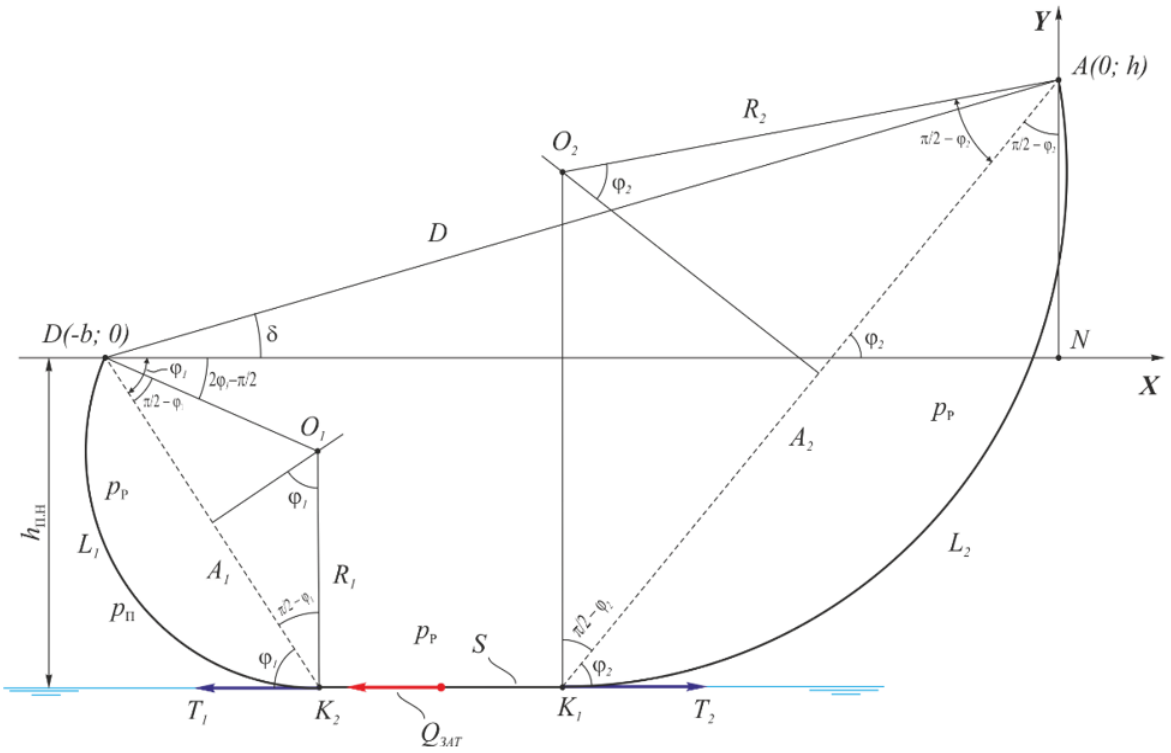


**Figure 2.**
**Diagram of forces (calculation scheme) acting on the flexible receiver of the BFS during hovercraft movement over still water after the transition mode**

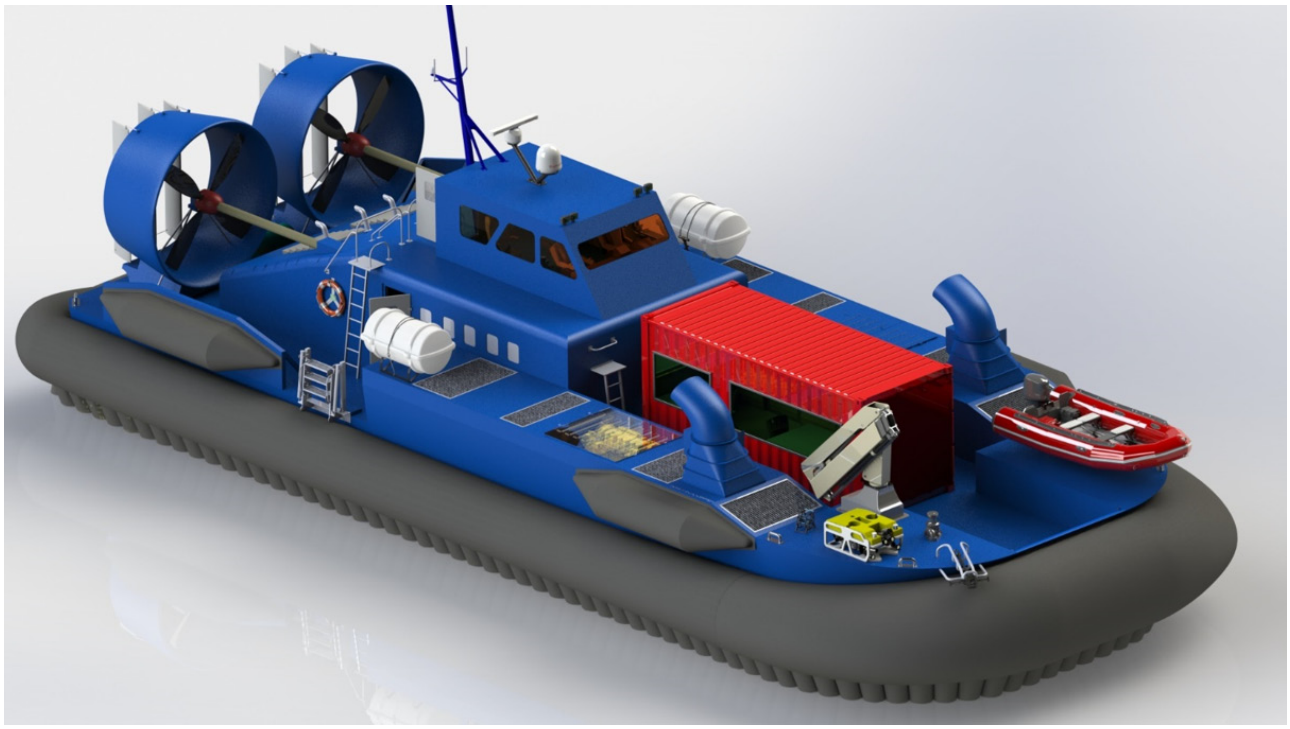

**Figure 3.**
**External view of hovercraft "ACV-70" (Design Bureau IMT project)**

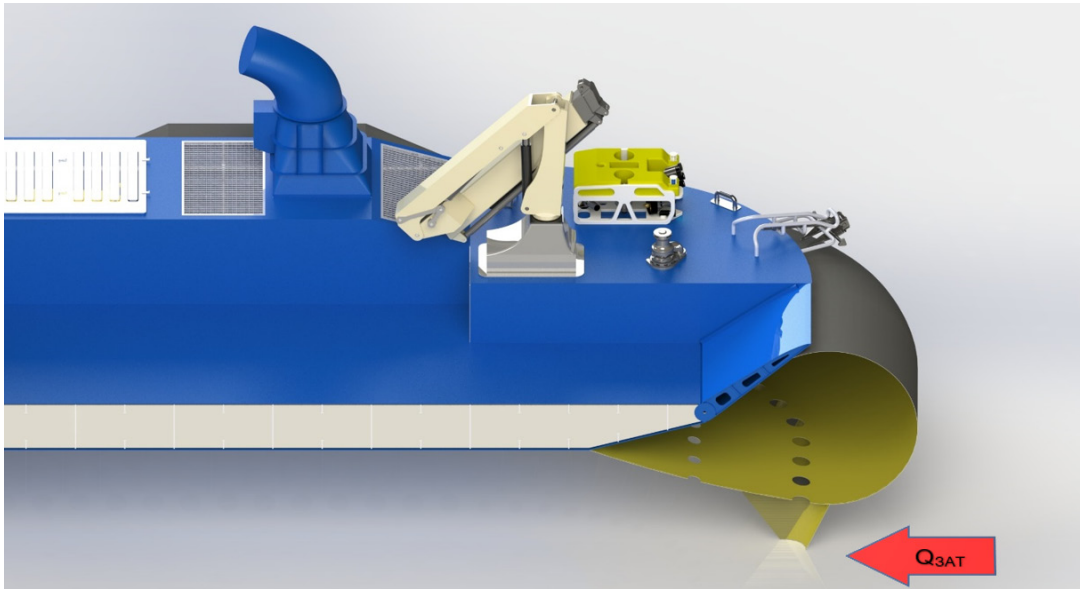


**Figure 4.**
**Direction of pulling forces acting on the bow flexible skirt of hovercraft "ACV-70" during its movement over still water in operational mode after the transition phase**

***Assumption.*** During hovercraft movement on the air cushion (AC) after the transition mode, the BFS will slide along the water surface (the attachment section of the RE $K_1K_2$ will be horizontal and will slide along the water surface). The RE will be pressed under the flexible receiver, and in the calculation scheme, only the shape resistance of the RE $Q_{\Phi}$, located in the water, will be considered. The horizontal element $K_1K_2$ does not experience longitudinal inclinations or rotations in the horizontal plane. Therefore, the fabric sections of the flexible receiver shell of the BFS will remain cylindrical during operation. There are no normal or tangential forces at the end sections of the flexible skirt shell.

The shell of the flexible receiver is subjected to stepwise air pressure loading. The section $AK_1$ is loaded by the pressure inside the flexible receiver $p_{\text{Р}}$, the section $DK_1$ - is loaded by the pressure difference between the air cushion $p_{\text{П}}$ and the receiver $p_{\text{Р}}$, that is, by the pressure $p_{\text{Р}}$ - $p_{\text{П}}$, and the receiver section $K_1K_2$ - is loaded by the pressure $p_{\text{Р}}$ and the pulling force $Q_{\text{зат}}$, applied along the surface of the horizontal section $K_1K_2$.

***Solution of the problem.*** The shape parameters of the bow receiver, considering its pulling under during the hovercraft's movement over still water, are determined by examining its cross-section after the transition mode (see Figure 2).

In the task of determining the shape parameters of the receiver under the influence of external forces, the following are considered: $p_{\text{Р}}$ - air pressure in the receiver, Pa; $p_{\text{П}}$ - air pressure in the air cushion, Pa; $Q_{\text{зат}}$ - resultant pulling force, directed parallel to the horizontal axis $NX$, N/m.

In addition to pressures and the pulling force, the following are considered as input data: $\boldsymbol{L}$ - length of the flexible receiver's cross-section (FRCS); $\boldsymbol{D}$ - distance between the attachment points of the receiver, m; $\boldsymbol{\alpha}_{\text{Р}}^{0}$ - BFS opening angle (structural angle between the cut of the bow section of the pontoon and the main plane (MP)), degrees (see Figure 5); $\boldsymbol{x}_{\text{П}}$ - abscissa of the air cushion center of gravity in the moving coordinate system, m; $\boldsymbol{L}_{\text{П}}$ - air cushion length, m; $\boldsymbol{\psi}$ - trim angle of the hovercraft «ACV-70» in hover mode, degrees, as a function of the heel angle $\boldsymbol{\theta}$, yaw angle $\boldsymbol{\varphi}$, drift angle $\boldsymbol{\beta}$, heading angle $\boldsymbol{\gamma}$, translational $\vec{V}^T = \begin{pmatrix} V_x & V_y & V_z \end{pmatrix}$ and angular

$$\vec{\omega} = \begin{pmatrix} \omega_x \\ \omega_y \\ \omega_z \end{pmatrix}$$

velocities of the hovercraft, longitudinal accelerations $\boldsymbol{a}_x$, lateral accelerations $\boldsymbol{a}_y$ and vertical accelerations $\boldsymbol{a}_z$ of the hovercraft:

$$\boldsymbol{\psi = f\left(\theta, \varphi, \beta, \gamma, \vec{V}, \vec{\omega}, \vec{a}\right)};$$

ν - kinematic viscosity coefficient, m²/s; $\zeta_{Ш}$ - surface roughness coefficient of the BFS.

Let's write the equilibrium equation for the horizontal section of the BFS element $\boldsymbol{K_1K_2}$, (see Figure 2):

$$-T_1 - Q_{зат} + T_2 = 0;$$
$$Q_{зат} = Q_{тр} + Q_{Ф};$$
$$T_1 = (p_Р - p_П)R_1;$$
$$T_2 = p_Р R_2,$$

where

$T_1$ - tension in the BFS shell acting on the inner section of the flexible receiver $DK_2$, N/m;
$T_2$ - tension in the BFS shell acting on the outer section of the flexible receiver $AK_1$, N/m;
$R_1$ - radius of curvature of the inner section of the receiver $DK_2$, m;
$R_2$ - radius of curvature of the outer section of the receiver $AK_1$, m.
$Q_{ТР}$ - friction resistance of the BFS against the water, N/m:

$$Q_{тр} = (\zeta_{ТР} + \zeta_{Ш})\frac{\rho_В \upsilon^2}{2} S;$$

where

$S$ - length of the horizontal section of the BFS element $K_1K_2$, m;

$\zeta_{ТР}$ - friction coefficient of an equivalent smooth plate

$$\zeta_{ТР} = 0{,}455(\lg \mathrm{Re})^{-2{,}58};$$

Re - Reynolds number

$$\mathrm{Re} = \frac{\upsilon L_С}{\nu};$$

υ - speed of the hovercraft "ACV-70" in hover mode, m/s;
$L_С$ - length of the hovercraft "ACV-70," m;
ν - kinematic viscosity coefficient, m²/s:

$$\nu = 1{,}57 \cdot 10^{-6};$$

$\zeta_{Ш}$ - surface roughness coefficient of the BFS:

$$\zeta_{Ш} = (0{,}5 \ldots 0{,}6) \cdot 10^{-6};$$

$Q_Ф$ - shape resistance force of the BFS removable element during hovercraft movement with bow trim when the BFS is pulled under the hull in transition mode, N/m:

$$Q_Ф = 0{,}5C_x(\alpha, h_{ЗАТ})\rho_В \upsilon^2 A_{ХАР}\frac{1}{B_П} = 0{,}5C_x(\alpha, h_{ЗАТ})\rho_В \upsilon^2 \frac{h_{ЗАТ}}{\sin\alpha};$$

$$A_{ХАР} = \frac{B_П h_{ЗАТ}}{\sin\alpha};$$

$v$ - forward speed of the hovercraft in hover mode, m/s;
$A_{ХАР}$ - characteristic area of the removable element during the pulling of the bow flexible skirt under the hovercraft hull, m²;
$\rho_В$ - density of seawater, $\rho_В = 1025\ kg/m^3$;
$C_x$ (α, $h_{ЗАТ}$) - shape resistance coefficient along the *NX* axis, determined by numerical experiments for the real RE structure of the BFS, dependent on the values of α and $h_{ЗАТ}$;

α - angle of inclination of the RE to the water surface, degrees (see Figure 4).

Geometric relationships for the bow receiver of the BFS:

$$D\cos\delta = A_1\cos\varphi_1 + S + A_2\cos\varphi_2;$$
$$D\sin\delta = A_2\sin\varphi_2 - A_1\sin\varphi_1;$$
$$A_1 = 2R_1\sin\varphi_1;$$
$$A_2 = 2R_2\sin\varphi_2;$$
$$L = L_1 + L_2 + S;$$
$$L_1 = R_1(2\varphi_1);$$
$$L_2 = R_2(2\varphi_2);$$
$$h_{\text{П.Н}} = h_{\text{ГО.0}} - \left(\frac{L_{\text{П}}}{2} + x_{\text{П}} - D\cos\delta\right)\tan\psi;$$
$$h_{\text{П.Н}} = R_1\left(1 + \sin\left(2\varphi_1 - \frac{\pi}{2}\right)\right).$$

where

$A_1$ - chord length of the inner section of the receiver $DK_2$, m;

$A_2$ - chord length of the outer section of the receiver $AK_1$, m;

$h_{\text{ro.0}}$ - height of the BFS at trim angle $\boldsymbol{\psi} = 0^{\text{o}}$;

**δ** - angle between the segments ***AD*** and ***ND*** or the rise angle of the outer line of attachment of the BFS to the hovercraft hull relative to the inner attachment line of the BFS;

$$\delta = \alpha_{\text{P}}{}^{0} - \psi;$$

$\alpha_{\text{P}}{}^{0}$ - opening angle of the BFS (structural angle between the cut of the bow section of the pontoon and the main plane (MP)), degrees (see Figure 5):

$\varphi_1$ - half of the central angle of the arc of the cross-section of the inner part of the receiver $DK_2$;

$\varphi_2$ - half of the central angle of the arc of the cross-section of the outer part of the receiver $AK_1$;

$L_1$ - length of the inner part of the cross-section of the flexible receiver of the BFS, m;

$L_2$ - length of the outer part of the cross-section of the flexible receiver of the BFS, m;

$h_{\text{П.Н}}$ - height of the air cushion at the inner part of the BFS receiver, m;

$\boldsymbol{x}_{\text{П}}$ - abscissa of the center of gravity of the air cushion, m;

$\boldsymbol{L}_{\text{П}}$ - length of the air cushion, m;

**ψ** - trim angle of the hovercraft “ACV-70” in hover mode, degrees.

**δ** - angle between the segments ***AD*** and ***ND*** or the rise angle of the outer attachment line of the flexible skirt to the hovercraft hull relative to the inner attachment line of the BFS;

$$\delta = \alpha_{\text{P}}^{0} - \Theta;$$

$\alpha_{\text{P}}{}^{0}$ - opening angle of the side flexible skirt (structural angle between the cut of the side section of the pontoon and the main plane (MP)), degrees (see Figure 5):

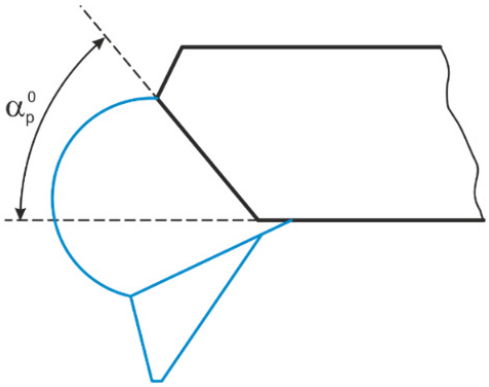


**Figure 5.**
**Opening angle of the BFS**

In the system of 14 equations with given values, we have: $D$, $L$, $\delta$, $x_{П}$, $L_{П}$, $\psi$, $f$, $p_{П}$, $p_{Р}$, and the unknowns are 14 variables: $L_1$, $L_2$, $A_1$, $A_2$, $S$, $R_1$, $R_2$, $T_1$, $T_2$, $Q_{ЗАТ}$, $\varphi_1$, $\varphi_2$, $\delta$ $h_{П\cdot Н}$.

Coordinates of point $K_2$ which connects the inner part of the cross-section of the flexible receiver of the BFS with the horizontal section $K_1K_2$ of the flexible receiver in the *XNY* coordinate system (see Figure 2):

$$X_{K_2} = -b + R_1 \cos\left(2\varphi_1 - \frac{\pi}{2}\right);$$
$$Y_{K_2} = -R_1\left(1 + \sin\left(2\varphi_1 - \frac{\pi}{2}\right)\right),$$

where

$b$ - horizontal projection of the distance between the receiver attachment points $b = ND = D \cos \delta$, m.

Coordinates of point $K_1$ where the outer part of the cross-section of the flexible receiver of the BFS connects with the horizontal section $K_1K_2$ of the flexible receiver in the *XNY* coordinate system (see Figure 2):

$$X_{K_1} = -b + S + R_1 \cos\left(2\varphi_1 - \frac{\pi}{2}\right);$$
$$Y_{K_1} = -R_1\left(1 + \sin\left(2\varphi_1 - \frac{\pi}{2}\right)\right).$$

Coordinates of the center of curvature $0_1$ of the inner part of the cross-section of the flexible receiver of the BFS in the *XNY* coordinate system (see Figure 2):

$$X_{O_1} = -b + R_1 \cos\left(2\varphi_1 - \frac{\pi}{2}\right);$$
$$Y_{O_1} = -R_1 \sin\left(2\varphi_1 - \frac{\pi}{2}\right).$$

Coordinates of the center of curvature $0_2$ of the outer part of the cross-section of the flexible receiver of the BFS in the *XNY* coordinate system (see Figure 2):

$$X_{O_2} = -b + S + R_1 \cos\left(2\varphi_1 - \frac{\pi}{2}\right);$$
$$Y_{O_2} = R_2 - h_{П.Н}.$$

## CONCLUSIONS

The described methodology for creating a mathematical model allows for the study of the pulling of the bow flexible skirt under the hull of amphibious air cushion vehicles during straight-course movement in operational mode over still water after the transition phase. Additionally, it enables simulation modeling of this process for hovercraft with six degrees of freedom, which will reduce the costs of designing and constructing the lead hovercraft with accurately predicted seakeeping and operational characteristics.

## REFERENCES

[1] З а й ц е в, Д.В. Исследование процесса затягивания носового гибкого ограждения без диафрагмы при эксплуатации судна на воздушной подушке на тихой воде / Зайцев Д.В., Зайцев В.В. // Зб. наук. праць НУК. - Миколаїв: НУК, -2008. - № 5 (422). - С. 37-41.

[2] З а й ц е в, Д.В. Расчет гибкого ограждения с учетом его затягивания в режиме движения судна на воздушной подушке / Зайцев Д.В. // Зб. наук. праць НУК. - Миколаїв: НУК, -2006. - № 4 (409). - С. 32-40.

[3] D m y t r o Zaytsev, Volodymyr Zaytsev, Pentscho Pentschev. Design Methods of Small Hovercrafts // Black sea 2014: Twelfth international conference on marine sciences and technologies. - Varna, Bulgaria: Varna Scientific and Technical Unions- Varna, - 2014. - P 107-108.

[4] L i a n g Yun. Theory and design of air cushion craft / Liang Yun, Alan Bliault - London: Yun and A. Bliault, 2000. - 632 p.

---

[1] Z a y t s e v, D.V., Zaytsev, V.V., «Issledovanie protsessa zatyagivaniya nosovogo gibkogo ograzhdeniya bez diafragmy pri ekspluatatsii sudna na vozdushnoy podushke na tikhoy vode,» (in Russian), *Zb. Nauk. Prats NUK*, no. 5 (422), pp. 37-41, 2008.

[2] Z a y t s e v, D.V., «Raschet gibkogo ograzhdeniya s uchetom ego zatyagivaniya v rezhime dvizheniya sudna na vozdushnoy podushke,» (in Russian), *Zb. Nauk. Prats NUK*, no. 4 (409), pp. 32-40, 2006.

[3] Z a y t s e v, D., Zaytsev, V., Pentschev, P., “Design methods of small hovercrafts,” in *Proc. 12th Int. Conf. Marine Sci. Technol. Black Sea 2014*, Varna, Bulgaria, 2014, pp. 107-108.

[4] Y u n, L., Bliault, A., *Theory and Design of Air Cushion Craft*. Oxford, U.K.: Butterworth-Heinemann, 2000, 632 pp.

# AN INVESTIGATION OF THE EFFECTIVENESS OF PARABOLIC BOW SHAPES FOR REDUCING SHIP RESISTANCE IN CALM WATER

**Stoyan SHAHLARSKI*, Nikita DOBIN***

**Abstract.** *The rapidly evolving geopolitical climate, technological advancements, globalization, and fluctuating fuel markets demand modernized maritime solutions. Many countries still utilize outdated vessels designed for the mid-20th century, which are ill-suited for current requirements. Compliance with International Maritime Organization (IMO) regulations further complicates fleet management. Enhancing maritime efficiency involves methods like innovative bow shapes, which reduce water resistance, fuel consumption, and increase speed. Parabolic bow shapes, a new alternative, improve seakeeping qualities. In Bulgaria, there is limited experience with this hull design. This research investigates a vessel with a parabolic bow shape through numerical analysis of hull geometry, supported by the Bulgarian Ship Hydrodynamics Centre (BSHC). Calm water simulations are conducted using Nushallo, a potential solver software, to evaluate the impact of different bow shapes.*
**Keywords:** *optimization, bow, geometry, ship, resistance.*

## INTRODUCTION

The bow of a vessel can be defined using relatively few parameters, especially compared to the extensive parameters required to determine the geometry of the entire hull surface [1].

Before discussing the impact of a bulbous bow on ship resistance and required power, it is essential to consider other hydrodynamic factors that play a crucial role in deciding whether to use a bulb. Changes in resistance affect the thrust load on the propeller and other propulsion characteristics, such as the quasi-propulsive coefficient, wake fraction, and thrust deduction fraction [2].

While bulbous bows may introduce some unfavorable effects, they generally do not significantly impact vessel stability or maneuverability, as evidenced by minimal changes in overshoot angle or zigzag test periods. Additionally, the bulbous bow is well-suited for housing bow thrusters and acoustic sounding equipment. [2].

In his publication Kracht subdivides the bulb into three types:

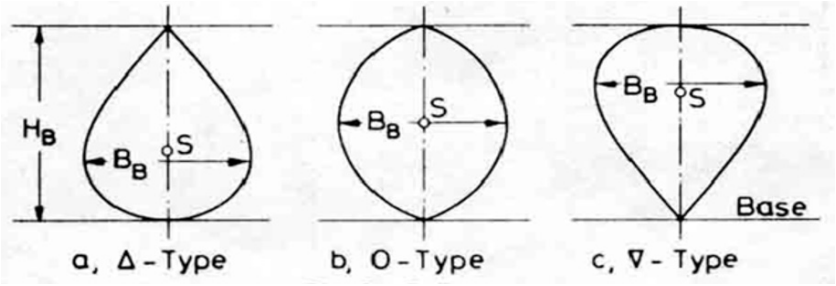


**Figure 1.**
**Types of bulbs**

The most basic effect of the bulbous bow shape is her impact towards the various resistance components and towards the required power. Alfred Kracht in his publication uses the following subdivision of the total resistance [2]:

$$R_T = R_V + R_{WF} + R_{WB} = R_F + R_{VR} + R_{WF} + R_{WB} \qquad \text{Eqn. 1}$$

***Institute of Metal Science, Equipment, and Technologies with Center for Hydro- and Aerodynamics "Acad. A. Balevski" at the Bulgarian Academy of Sciences - (IMSETHC-BAS), Varna, Bulgaria**

where,

$R_V$ - viscous resistance;
$R_F$ - frictional resistance;
$R_{VR}$ - viscous residual resistance;
$R_{WF}$ - resistance of the generated waves;
$R_{WB}$ - wave-breaking resistance.

The last two components are related with the formation of waves. Their contributions towards the total resistance are completely different for vessels with different block coefficients and speeds. Here, the explanation could be found due to the fact, that the lesser resistance due to bulb with full, slow ships can overtake the wave resistance from itself, which at $F_N < 0.2$ is an insignificant part of the total resistance [2].

The additional bulb surface always increases the resistance due to friction $R_F$, which is the main component of the viscous part $R_V$ [2].

The wave resistance *RWB* depends closely from the elevation and the development of free, as and local waves near the forward part of the body and is also a matter of the spraying phenomenon [2].

## MOTIVATION

The motive behind that investigation is ought to the bow hull shape of Rolls Royce, Rolls Royce Environship Leadge Bow and the New Zealand vessel HMNZ Aotearora:

**Figure 2.**
**New Zealand vessel HMNZ Aotearora [3]**

According to Wikipedia Aotearoa has ice-breaking qualities as well: Aotearoa is a Polar-class Logistics Support ship designed and built with specialised winterisation capabilities for her operations in Antarctica [4].

## METHODOLOGY

The methodology of the investigation consists of

1) Geometric manipulation in Rhinoceros
2) Transferring the geometry from Ansys Aqwa via Ansys Spaceclaim
3) Mesh generation in Ansys Aqwa
4) Nushallo calculations
5) Data analysis

## PROCEDURE

The Original Hull was opened from an IGES File provided by BSHC.

First geometry is the so-called “Original Hull”

**Figure 3.**
**"Original hull", bow profile**

**"Bulbless Hull"**

Before the start of the parabolic bow shapes generation, it was decided geometry without a bulb to be created, upon which the parabolic bow shapes to be added. The Rhinoceros commands were used [5]. The second geometry represents the original hull without a bulb:

**Figure 4.**
**"Bulbless geometry", bow profile**

In order to investigate the impact of different bow shapes, it was decided two bulb variants to be integrated into the original hull. The new bow shapes were labelled as "Geometry with big parabolic bulb" and "Geometry with small parabolic bulb", based upon the bulb size and bulb volume.

**"Geometry with big parabolic bulb"**

**Figure 5.**
**"Geometry with Big Parabolic Bulb", bow profile**

**"Geometry with small parabolic bulb"**

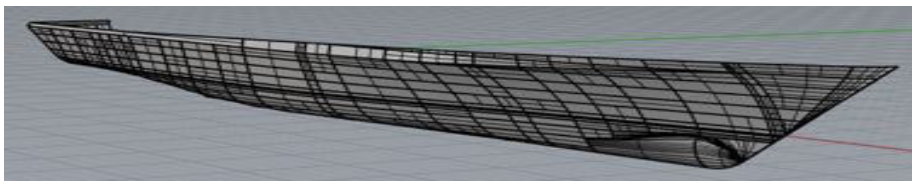

**Figure 6.**
**"Geometry with small parabolic bulb", bow profile**

**Table 1. Analysis**

| Parameter | "Original Hull" | "Bulbless Hull" | "Geometry with big parabolic bulb" | "Geometry with small parabolic bulb" |
|---|---|---|---|---|
| Volume, $m^3$ | 1553.49 | 1516.46 | 1614.83 | 1560.54 |

**Spaceclaim Procedure**

In Ansys Spaceclaim, the direction of the normalls, was checked as an insurance. The requirement of Aqwa to make a mesh on any of the geometries is the normalls to be directed outwards, whilst the Nushallo requirement for the direction of normalls is they to be inwards.

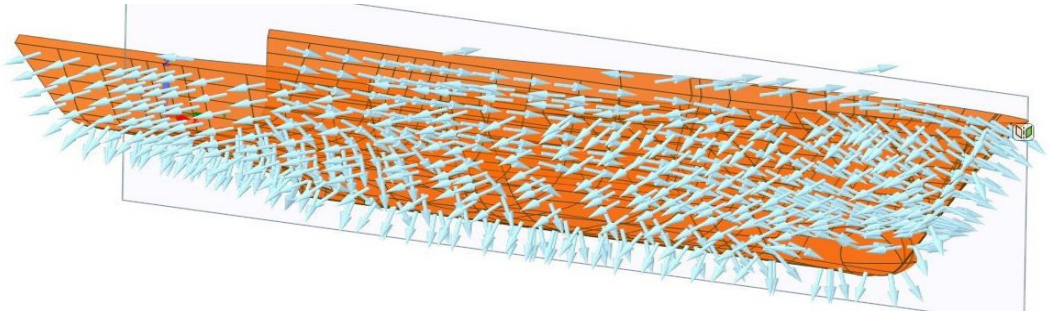

**Figure 7.**
**"Original hull" normalls in Ansys Spaceclaim**

**Mesh generation**

The meshes were made with the use of the Ansys Aqwa Interface [6]:

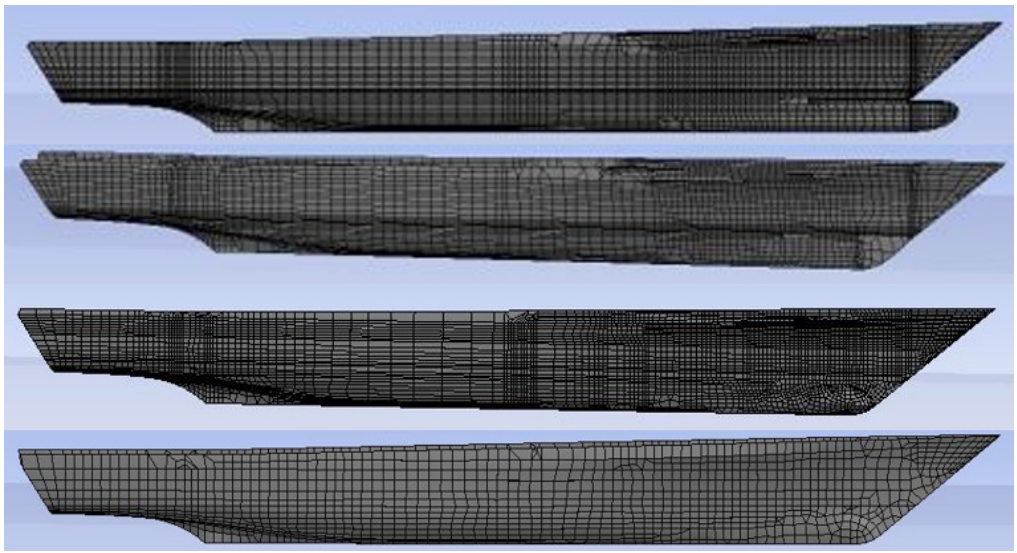

**Figure 8.**
**From top to bottom"Original hull" mesh, "Bulbless geometry" mesh,**
**"Geometry with big parabolic bulb" mesh, "Geometry with small parabolic bulb" mesh.**

The calculations were done with the full use of the Nushallo interface [7].

Before showing the results, the velocities in knots were converted into meters per second and into Froude:

**Table 2. Froude numbers**

| Velocity, kn | Velocity, m/s | Fn |
|---|---|---|
| 14 | 7.20 | 0.26 |
| 18 | 9.26 | 0.34 |
| 20 | 10.29 | 0.38 |
| 24 | 12.35 | 0.45 |
| 28 | 14.40 | 0.53 |

**Table 3. Total resistance in calm water**

| Total resistance in calm water, kN | | | | |
|---|---|---|---|---|
| Velocity, m/s | "Original Hull" | "Bulbless Hull" | "Geometry with big parabolic bulb" | "Geometry with small parabolic bulb" |
| 7.20 | 82.50 | 73.73 | 87.54 | 63.09 |
| 9.26 | 119.91 | 104.53 | 118.00 | 90.64 |
| 10.29 | 160.79 | 142.90 | 171.21 | 126.96 |
| 12.35 | 324.10 | 315.79 | 372.14 | 294.68 |
| 14.40 | 525.16 | 508.98 | 573.97 | 488.63 |

**Table 4. Percentage difference in the total resistance towards the original hull**

| | Percentage difference in the total resistance towards the original hull | | |
|---|---|---|---|
| Velocity, m/s | "Bulbless Hull" | "Geometry with big parabolic bulb" | "Geometry with small parabolic bulb" |
| 7.20 | 10.63 | -6.12 | 23.53 |
| 9.26 | 12.83 | 1.59 | 24.41 |
| 10.29 | 11.13 | -6.47 | 21.04 |
| 12.35 | 2.56 | -14.82 | 9.08 |
| 14.40 | 3.08 | -9.29 | 6.96 |

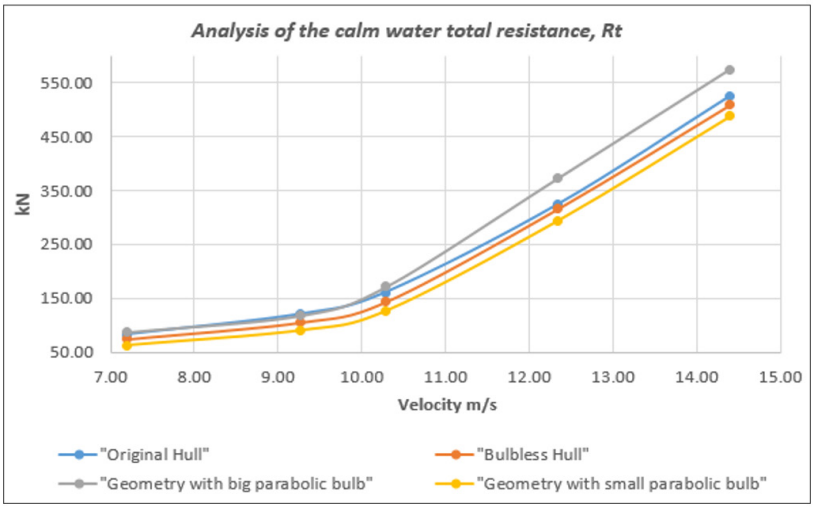


**Figure 9.**
**Comparisson of Rt, Cw and Rr**

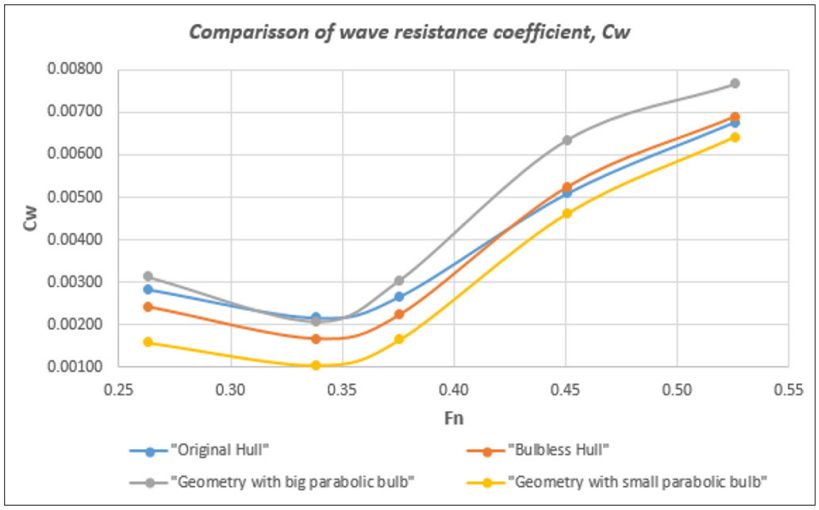


**Figure 9.**
**Comparisson of Rt, Cw and Rr**

The graphs of Ct (total resistance coefficient) and Cr (residuary resistance coefficient) have the same graphical behavior as Cw (wave resistance coefficient). They are not shown due to the publication's size limit.

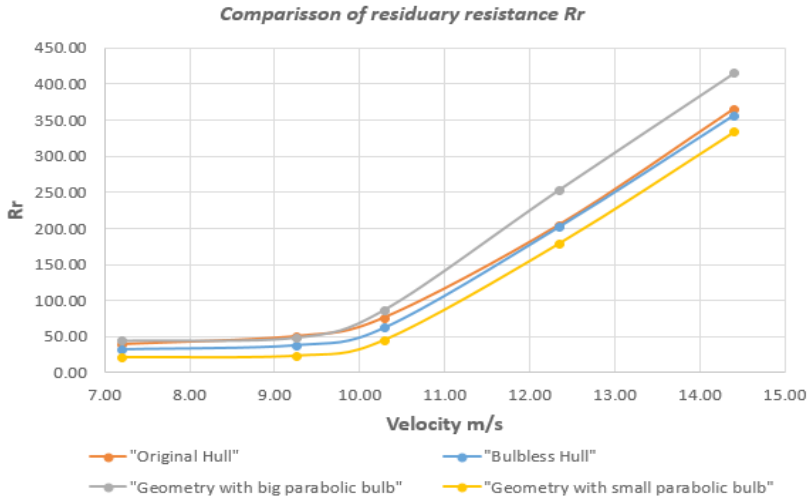


**Figure 9.**
**Comparisson of Rt, Cw and Rr**

## CONCLUSIONS

In conclusion, this investigation presents an effective method for assessing calm water resistance in modern fast vessel designs, encompassing the entire speed range and providing valuable guidance for designers seeking optimized resistance characteristics.

The results demonstrate that a small parabolic bulb geometry offers maximum efficiency and minimal calm water resistance, while a larger parabolic bulb has the opposite effect. This inefficiency is likely due to the increased transverse area and wetted surface resulting from the larger bulb volume.

The findings validate the relevance of the chosen design parameters and will inform the subsequent stages of this research.

The future stages of the current research are:

- 90-Degree Bow Shapes in accordance with the HMNZ Aoeateaora to be investigated;
- Inverted Bow Shapes in accordance with the class vessels Zumwalt(USA) and Belhara(France) to be investigated;
- Results' validation.

## REFERENCES

[1] N o b l e s s e, F., Delhommeau, G., Liu, H. et al. Ship bow waves. J Hydrodyn 25, 491-501 (2013).
[2] DESIGN OF BULBOUS BOWS Alfred M. Kracht, Visitor, SNAME Transactions, Vol. 86, pp. 197-217.
[3] https://www.navalnews.com/naval-news/2019/04/royal-new-zealand-navys-aotearoa-auxiliary-ship-launched-in-south-korea/.
[4] https://en.wikipedia.org/wiki/HMNZS_Aotearoa.
[5] R h i n o c e r o s Manual.
[6] A n s y s Aqwa Manual.
[7] N u s h a l l o User Guide Manual.


# MARITIME TRANSPORTATION AND PORT OPERATIONS

# AN APPROACH FOR NEAR REAL-TIME OBJECT RECOGNITION THROUGH VIDEO PROCESSING IN UNMANNED AERIAL VEHICLES

**Veselin ATANASOV***

**Abstract.** *In recent years, advancements in video processing technology have opened up new avenues for real-time object recognition, particularly in the domain of Unmanned Aerial Vehicles (UAVs). This paper delves into the potential of video processing for recognizing objects in near real-time scenarios. The experimental setup involved a diverse range of UAVs equipped with video streaming capabilities, a central streaming server, and a sophisticated video signal processing application tailored for object detection and recording.*
**Keywords:** *UAV, near real time video process, streaming, artificial intelligence, objective detection.*

## INTRODUCTION

### Background

The importance of real-time object recognition in UAV applications has been growing significantly due to its crucial role in various practical scenarios such as surveillance, monitoring, emergency response, and agriculture. The integration of UAVs with advanced object recognition technologies enhances the capabilities of these systems to perform complex tasks like detecting changes in environments, identifying specific objects or anomalies, and providing timely data for decision-making processes[1], [2]

### Research Objective

The main objective of this research is to develop and validate a system capable of performing real-time object recognition by processing video streams directly from UAVs. The system utilizes a custom streaming server and a Python application integrating YOLOv5, a cutting-edge deep learning model known for its efficiency in object detection tasks. This setup aims to demonstrate the feasibility and effectiveness of using UAVs equipped with AI-driven analytical tools to enhance real-time surveillance and monitoring capabilities

The experimental setup for real-time object recognition using UAVs comprises several interconnected components that work together to capture, transmit, and analyze video data efficiently. The setup includes:

## THE ARCHITECTURE OF THE EXPERIMENTAL SETUP

This architecture highlights the integration of advanced aerial and processing technologies to achieve near real-time analysis for practical applications like surveillance and monitoring.

1. **Unmanned Aerial Vehicle (UAV)**: A DJI drone equipped with a high-resolution camera, optimized for clarity in various lighting and movement conditions, ensures quality data capture for object detection.
2. **Video Streaming**: The drone is operated remotely via a WiFi connection, which transmits the video data in real-time to the operator's control station. This setup uses RTMP (Real-Time Messaging Protocol) to efficiently deliver live video streams to the internet.
3. **OWN Streaming Server**: A custom server receives the RTMP video stream, designed to handle high throughput and low latency. It temporarily stores and conditions the video for further processing.
4. **Object Detection Application**: A Python application processes the video stream, which includes resizing images and normalizing pixel values. It uses the YOLOv5 algorithm for rapid and accurate object detection and logs the detected objects with detailed statistics.

*** Nikola Vaptsarov Naval Academy, Varna, Bulgaria**

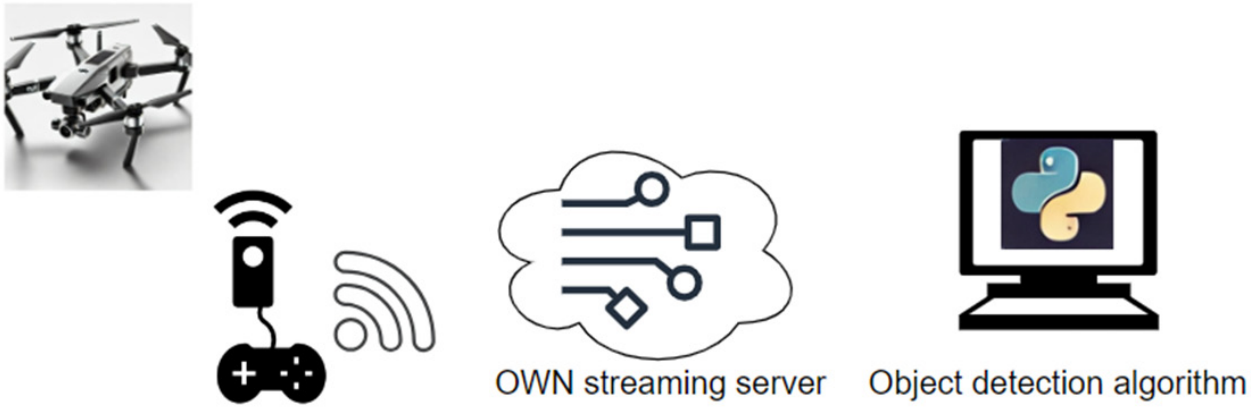


**Figure 1.**
**The architecture of the experimental setup**

## SYSTEM OVERVIEW

### UAV Selection and Setup

For this experiment, a DJI drone model was selected due to its high reliability and advanced hardware specifications which are ideal for real-time data capture and processing. The UAV is equipped with a high-resolution camera capable of capturing detailed video footage, essential for the accurate detection and classification of objects. This drone model was chosen specifically for its stability in various atmospheric conditions, long battery life, and integrated GPS functionality, which allows for precise navigation and tracking during flight missions.

### Video Streaming Setup

The video data captured by the UAV is streamed in real-time using the Real-Time Messaging Protocol (RTMP). RTMP is a widely used protocol for streaming audio, video, and data over the Internet, primarily designed to maintain low latency connections. To stream the video, the drone is connected to a remote operator's console via a WiFi network, which transmits the captured video to the RTMP server. This setup involves configuring the drone's onboard camera to encode the video stream into an RTMP format directly before transmission. The stream is then sent to the OWN server at a specified resolution and bitrate, which can be adjusted based on network bandwidth and latency requirements.

### OWN Server Configuration

The OWN server plays a crucial role in this system as it receives, processes, and manages the incoming video streams from the UAV. The server is configured with high-performance hardware capable of handling multiple real-time video streams without significant delays. It includes a powerful CPU, ample RAM, and dedicated graphics processing units (GPUs) to facilitate efficient video processing and object recognition tasks. The server runs specialized software that buffers the incoming RTMP streams, ensuring smooth video playback and minimizing the loss of critical data during transmission. Additionally, the server is equipped with software capable of interfacing with the Python application, which performs the actual object detection using the YOLOv5 algorithm. This setup enables the server not only to manage video streams but also to serve as a bridge between the raw video data and the processing application, which analyzes the content to detect and classify objects in real time.

## OBJECT RECOGNITION USING YOLOV5

### YOLOv5 Overview

YOLOv5 (You Only Look Once version 5) is the latest iteration in the YOLO series of object detection models, known for its speed and accuracy in detecting objects in images in real-time. YOLOv5 is designed to

process images at high speeds, making it well-suited for scenarios where real-time detection is crucial, such as surveillance, autonomous driving, and in this case, UAV-based monitoring. This algorithm is particularly efficient because it treats object detection as a single regression problem, straight from image pixels to bounding box coordinates and class probabilities. This simplification allows it to run significantly faster than models that handle parts of the detection as separate components.

**Integration with Python**

YOLOv5 is implemented within the Python environment using a combination of libraries, primarily PyTorch, which is a popular framework for deep learning applications. The integration process typically involves loading the pre-trained YOLOv5 model, configuring it with custom settings for the specific application (such as adjusting the input size or the confidence threshold), and then running it on the video frames received from the UAV. Python's flexibility and the rich ecosystem of data processing libraries make it an ideal choice for implementing complex object recognition tasks that require real-time processing and high accuracy.

**Data Processing Flow**

The data processing flow from video capture to object recognition includes several key steps:

**1. Video Capture**: The UAV captures high-resolution video footage which is streamed in real-time to the server via RTMP.

**2. Video Preprocessing**: Upon receipt, the Python application processes the video stream. This preprocessing step typically involves decoding the video stream, resizing and normalizing images, and converting them into a format suitable for the detection model. These steps are crucial for maintaining the quality of the video data and ensuring it meets the input requirements of the YOLOv5 model.

**3. Object Detection**: The preprocessed video frames are fed into the YOLOv5 model. The model uses its trained neural network to detect objects in each frame, identifying their locations and classifying them based on the learned object categories.

**4. Output Generation**: For each detected object, the model outputs a bounding box, a class label, and a confidence score. These outputs are then post-processed to apply thresholds, remove overlaps using non-maximum suppression, and format the data for display or logging.

**5. Real-time Challenges**: The main challenges in real-time processing include handling variable network latencies, maintaining high throughput under limited computational resources, and ensuring the accuracy of object detection under dynamic conditions (e.g., changing light, fast-moving objects). Solutions often involve optimizing the model for speed (e.g., model pruning, using lighter network architectures), employing more efficient video processing techniques, and scaling resources dynamically based on load.

By addressing these steps and challenges efficiently, the system can deliver robust real-time object recognition capabilities, leveraging YOLOv5's strengths to provide timely and accurate data for decision-making and response.

## RESULTS AND DISCUSSION

### Object Recognition Performance

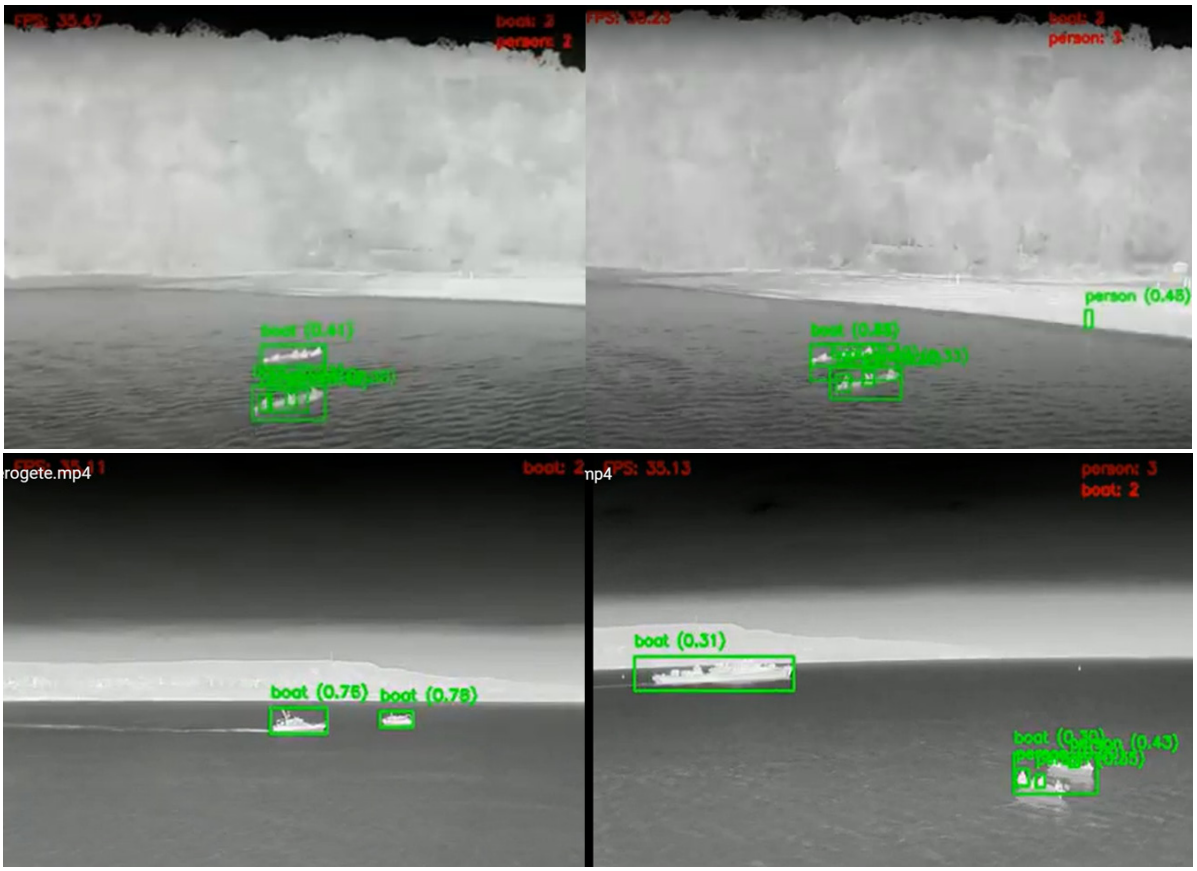


**Figure 2.**
**Display images depicting the output of the object recognition algorithm**

The object recognition system using YOLOv5 demonstrated high accuracy, speed, and reliability in real-time scenarios. The model accurately identified various objects with a high detection rate, showcasing its robustness in diverse environments and under different lighting conditions. Speed-wise, the system processed video streams at a rate that supported real-time analysis, typically maintaining frame rates that meet the operational requirements of UAV surveillance applications. The system's reliability was evident in its consistent performance across multiple test sessions, showing minimal downtime and error rates.

### Statistics Generated

The types of statistics generated included the number of objects detected, classification accuracies, frame processing times, and detection confidence levels. These statistics are crucial as they provide quantitative insights into the system's performance, such as detection efficiency and operational throughput. By analyzing these metrics, the team could gauge the system's effectiveness in real-world conditions and make data-driven decisions to refine the detection algorithms and system configurations.

### Event Logging

The system incorporated a detailed event logging mechanism that recorded every detection event along with timestamp information, detected object types, and their locations within the video frames. This logging is instrumental in tracking the system's operational history, diagnosing issues, and understanding patterns in object appearances and system responses. Insights gained from these logs help in optimizing the system setup and improving future deployments by pinpointing areas needing enhancements.

**Achievements**

The setup achieved significant milestones in technology integration and real-time processing capabilities. It seamlessly integrated cutting-edge AI object detection with UAV technology, providing a robust platform for advanced surveillance and monitoring. The real-time processing capabilities enabled by YOLOv5 and the Python-based application framework allowed for immediate object recognition and response, crucial for dynamic environments like urban surveillance or natural disaster monitoring.

**Limitations**

Despite its successes, the system faced limitations, particularly in handling extremely high-resolution video without compromising the frame rate. Additionally, the system's dependency on stable network conditions for seamless video streaming could affect performance in less ideal environments. Future work could focus on enhancing the model's efficiency with compression algorithms to reduce bandwidth usage without loss of detection accuracy. Improving fault tolerance and adaptive streaming capabilities might also be areas to explore.

**Comparative Analysis**

When compared with other existing systems, this setup showed comparable or superior performance in terms of detection accuracy and processing speed. Most competing systems struggle with the balance between speed and accuracy, especially in real-time scenarios. This system's use of YOLOv5, known for its efficiency in real-time settings, provides it with an edge in maintaining this balance. Further comparative studies could be beneficial, particularly those involving side-by-side comparisons in identical conditions, to more precisely measure performance enhancements and identify specific areas for improvement relative to peer technologies.

## CONCLUSIONS

In conclusion, this study presents a novel approach to near real-time object recognition through video processing in unmanned aerial vehicles (UAVs). By integrating advanced video streaming protocols and the YOLOv5 object detection model, the system demonstrates high accuracy and speed in real-world scenarios. While the experimental setup achieved significant milestones in terms of performance and reliability, limitations related to network dependencies and handling of extremely high-resolution videos without compromising frame rates were identified. Future work will focus on optimizing video compression, enhancing fault tolerance, and adapting the system for various environmental conditions, which will further improve its applicability in dynamic situations such as surveillance, monitoring, and disaster response. This system has the potential to set a new standard for UAV-based real-time object recognition, offering efficient and reliable solutions in critical applications.

## ACKNOWLEDGMENT

This article has been developed as a necessary component of the programme established under the National Research Development Strategy 2017-2030 (NRDS). The programme is designed to enhance the national security and defense research capacity, aligning with the strategic objectives set forth by the NRDS to advance technological and scientific capabilities in these critical areas.

## REFERENCES

[1] C a o, Z., Kooistra, L., Wang, W., Guo, L., Valente, J., "Real-Time Object Detection Based on UAV Remote Sensing: A Systematic Literature Review," Oct. 01, 2023, *Multidisciplinary Digital Publishing Institute (MDPI)*. doi: 10.3390/drones7100620.

[2] Y a n g, S. Y., Cheng, H. Y., Yu, C. C., "Real-Time Object Detection and Tracking for Unmanned Aerial Vehicles Based on Convolutional Neural Networks," *Electronics (Switzerland)*, vol. 12, no. 24, Dec. 2023, doi: 10.3390/electronics12244928.

# VESSEL TRAFFIC DATA THROUGH THE BULGARIAN EXCLUSIVE ECONOMIC ZONE

**Angel ANGELOV***

**Abstract**. *Maritime traffic is recognized as a significant source of primary atmospheric emissions in coastal regions, leading to the degradation of air quality along European coastlines. Over the past 20 years, the International Maritime Organization (IMO) has been actively working to introduce technical measures to reduce harmful emissions. In addition, Emission Control Areas are introduced, which are often linked to a country's exclusive economic zone. The Bulgarian Exclusive Economic Zone (EEZ) includes three main corridors of ship traffic in the Black Sea: from the Bosphorus to Constanta, Bulgarians ports the mouth of the Danube River, Odessa and vice versa. The paper presents the characteristics of ships crossing the EEZ for approximately 70 days at beginning of 2024 based on AIS data.*
**Keywords:** *AIS, vessel traffic, Exclusive Economic Zone, gas emissions.*

## INTRODUCTION

Ships transport about 90% of the world's goods and shipping is considered the least environmentally harmful mode of transport [1]. Today, transport generates one third of CO2 emissions in the EU. Land transport handles 72% of emissions, water for 14%, air for 13% and the rest mainly for rail transport [2].

The International Maritime Organization (IMO) for about 20 years, through the Marine Environment Protection Committee (MEPC) continuously adopts new resolutions and recommendations related to the prevention of pollution from shipping, including oil pollution, chemical pollution, wastewater, air pollution and greenhouse gas (GHG) emissions, ballast water management, bio-pollution, ship recycling, port reception facilities.

A significant number of studies in recent years have been related to the analysis of the impact of emissions on coastal areas, both in Europe and in other regions of the world [3]. As a measure to reduce this influence, the definition of emission control areas along the coastlines of various countries has been set up. These are part of the organizational measures to mitigate the harmful impact of emissions from shipping.

In a study[3], the impact of emissions from ships anchoring before entering the port of Varna was evaluated. It has been proved that the probability of exceeding the NOx pollution norms at certain points in coastal areas found 1000 meters away from the source can reach 10-15% during a 10-12-week period of recurrence.

Another study [4] examines the emissions from floating ships along the canal to Varna-West. Even in smaller quantities, the emissions in the areas near the canal can also pose a danger to those living there.

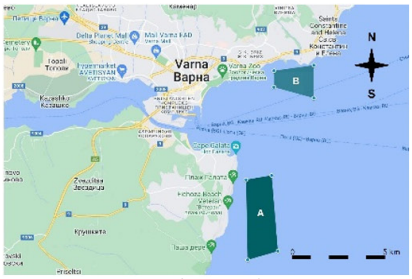


**Figure 1.**
**Anchoring area A (summer) and B (winter) at the port of Varna [3]**

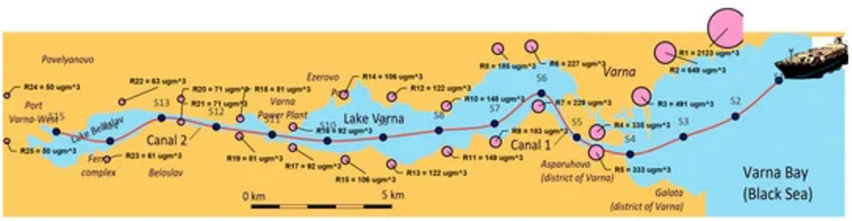


**Figure 2.**
**The route to the ship through the canal to the port of Varna-West and level of NOx emissions [4]**

* **Technical University of Varna, Bulgaria**

The goal of this study is to show that the main transport corridors in the Black Sea are between the Bosporus, Bulgarian ports, Constanta, the mouth of the Danube River, and Odessa. The study is the first step in assessing maritime traffic through Bulgaria's exclusive economic zone (EEZ), an analysis of the types and sizes of ships and their routes for a certain period in a pre-defined area up to the eastern border of Bulgaria.

## EMISSION CONTROL AREAS

Reducing sulphur emissions near coastal areas helps improving air quality and contributes to more sustainable shipping with less impact on the environment. To address the need for less pollution near coastal areas, emission control areas (ECAs) have been appointed where stricter controls are in place to minimize ship emissions. Existing and planned emission control zones are shown in Figure 3.

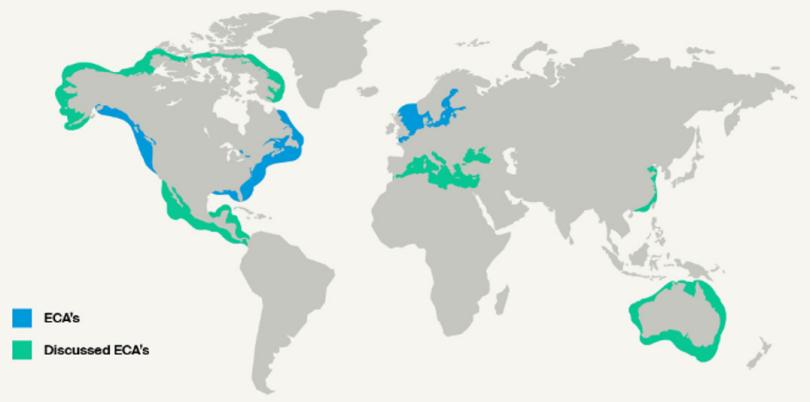


**Figure 3.**
**Existing and discussed Emission Control Areas [5]**

The MARPOL regulation says that ships sailing in certain ECAs must stop using Very Low Sulphur Fuel Oil (VLSFO - with a sulphur content of 0.5%) or Heavy Fuel Oil (HFO) with the use of scrubbers. In these zones, ships must use Ultra Low Sulphur Fuel Oil (ULSFO) with a maximum sulphur content of 0.1%.

A decision has already been made for one of the discussed zones, and the entire Mediterranean Sea (Figure 4) will become a control zone for sulphur oxide emissions from May 1, 2025. At the same time, MEPC (81) approved two proposals to designate emission control areas: 1) ECA proposal for Canadian Arctic waters, for NOx, SOx and particulate matter (Figure 5); 2) ECA proposal in Norway for NOx and SOx (Figure 6). The earliest date of entry into force of the proposals will be 1 March 2026.

**Figure 4.**
**Mediterranean Sea SECA [6]**


**Figure 5.**
**Proposed Canadian Arctic ECA [7]**

Figure 6 shows that Norway's proposed zone fully covers the country's Exclusive Economic Zone. This fact confirms the need to conduct such an analysis for the EEZ of Bulgaria.

## MARITIME TRANSPORT IN THE BLACK SEA AND BULGARIAN *EEZ*

### Typical characteristics

The transport of goods by sea between the main ports of the EU Member States and ports found in geographical Europe or in non-European countries on the Mediterranean and Black Seas is defined as "short sea shipping". Eurostat supports statistics on this transport and according to the latest data (for 2022) the main highlights are [8]:

- The volume of short-distance sea transport for the EU in 2022 decreased by 1.3% compared to 2021.
- Transport in Italy, the Netherlands and Spain is more than 40% of total short sea shipping for the Union.
- Liquid cargo is still the dominant type of cargo in European short sea shipping.


**Figure 6.**
**Proposed Norwegian Sea ECA [7]**

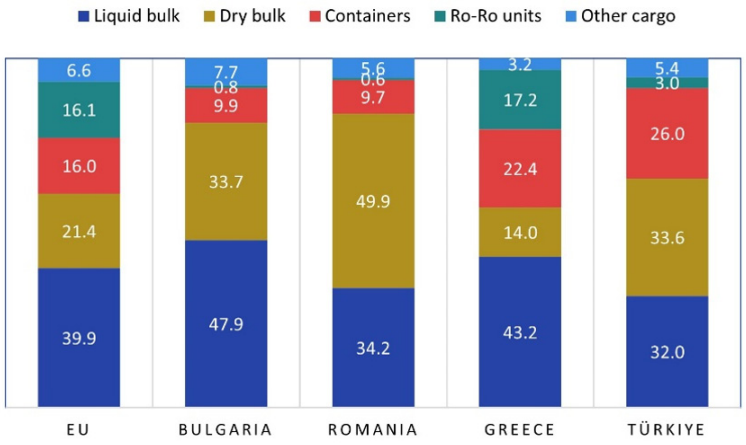


**Figure 7.**
**Comparison of short sea shipping (% of total volume)**
**by type of Black Sea countries and Greece (based on Eurostat data)**

- Short-distance container transport between the Union's main ports decreased by 2.3% between 2021 and 2022.

Figure 7 compares the percentage types of cargo transported by short sea transport for Black Sea countries, together with Greece and the EU. In terms of containers percentage Bulgaria and Romania have the same share of their shipments. For all countries compared, there is a different ratio in percentages between liquid and dry loads.

**Transport corridors by type of cargo**

The website https://www.vesselfinder.com/ provides an opportunity to create maps of the Black Sea with traffic density by type of cargo (Figure 8 - Figure 13). On can see that the highest traffic density is for general cargo ships, which follow clearly defined routes from the Bosphorus to Constanta, Bulgarian ports, the mouth of the Danube River, Odessa, and vice versa. Tankers carrying liquid cargoes use the Novorossiysk-Bosphorus route. The lines of container ships are visible, between the Bosphorus and Constanta, Odessa, and Novorossiysk, as well as those that consistently serve Bulgarian ports. Figure 11 shows Ro-Ro transports from Burgas to ports in Georgia. Traffic density for chemical cargoes is like that of dry bulk cargoes.

**Bulgarian Exclusive Economic Zone**

The United Nations Convention on the Law of the Sea (https://www.unclos.org/) regulates areas over which states have special rights with respect to the exploration and exploitation of marine resources. Exclusive economic zones range from the baseline to 200 nautical miles from shore. Figure 14 shows the boundaries of the exclusive economic zones of the six countries along the Black Sea, and Figure 15 presents a map of the maritime spaces of Bulgaria.

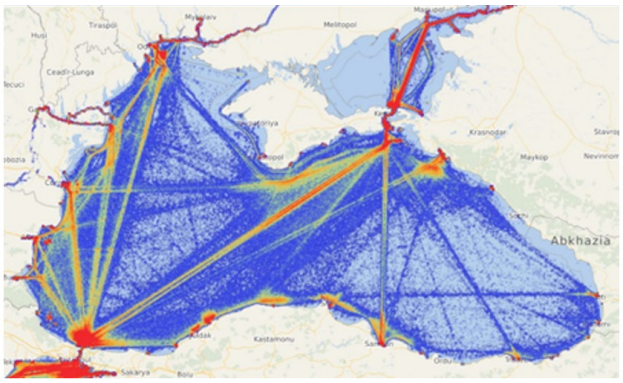


**Figure 8.**
**General cargo corridors**

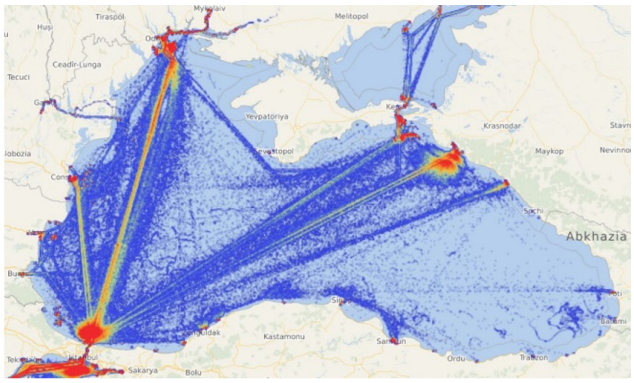


**Figure 9.**
**Dry bulk cargo corridors**

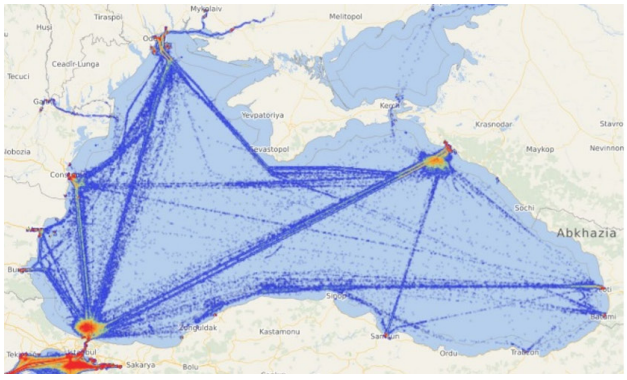


**Figure 10.**
**Containers corridors**

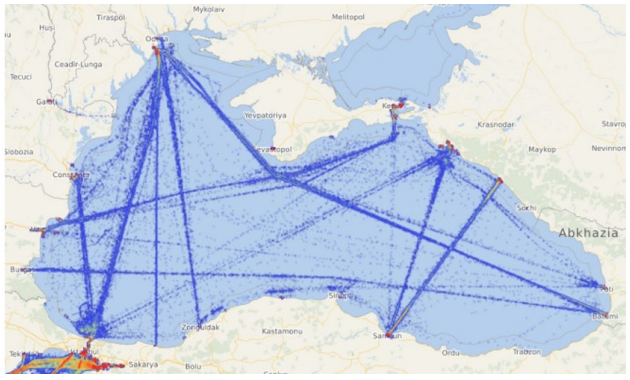


**Figure 11.**
**Ro-Ro cargo corridors**

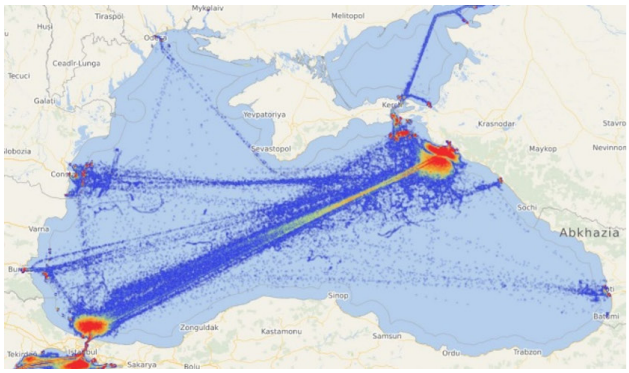


**Figure 12.**
**Liquid cargoes corridors**

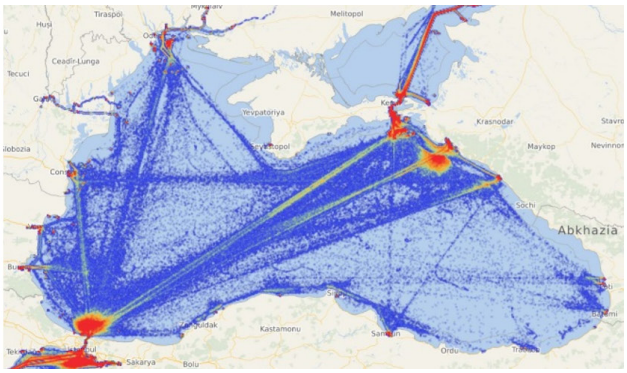


**Figure 13.**
**Chemical cargoes corridors**

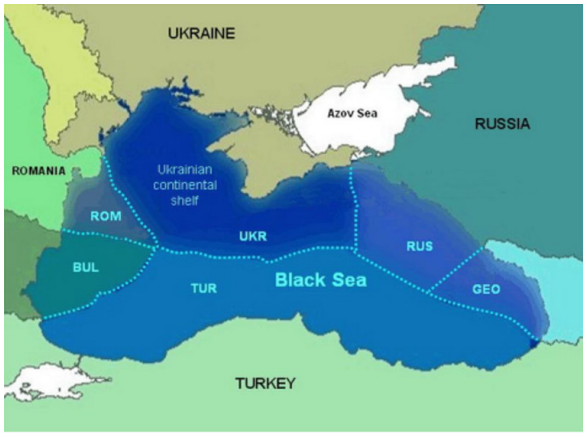


**Figure 14.**
**Boundaries of EEZ between the states of the Black Sea (https://vmh-bg.com/)**

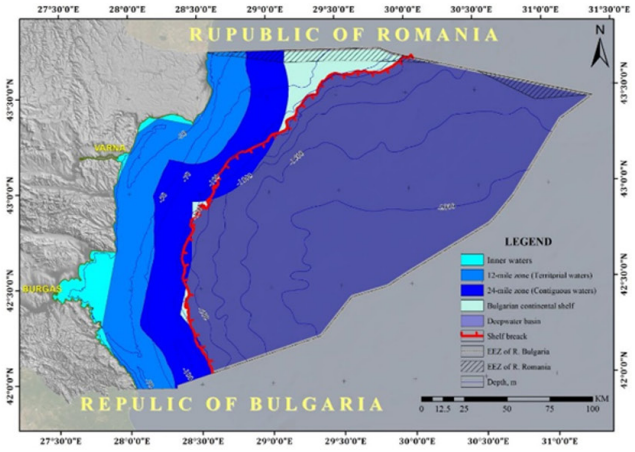


**Figure 15.**
**Maritime Space of the Republic of Bulgaria [9]**

## TRAFFIC RESEARCH AREA AND SOURCE OF DATA

### Traffic research area

Figure 16 presents a general scheme of the study area. The map includes as a background the Black Sea map, the density of traffic for general cargoes and some added objects.

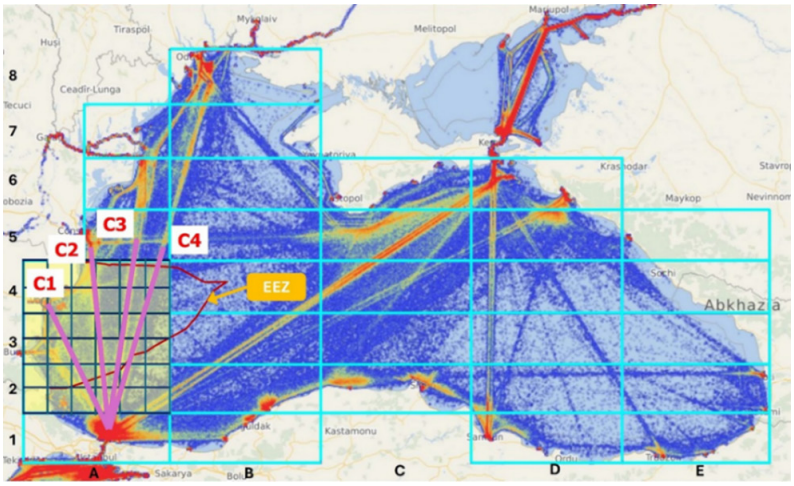


**Figure 16.**
**Traffic Research Scene**

The grid (lines in cyan) sets navigation zones defined in [10]. They are found between the extreme (east, west, north-south) points of the Black Sea. For these rectangular zones, data on wave height and peak period, direction and wind speed were extracted from the Copernicus Marine Service [11]. These data are used to estimate ship emissions, considering real sailing conditions in the Black Sea [10].

The red line shows the borders of the EEZ of Bulgaria. In yellow are marked 3 of the navigation zones-A2, A3 and A4, which coincide with the EEZ. The scheme also marks the main corridors C1, C2, C3 and C4 for which it is clearly seen that they pass entirely in the EEZ of Bulgaria. To assess the likelihood of a ship falling into the EEZ, the three navigation zones are further divided into 6 x 6 =36 smaller sectors. The size of such a sector is 40 x 40 km.

**Source for marine traffic data**

Traffic data in the Bulgarian EEZ are extracted from the specialized site MarineTraffic (https://www.marinetraffic.com/). It provides access to real-time ship tracking data with over 6,600 receivers worldwide. With AIS receivers along the coast, in the ocean and in space, the network captures AIS transmissions 24/7. The most important AIS messages have data on the position of ships and their movement parameters. Position reports are broadcast at short intervals (between 2 and 10 seconds depending on the speed of the vessel, or 3 minutes for stationary vessels), while static messages are broadcast at 6-minute intervals. The services of the MarineTraffic site are paid for, and for this research the choice of defining a custom area in the sea in which the entry of a ship into this area is watched was used. In such an event, the platform sends an e-mail with the data provided by the ship via AIS.

To collect information about those passing through the EEZ of Bulgaria, a custom area has been defined in the MarineTraffic platform (Figure 17).

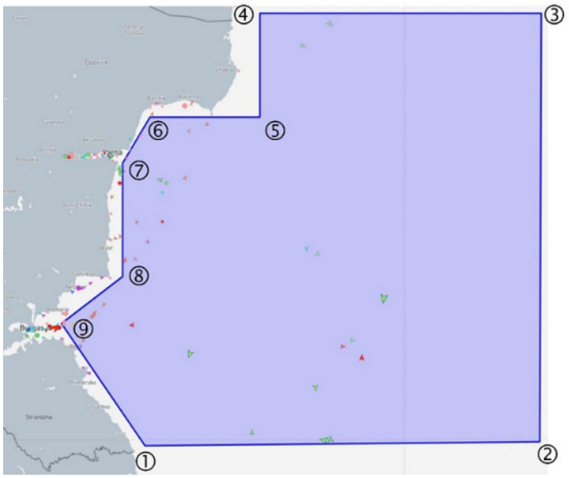


**Figure 17.**
**Traffic Research Scene**

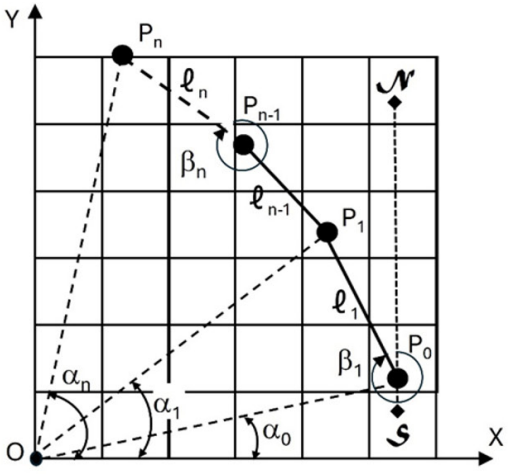


**Figure 18.**
**Description of the route of a ship in the XY plane**

## SHIP CHARACTERISTICS

In the period 02.01.2024 (14:18)-14.03.2024 (17:56), which is 72 days, 3 hours and 38 minutes, 1560 crossings of ships through the defined area were recorded. For each of them, the described data on the route, as well as the main characteristics of the ship were taken. The latter are also extracted from the internet platform MarineTraffic and statistics of them is included in this section.

For each route of the ship crossing the defined area, the following is registered:

- coordinates latitude and longitude of the starting point when entering the area;
- a maximum of 10 legs of the route, represented as a polyline;
- for each leg, the course angle and length.

Based on the coordinates of the starting point and the data for the legs, the geographical coordinates of the points of the polyline of the route are calculated. The geographical coordinates for all points of the route are

recalculated to move to coordinates in the XY plane (Figure 18). These results will be analysed and presented in the next article.

A statistical description of the characteristics of ships crossing the exclusive economic zone (EEZ) shall offer further insight into the quality and condition of those ships. Figure 19 shows the number of crossings as a percentage for the type of ship, and the load of the ships. The load states according to MarineTraffic platform are under load, partially loaded, ballast and unknown state.

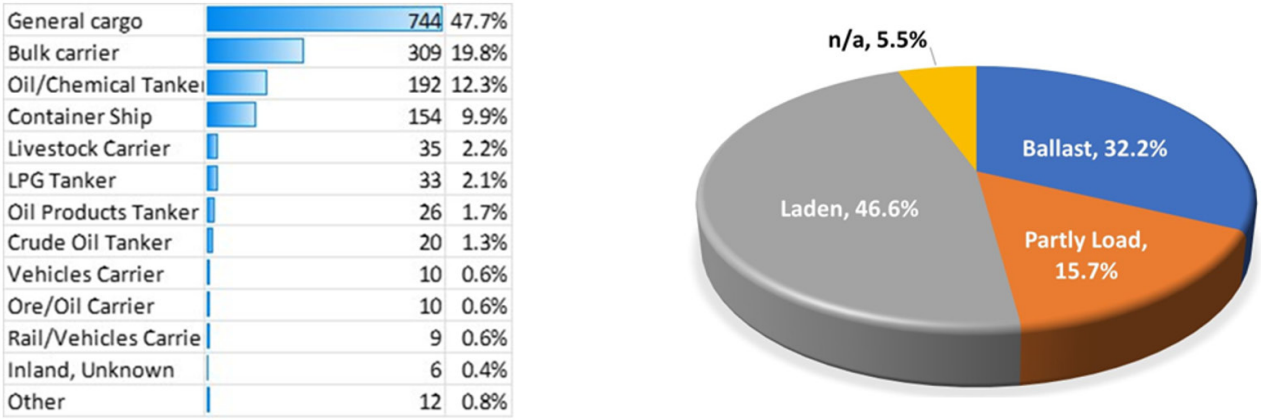


**Figure 19.**
**Type of vessels in the EEZ and distribution by type of load**

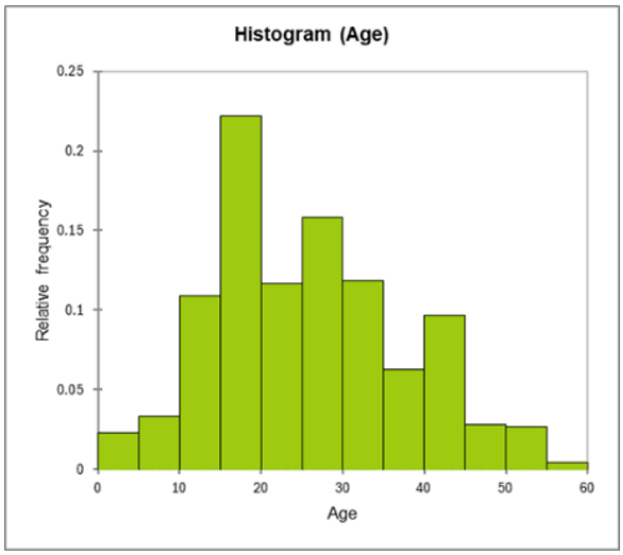


| Lower bound | Upper bound | Frequency | Relative frequency | Density |
|---|---|---|---|---|
| 0.000 | 5.000 | 36 | 0.023 | 0.005 |
| 5.000 | 10.000 | 52 | 0.033 | 0.007 |
| 10.000 | 15.000 | 170 | 0.109 | 0.022 |
| 15.000 | 20.000 | 346 | 0.222 | 0.044 |
| 20.000 | 25.000 | 182 | 0.117 | 0.023 |
| 25.000 | 30.000 | 247 | 0.158 | 0.032 |
| 30.000 | 35.000 | 185 | 0.119 | 0.024 |
| 35.000 | 40.000 | 98 | 0.063 | 0.013 |
| 40.000 | 45.000 | 151 | 0.097 | 0.019 |
| 45.000 | 50.000 | 44 | 0.028 | 0.006 |
| 50.000 | 55.000 | 42 | 0.027 | 0.005 |
| 55.000 | 60.000 | 7 | 0.004 | 0.001 |

**Figure 20.**
**Age of vessels from all crossings of the zone**

As should be expected, general cargo ships have the highest percentage of transits through the EEZ (47.7%), followed by bulk cargo ships with 19.8%. The percentage of ships with cargo is practically the same as that under ballast plus partially loaded. Here it is possible to look for a difference in the required power and hence corresponding emissions for ships under load and with greater draught, where there is greater water resistance. The data about the age of the ships are presented in Figure 20. Vessels aged between 20 and 40 years accounted for nearly half (45.7%) of all crossings.

The number of crossings is 1560, but the unique ships are less. Half of the ships have made two or more crossings - typical for container ships, for example. Figure 21 shows the total number of crossings and the number of unique vessels by type. The general cargo ships almost every at least twice crossed the EEZ of Bulgaria. It is also the largest group of ships.

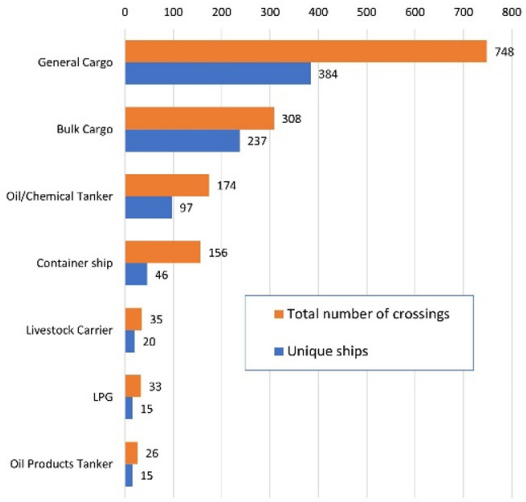


**Figure 21.**
**Comparison of the number of crossings and the number of unique vessels by type**

The features of general cargo ships, being the largest category in the traffic passing through Bulgaria's EEZ, are displayed in Table 1. Figure 22 presents the histograms of length between perpendiculars, total installed power, design speed and age of the ships.

**Table 1. Statistical description of general cargo vessel characteristics**

| Variable | Observations | Minimum | Maximum | Mean | Std. deviation |
|---|---|---|---|---|---|
| DWT, t | 383 | 1000.000 | 33383.000 | 6158.979 | 4696.627 |
| GT | 384 | 398.000 | 22070.000 | 4221.664 | 3116.905 |
| Lbp, m | 383 | 47.650 | 192.000 | 96.823 | 21.053 |
| Power, kW | 384 | 400.000 | 9730.000 | 2461.008 | 1503.777 |
| Speed, kn | 384 | 8.000 | 20.000 | 12.524 | 1.917 |
| Age, years | 384 | 1.000 | 56.000 | 29.438 | 10.485 |

Of interest are the GT values for the observed general cargo ships. Of all 384 ships crossed Bulgarian EEZ in the period under review, 283 (73.7%) have a GT less than 5,000. This means that these ships are not obliged to conduct MRV (Monitoring, Reporting, Verification) procedure, i.e. to report annual $CO_2$ emissions. This suggests that they are out of control in terms of carbon emissions. Only one ship has a GT = 398, less than the 400 limit that will be introduced soon.

Similar statistics have been extracted for bulk cargo vessels - the second largest group. The total number of unique ships is 237.

## CONCLUSIONS

This article is the beginning of an extensive study related to the assessment of the effect of maritime traffic in the Bulgarian Exclusive Economic Zone on the coastal area. The problem is considered serious because the maps of the traffic density in the Black Sea show that the main corridors connecting the Bosphorus with the major ports on the west coast pass through the EEZ of Bulgaria. 1560 crossings were registered with 19 types of ships-some with a single crossing. General cargo ships have the highest number of crossings of the zone 748 (48%) followed by those of bulk cargo ships 308 (20%). The number of unique ships is smaller-384 and 237, respectively.

The routes of the ships through the zone are recorded by the geographical coordinates of the points of the polyline being the respective route. Vessel route data is obtained from the MarineTraffic platform based on the vessels' AIS information.

In addition to the routes for all ships, the main dimensions and general particulars are extracted. Statistical

data on these values are presented. The following important circumstances should be noted:

- The average age of general cargo ships is 29.4 years and that of bulk cargo ships is 17.4 years;
- No statistical assessment has been made, but a large part of these ships is under so-called “Grey” and “Black” flags;
- Of all general cargo ships passing through the defined area, 73.7% are with GT < 500, therefore they are not obliged to report annual $CO_2$ emissions, which takes them out of control;
- Bulk carriers with GT < 5,000 are 3%.

The next results of the study will be related to the probabilistic assessment of the density of shipping along the four corridors-from the Bosphorus to the port of Varna, Constanta, the mouth of the Danube River and Odessa and vice versa.

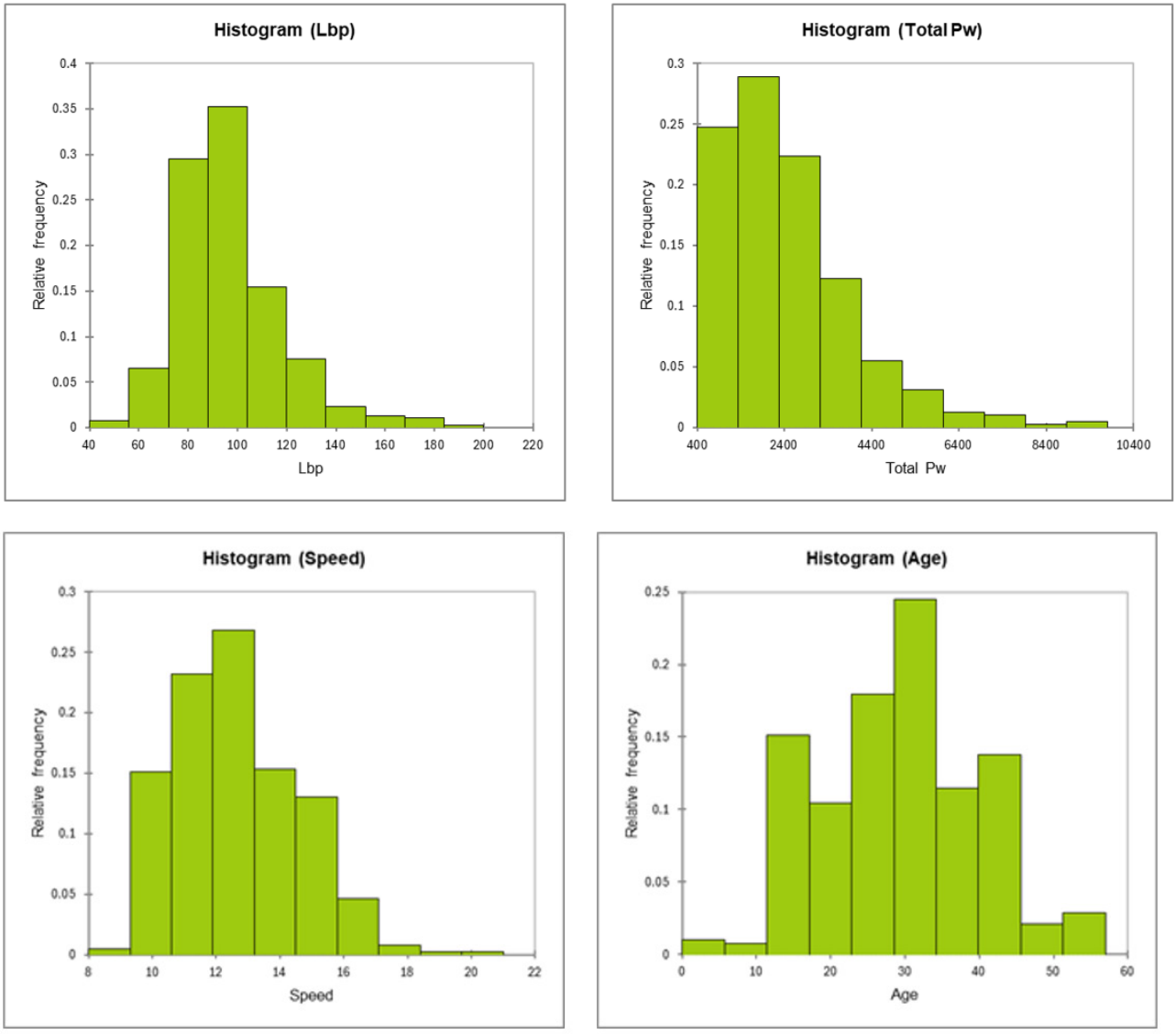


**Figure 22.**
**Histograms of general cargo ship characteristics**

**ACKNOWLEDGEMENTS**

This work has been performed within the Technical University of Varna Research Plan, funded by the State Budget under the contract PD13-2024.

**REFERENCES**

[1] UNCTAD. Review of Maritime Transport 2019; United Nations: Geneva, 2020.
[2] European parliament. $CO_2$ emissions from cars: Facts and figures. 28 2 2020. https://www.europarl.europa.eu/news/en/headlines/society/20190313STO31218/co2-emissions-from-cars- facts-and-figuresinfographics.
[3] Garbatov, Y., Georgiev, P., Fuchedzhieva, I. Extreme Value Analysis of NOx Air Pollution in the Winter Seaport of Varna. Atmosphere. 2022; 13(11):1921. https://doi.org/10.3390/atmos13111921.
[4] Garbatov, Y.; Georgiev, P. Air Pollution and Economic Impact from Ships Operating in the Port of Varna. Atmosphere 2022, 13, 1526.
[5] Kuehne + Nagel, Reducing Sea Freight Emissions. https://home.kuehne-nagel.com/en/-/knowledge/emission-control-areas (Accessed online 15 August 2024).
[6] Eason, C. IMO approves plans for whole Med Sea SOx ECA in 2025. https://fathom.world/imo-approves-plans-for-whole-med-sea-sox-eca-in-2025/ (Accessed online 12 March 2024).
[7] ABS. 2024. News Brier. MEPC 81. March 22, 2024.
[8] Eurostat. https://ec.europa.eu/eurostat/statistics-explained/index.php?title=Maritime_transport_statistics_-_short_sea_shipping_of_goods (accessed on 22 August 2024).
[9] Dimitrov, L. Maritime spatial plan of the Republic of Bulgaria 2021-2035. Geology and geomorphology. https://mspbg.ncrdhp.bg/?lg=en (Accessed 20 September 2024).
[10] Garbatov, Y.; Georgiev, P. Carbon Intensity Assessment of a Bulk Carrier Operating in Different Sea State Conditions. *J. Mar. Sci. Eng.* 2024, *12*, 119. https://doi.org/10.3390/jmse12010119.
[11] Copernicus Marine Service. (https://data.marine.copernicus.eu/product/wind_glo_phy_ l4_my_012 _ 006/services).

# VARNA SCIENTIFIC AND TECHNICAL UNIONS

# SEVENTEENTH INTERNATIONAL CONFERENCE ON MARINE SCIENCES AND TECHNOLOGIES

**Correction by LARGO CITY Ltd. - DOBRICH**
**Computer layout by Donika Sarkoleva-Zlateva**
**Total print: 30, Format 60/84/8**

**LARGO CITY Ltd. - DOBRICH**
**DESIGN, PRE-PRESS AND PRINTING**

**ISSN 1314 - 0957**